Immunomodulatory porous regenerative scar-free scaffolds for *in-situ* vascular engineering (IMPRESSIVE)

Le Zhen

A dissertation

submitted in partial fulfillment of the

requirements for the degree of

Doctor of Philosophy

University of Washington

2020

Reading Committee:

Buddy Ratner, Chair

David Castner

Cole Deforest

Program Authorized to Offer Degree:

Chemical Engineering

University of Washington

Abstract

Immunomodulatory porous regenerative scar-free scaffolds for *in-situ* vascular engineering (IMPRESSIVE)

Le Zhen

Chair of the Supervisory Committee:

Buddy Ratner

Bioengineering and Chemical Engineering

Tissue Engineering has long promised to regenerate tissues for restoring health in patients. However, the requirements of cell harvesting, *in vitro* expansion, cell seeding, maturation in bioreactors, and decellularization involved in traditional tissue engineering often make the time and costs for engineering tissues unaffordable to patients. As a result, there's currently no tissue engineered product that withstands the test of the market, hindering the delivery of the promise of regeneration to patients. *In situ* tissue engineering, by recruiting cells from the body directly to the site to be regenerated and using the body as the bioreactor, bypasses all the *in vitro* works, eliminating the time and costs associated with them. Thus such an approach is more likely to be translational. The research from the Ratner Lab has demonstrated that precision-engineered porous material with pore sizes in the range of 30-40 μm maximizes the recruitment of macrophages which in turn orchestrate blood vessels and other tissues to integrate into the material. Here, we focus on *in situ* tissue engineered vascular grafts using such angiogenic and regenerative materials for the replacement of blood vessels. First, we developed a biostable elastic polymer (elastomer) with tunable mechanical property able to match that of the native

blood vessels. Second, we demonstrated, in a mouse subcutaneous implant model, the precision-engineered elastomer eliminates the foreign body capsule (FBC) and maximizes the ingrowth of capillary blood vessels. Such effects are accompanied and potentially explained by the increase of macrophage recruitment and the decrease of inflammatory macrophages. Third, we manufactured the vascular graft by integrating the porous elastomer, a reinforcement fabric, and a sealant with tunable degradation rate. Fourth, we are conducted short-term implantation studies in both pig and sheep models. We hypothesize that, combining the pro-angiogenic effect, matching mechanical property, and reduction of FBC, our vascular graft will improve healing and reduce intimal hyperplasia (IH). Our first target for clinical application is to improve the performance of vascular grafts for hemodialysis access, which currently have a failure rate of 50% within the first year. If proven successful, such vascular graft can be easily applied to address to broad clinical problems of cardiovascular diseases (CVDs) that are responsible for one in every three deaths. The strategy of co-optimizing porous structure, mechanical property, and bio-degradability is also being applied to developing skin grafts and grafts for regeneration after spinal cord injury (SCI).

Dedication

This little book is dedicated to my grandmother, Xingzhi Chen (1930-2019), who taught me (not by words, but by actions) to face the challenges in life without fear, and to love without condition.

Table of Contents

List of Figures

List of Tables

Chapter 1. Introduction

1.1 Current problems of vascular grafts and proposed solution

Cardiovascular diseases (CVDs) lead to one in every three deaths in the US (Benjamin et al. 2018). Almost one million people in the US suffer limb amputation due to peripheral artery disease (Ziegler-Graham et al. 2008). There is currently no FDA approved vascular graft for the replacement of small-diameter (<5mm) blood vessels that fail due to CVD. Also, vascular grafts for hemodialysis have more than 50% failure rate within one year of implantation (Cinat, Hopkins, and Wilson 1999), demonstrating poor performance of larger diameter vascular grafts. These facts underline the need for better vascular grafts. We attribute the failure of vascular grafts to 1) poor blood compatibility due to the absence of an endothelial lining; 2) inability to dilate due to mechanical mismatch; 3) the foreign body response (FBR) that exacerbates the mechanical mismatch and inhibits healing. Considering all these factors, we hypothesize that a material that simultaneously induces endothelial cell ingrowth, matches mechanical property with native blood vessels, and reduces the inflammatory FBR will substantially improve vascular grafts performance. We developed a precision-engineered porous polyurethane (PU) material that addresses the issues leading to graft failure. Thus, we propose an *in-situ* tissue engineering approach to generate a semi-living vascular graft.

1.2 Tissue engineering and *in situ* tissue engineering

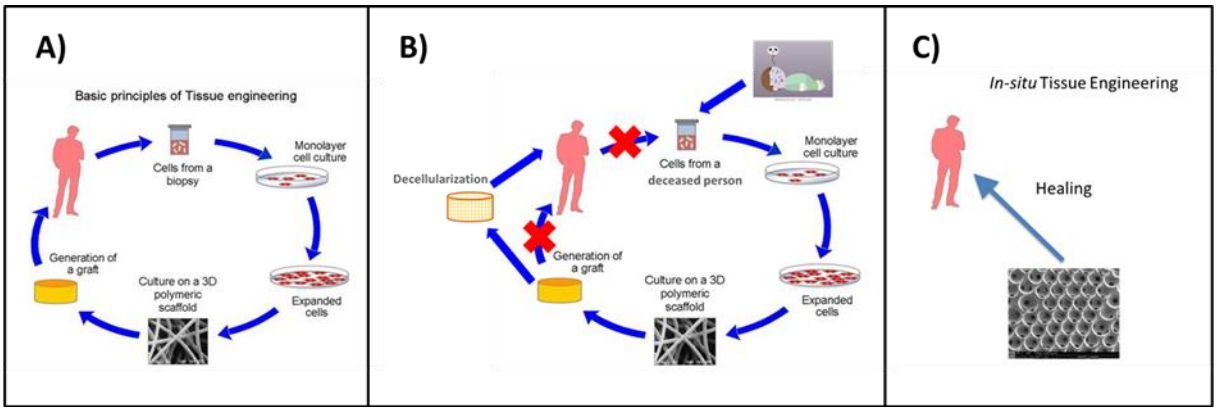

Figure 1.1 Paradigm shift from tissue engineering to *in situ* tissue engineering. A) *in vitro* tissue engineering from autologous cells; B) in vitro tissue engineering from allogenic cells + decellularization (the Humacyte® approach); C) cell-free *in situ* tissue engineering (our approach).

Tissue Engineering offers an opportunity to solve all the problems associated with synthetic vascular grafts by using human cells to construct vascular grafts (L'heureux et al. 1998; Niklason et al. 1999; Soletti et al. 2010; Hashi et al. 2007; McAllister et al. 2009; Zhu et al. 2004a; Soffer et al. 2008; Teebken et al. 2000; Jeong et al. 2007; Roh et al. 2010). The classical tissue engineering paradigm envisioned taking a patient's own cells to engineer a new organ *in vitro*, and transplanting it back to the same patient (**Fig 1.1A**.) more than 30 years ago. However, high cost, long time for production, significant technical and regulation hurdles often render such an approach futile in clinical translation. To reduce patient waiting time and produce an "off-the-shelf" tissue engineered vascular graft (Syedain et al. 2017; Kirkton et al. 2019; Lawson et al. 2016), Humacyte® pioneered the clinical translation of the *in vitro*, allogenic tissue engineering approach (**Fig 1.1B**.) To avoid transplant rejection and prolong shelf life, the final product is a decellularized scaffold. Although such a scaffold does not solve the problem of high cost and long production time, it demonstrated the ability to recruit the patient's own cells and reconstruct

blood vessel *in situ* (Kirkton et al. 2019). In light of such observations, we aim at *in situ* tissue engineering of blood vessels using synthetic and biologic hybrid scaffold that completely eliminates *in vitro* cell works. (**Fig 1.1 C**.) Such approach has the potential to achieve healing response similar to that of Humacyte®, while significantly reducing cost, production time, and improve safety.

1.3 Precision-engineered porous material induced angiogenic regeneration

The Ratner Lab invented a new class of materials of which the microporous structure and pore size can be precisely controlled through the "6S" process (see Section 2.3.3.2 in Chapter 2). We discovered that maximum vascularization and minimum foreign body capsule formation are achieved when the pore size is between 30-40 μm. (Ratner and Marshall 2008; Madden et al. 2010; Sussman et al. 2013) Healionics, a spin-out company from our lab, is pioneering the clinical trial on the STARgraft®, a PTFE graft externally coated with a silicone-based 6S material. The highly angiogenic and scar-free healing induced by the 6S material is expected to reduce infection risk and compliance lost due to foreign body response. However, such a coating approach does not improve tissue regeneration on the luminal surface because the PTFE layer and the adhesive between the PTFE and 6S material are impermeable to cells. To address this problem, we developed a vascular graft made of a polyurethane-based elastic 6S material throughout the wall. We will test if this graft induces angiogenic regeneration on the luminal surface and ultimately leads to complete endothelialization.

1.4 Immunomodulation and pro-healing effects of 6S materials

The response of innate immune cells, macrophages, to vascular grafts is essential in directing vascular graft healing (Hibino et al. 2011; Koyal Garg et al. 2013b; Z. Wang, Cui, Wang, Yang,

Wu, Wang, Gao, Li, Li, Zheng, et al. 2014). 6S materials induce tissue regeneration by attracting macrophages into the porous structure and the porous structure modulates the macrophages towards a pro-healing phenotype. (Sussman et al. 2013) In Chapter 3, we discuss some nuances of accessing such phenotypes. The pro-healing macrophages in turn recruit endothelial and other cells to grow in and around the material. Thus 6S materials have the potential of achieving *in situ* tissue regeneration without the loading of any growth factor, cells, or other pre-conditioning.

1.5 Mechanical property mismatch and patency

The mismatch of mechanical property between vascular grafts and native blood vessels leads to constant flow disturbance and damage of native blood vessels at the anastomosis (Ballyk et al. 1997; Abbott et al. 1987; Walden et al. 1980; Kidson 1983; Sarkar et al. 2006). These factors induce intimal hyperplasia and reduce patency. Thus it's not surprising that patency of different vascular grafts negatively correlates to their mechanical mismatch with native blood vessels (Salacinski et al. 2001). Vascular grafts that are more compliant and have a better match with the mechanical property to the native blood vessel tends to perform better than mechanically mismatched grafts such as PTFE and Dacron. Such observation entails the hypothesis that vascular grafts perfectly that match the mechanical property with the native blood vessels will have perfect patency. In Chapter 2, we discuss how we created the material to match the mechanical property of the native blood vessel. In addition, the foreign body response to traditional vascular grafts leads to their encapsulation by a dense and stiff collagen layer, called the foreign body capsule. The encapsulation further reduces the compliance of traditional vascular grafts and intensifies the mechanical mismatch over time. Our grafts simultaneously match mechanical properties with native blood vessels and reduce foreign body capsule formation (Chapter 3). Thus, we expect this product to maintain matched mechanical properties

both initially and in long term. We expect such properties to mitigate intimal hyperplasia and improve patency.

1.6 The manufacturing process of IMPRESSIVE grafts

In Chapter 4, we will discuss, in detail, the manufacturing process of the full IMPRESSIVE grafts and the tests we conducted to ensure safety for large animal studies.

1.6.1 "6S" process for manufacturing precision-engineered porous material

To help understand the manufacturing process of the IMPRESSIVE grafts, we first describe the "6S" process of manufacturing a simple piece of precision-engineered porous material. (**Fig 1.2**) Typically, PMMA beads with a broad size distribution were **S**ieved to obtain mono-dispersity. In this case, all the PMMA beads are around 40 μm in diameter. The beads were then loaded into the space between a 6-mm-diameter glass rod and 8-mm-inner-diameter glass tube held concentric by two Teflon caps at the ends. The beads were **S**haken in a sonicator for 1 hour to obtain close packing and then **S**intered under 175 °C for 20 hours to obtain interconnection between each adjacent bead. The bead cake was taken out from the glass tube submerged in the freshly mixed polyurethane components. The whole mixture was placed in vacuum for 5 minutes for the gas in the bead cake to be sucked out. When the vacuum was purged by nitrogen, the bead cake and its internal space were **S**urrounded by the mixture of the four components. Then the bead cake was taken out of the mixture and wrapped with Teflon films and mixture in the bead cake was allowed to **S**olidify under 55 °C for two days. After the reaction, the PMMA template was **S**olubilized by organic solvents, leaving behind the precision engineered porous material. Note that the traditional sieving process was omitted since we identified commercial source of mono-dispersed PMMA beads.

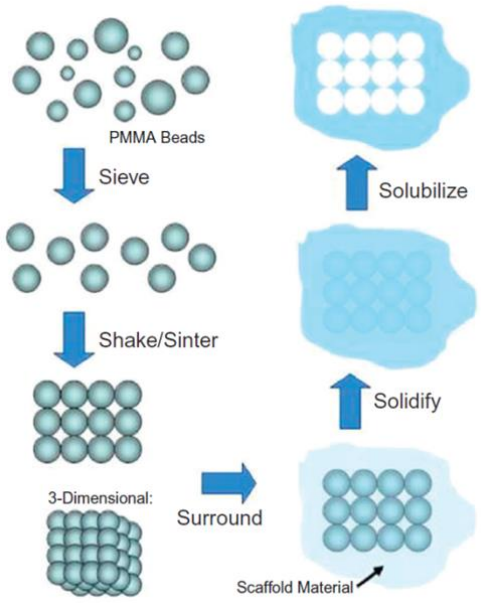

Figure 1.2 Schematic representation of the "6S" manufacturing process for the precision-engineered porous material.

1.6.2 Manufacturing process for IMPRESSIVE grafts

A modified version of the 6S process was used to manufacture IMPRESSIVE grafts. First the polyester mesh was wrapped around a 6-mm-diameter glass rod twice. The wrapped glass rod was then put into an 8-mm-id glass tube. All three parts were sterilized with 70% ethanol, and then dried in an 80 °C oven for two days. The glass rod and glass tube were held concentric by two custom-made Teflon caps. 40 μm PMMA beads were poured into the space between the glass rod and the class tube and sonicated for 1 hour to allow close packing. Interconnects between PMMA beads were formed by sintering in 177 °C for 28 hours. The glass rod and mesh embedded bead cake were taken out of the class tube and submerged in PU 4344 pre-polymer mixture. The submerged beak cake was subjected to -25 in. Hg for 5 mins. The vacuum was purged with N_2. One more repetition of this vacuum-purge process secured the interstices of the

bead cake were completely filled with the pre-polymer mixture. The bead cake was taken out of the pre-polymer mixture and immediately wrapped with low density PTFE tape. Polymerization was completed in 55 °C for 48 hours. The PTFE tape was removed and the nonporous film formed on the surface of the bead cake was scraped off. The glass rod was taken out after soaking in 70% ethanol overnight. The PMMA beads were solubilized and removed by soaking in acetone for 3 days with 1 change per day, then washed DCM for 7 days with 1 change per day, then acetone for 3 days with 1 change per day. The vascular graft was gradually changed into 70% ethanol, then thoroughly washed with DI water and lyophilized overnight. The vascular graft was impregnated with a 5% gelatin solution with the same vacuum-purge process described above for 3 times. The gelatin impregnated graft was refrigerated overnight. The impregnation and refrigeration were repeated one more time. The gelatin was crosslinked with EDC/NHS chemistry (gelatin solution/crosslinker solution=1:50 (v/v), NHS/EDC (molar ratio=0.2, EDC/(-COOH) in gelatin (molar ratio)=2) for 16 hours in 4 °C. The crosslinking reaction was quenched with ph8.5 PBS for 2 hours then washed with DI water. The gelatin sealed vascular graft was sterilized with 70% ethanol then thoroughly washed with DI water. After lyophilization, the graft was double wrapped and sterilized with ethylene oxide treatment before implantation.

1.7. Significant physical and performance characteristics

1.7.1 Vascular graft structure overview

IMPRESSIVE grafts consist of three components: the 6S material graft wall, gelatin sealant to prevent hemorrhage, and polyethylene terephthalate (Dacron) mesh embedded within the graft wall to provide suture strength. (**Fig 1.3A**.) The graft has a 6-mm inner diameter, and can be made in arbitrary length. (**Figure 1.3B.**)

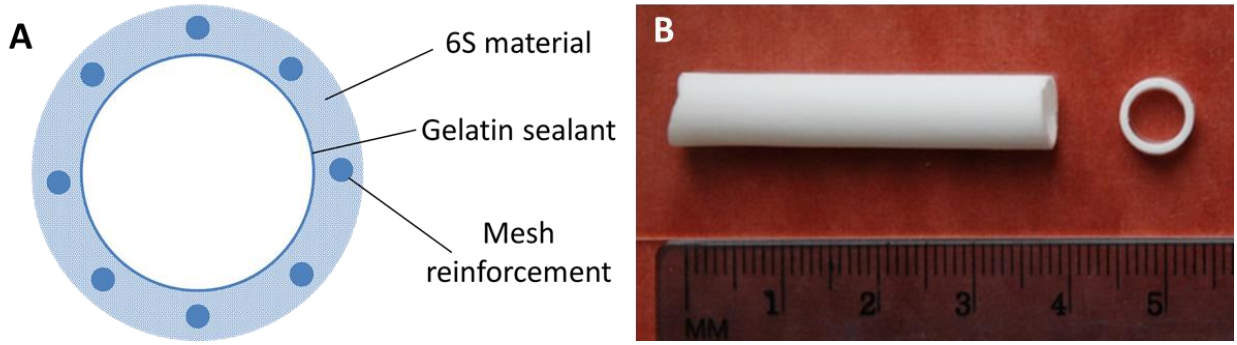

Figure 1.3 Overview of IMPRESSIVE graft structure. **A)** Illustration of the cross-section of the vascular grafts showing the all three components; **B)** Photograph of the side view and cross-section of the vascular graft.

1.7.2 Precision-engineered porous material

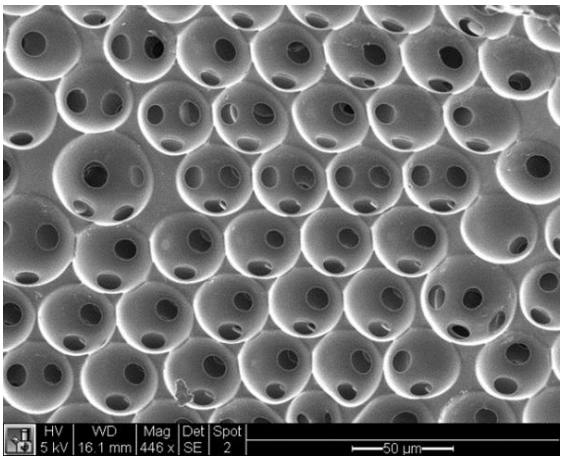

Figure 1.4. Scanning electron micrograph of the precision-engineered porous structure.

The 6S material has precision-engineered spherical pores with diameters all around 40 micrometers. Each spherical pore is interconnected with surrounding pores by 10-15 micrometers round holes. (**Fig 1.4**) Such structure allows the whole graft wall to be permeable by cells. More importantly, it is optimized for vascularization.

1.7.3 Fast degradable gelatin sealant

To prevent initial hemorrhage from the porous graft wall, the pores were sealed with crosslinked gelatin. The gelatin sealant was optimized to degrade within two to three weeks *in vivo*. Such a fast degradation rate corresponds to the rate of healing. Thus the gelatin should be rapidly replaced by cells *in vivo*, and does not cause foreign body capsule formation.

1.7.4 Polyethylene terephthalate (Dacron) mesh

To provide the suture strength, a polyethylene terephthalate (Dacron) surgical mesh was embedded within the graft wall. The pores of the mesh are large enough (≥ 1mm) that they should have negligible effect on the microporous structure of the graft wall and will not block cell infiltration. Dacron is also widely used for FDA approved vascular grafts. It has excellent biostability, which helps to prevent aneurysms during long-term implantation.

1.7.5 Tunable Young's modulus of porous material

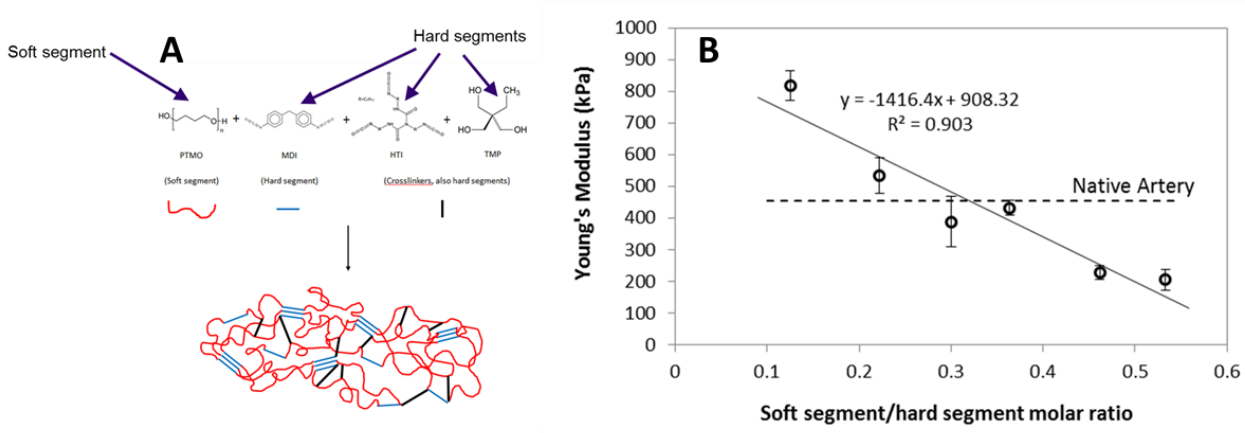

Figure 1.5. Tuning the Young's modulus of the porous material. **A)** The chemical composition of the elastomer used for making the porous material; **B)** The Young's modulus of the porous material linearly correlates to the soft to hard segment ratio.

The porous material of the vascular graft is made from a novel polyurethane elastomer consisting four components: poly(tetramethylene oxide) (PTMO), 4,4'-methylene diphenyl diisocyanate (MDI), 6-(3-(6-isocyanatohexyl)-2,4-dioxo-1,3 diazetidin-1-yl]hexyl N-(6-isocyanatohexyl) carbamate (HTI, or Desmodur N-3200), and 1,1,1-tris(hydroxymethyl) propane (TMP). (**Fig 1.5 A**.) In these components, PTMO is the soft segment that provides elasticity. MDI, HTI, TMP are the hard segments that provide mechanical strength. The Young's modulus of the porous material can be tuned by varying the soft segment to hard segment ratio. (**Fig 1.5 B.**) When the soft/hard segment ratio equals 0.36, or PTMO/MDI/HTI/TMP=4/3/4/4 (PU4344), the mechanical property of the porous material perfectly matches that of the native blood vessel. Thus we chose such composition for making the vascular graft. In addition, from the standpoint of a crosslinked polymer, PTMO and MDI are the linear components, while HTI and TMP are crosslinkers. In the mechanically optimal composition, the crosslinker to linear ratio is more than 1:1, which is considered extremely highly crosslinked. Such a high degree of crosslinking provides the novel material extra biostability compared to traditional biostable linear polyurethanes. Such property also helps to reduce the risk of aneurysm over long-term implantation.

1.7.6 Suture strength of vascular graft

With the reinforcement, the suture strength of the material is 4.77±0.36 N, which is much higher than the suture strength of native blood vessels (~ 2N). This shows that the vascular graft is

suturable. In addition, the grafts have been sutured end-to-end as interposition artery graft in sheep for 4 weeks and demonstrated excellent suture retention.

1.7.7 Pro-healing property

Side-by-side comparison of the luminal surfaces of an IMPRESSIVE graft and a PTFE graft after 4 weeks implantation in sheep shows that the IMPRESSIVE graft was almost completely covered by tissue and very few red clots, while PTFE was completely covered by red clots. (**Fig 1.6**) This preliminary result demonstrates the pro-healing property of the IMPRESSIVE graft.

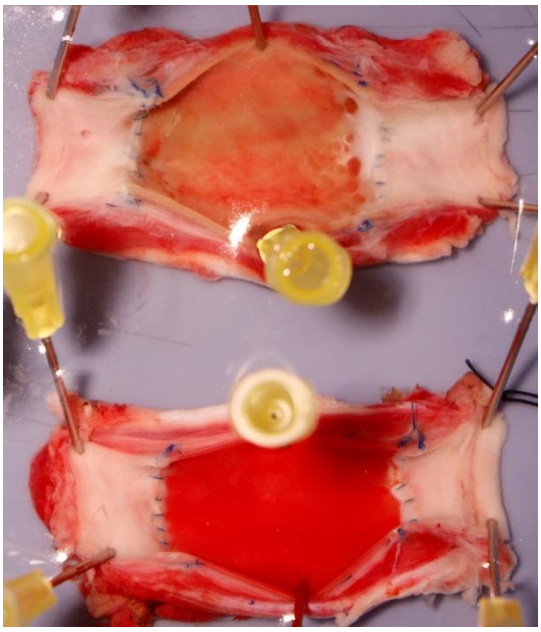

Figure 1.6. Representative photograph of the luminal surfaces of the IMPRESSIVE graft (top) and PTFE (bottom) after 4 weeks of implantation as interposition grafts in each side of the carotid arteries in the same sheep.

1.8 A pathway towards first in human (FIH) clinical trial

In Chapter 6, we discuss the clinical backgrounds of vascular grafts used as blood access. Based on the clinical background, we proposed a battery of tests to justify a FIH clinical trial.

1.9 Pushing the boundary of small diameter vascular grafts

In Chapter 7, we propose to expand the IMPRESSIVE approach to address small diameter vascular grafts. Incorporating *de novo* designed pro-healing cytokine IL-4 mimic, we expect to further improve healing and reduce FBR. We hope to finally create high performance vascular grafts to replace femoral and even coronary arteries.

Chapter 2. Precision-engineered Porous Material with Tunable Mechanical Property for Vascular Graft Application

2.1 Abstract

We investigate the in vitro biostability and mechanical property of a polyurethane elastomer for vascular graft application. The polyurethane was synthesized in a one-step, catalyst-free, solvent free reaction, which is compatible with the precision engineering of porous vascular graft. The in vitro biostability characterized by H_2O_2 oxidation and examined with ESCA, which shows equivalence or improvement compared to commercialized product Pellethane 2363-80A. The precision engineered porous structure of the vascular graft is proven to be optimized for endothelial cells ingrowth in vivo. In addition, the mechanical property (Young's Modulus) of the vascular graft can be fine-tuned to match that of the native blood vessels.

2.2 Introduction

The failures of blood vessels result in one in every three deaths. Autologous blood vessels are the golden standard for blood vessel replacement. However, they are limited by their availability. As an alternative, synthetic vascular grafts are in great demand. But their failure rate is much higher. The major causes of vascular graft failures are stenosis (narrowing) and infection. Stenosis is mainly initiated by acute events such as thrombosis (blood clotting), or long term events such intimal hyperplasia (IH, smooth muscle cells over proliferation at the blood vessels- synthetic graft suture line, or anastomosis). The mismatch of mechanical property between current vascular graft materials (ePTFE and Dacron, which are very rigid) and native blood vessels (elastic), which creates turbulence and repeated damage to the native blood vessel

under the cyclical, pulsatile blood flow, is one of the main contributing factors to IH. For this reason, *developing a graft material that matches the elasticity with native blood vessel is crucial in that it has a high potential for reducing IH*, one of the major failure modes of vascular grafts. The suboptimal blood compatibility of current vascular graft materials induces thrombosis. In healthy native blood vessels, a single layer of endothelial cells form an inner lining called endothelium which has the optimal blood compatibility dictated by evolution. In addition, a healthy endothelium cells can also suppress smooth muscle cell proliferation. Therefore, *the complete healing of endothelium is long hypothesized to reduce thrombosis and IH*. However, the healing of endothelium seldom crosses the anastomosis more than 1 cm and complete healing of endothelium has not been observed in current vascular grafts in patients. Another devastating complication not only hindering the application of vascular grafts but all implantable devices is infection. Current biomaterials generally elicit a cascade of reactions (foreign body reaction, or FBR) orchestrated by macrophages that result in a scar layer that separates the material from the rest of the body. This separation creates regions devoid of the body's natural defense system. *These defenseless regions in biomaterials are heavens for bacterial infections.*

Our lab has developed the precision engineered microporous structure that simultaneously optimizes angiogenesis and reduces scar layer formation *in vivo*.(Lauran R. Madden et al. 2010) Materials with this structure elicit a healing and integration reaction from the body distinctively different from the classic FBR by attracting macrophages to reside in the porous structure and turning them into a pro-healing state which orchestrates healing.(Sussman et al. 2014) Different materials with such microstructure have demonstrated a seamless healing pattern in skin, sclera, bone, and heart stroma. In addition, such porous materials have received a CE mark and have

been translated in human implantation. Inspired by Clowes et al.'s research (1986) on transmural healing of endothelium (**Fig 2.1.**), we hypothesize that *a vascular graft with the precision-engineered microporous structure will allow endothelial cells to grow through the vascular graft wall and cover the whole lumen of the vascular graft.* This complete healing can also *eliminate the defenseless regions in the biomaterial, which is likely to reduce vascular graft infection.*

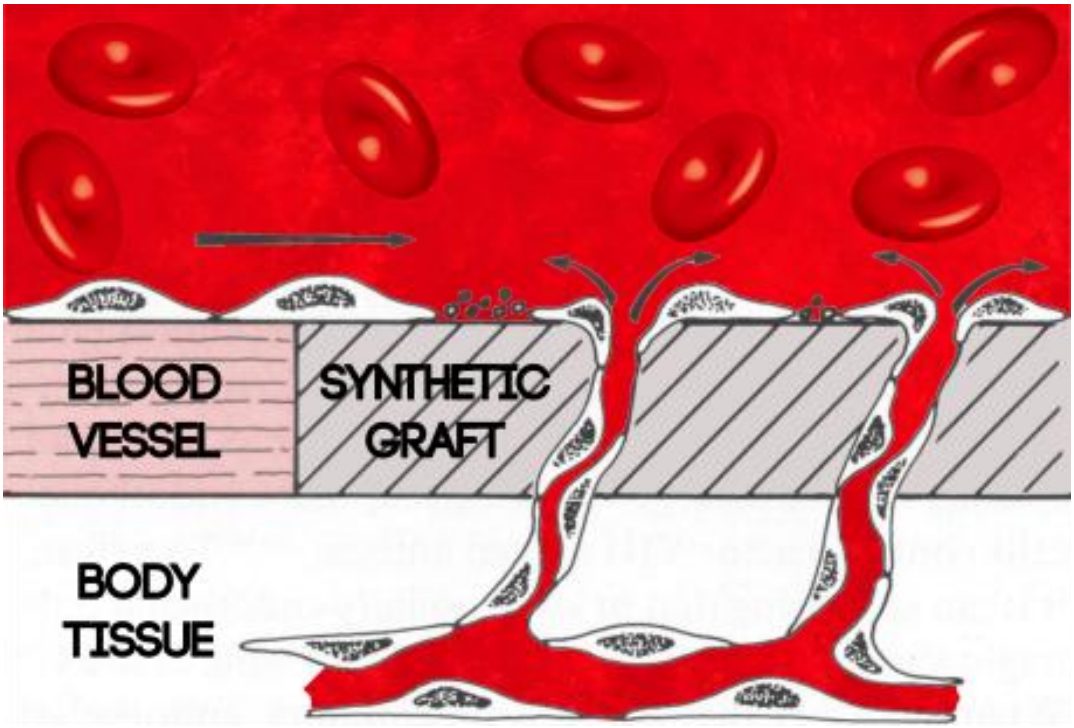

Figure 2.1. Scheme for complete endothelium healing. Endothelial cells from surrounding tissue grow in through the porous structure of the vascular graft and ultimately cover the entire lumen. (Image modified from (Clowes, Kirkman, and Reidy 1986).)

Polyurethanes are a class of extremely versatile polymers with tunable mechanical properties, bio-stability/biodegradability, and functionalities. Thus many research have been done to apply polyurethanes to make vascular graft (Tai et al. 2000a; Zhu et al. 2004b; Doi and Matsuda 1997;

Hsu and Chen 2000; Seifalian et al. 2003; Uttayarat et al. 2010; Jun, Taite, and West 2005; Jeschke et al. 1999; Z. Zhang et al. 2004; Chuang and Masters 2009). However, most of polyurethane grafts in the literature have poorly controlled porous structure. In addition, many of the linear polyurethanes used are not compatible with the solvent extraction in the "6S" processes.

In this research, we focus on developing the proper material for the pro-healing vascular graft. Such a material will need to satisfy several design principles: 1) the reaction system needs to be compatible with the manufacture process of the porous material; 2) the mechanical property of the material needs to be tunable to match that of the native blood vessels; 3) the material needs to have the strength to withstand suture; 4) the material needs to be stable in the body for long term. To satisfy these requirements, we developed a crosslinked polyurethane material that can be synthesized in a *one-step, catalyst-free, solvent free reaction*. This material can be manufactured into the *precise pro-healing porous structure*. The Young's modulus of the porous material can be tuned to *completely match that of the native blood vessel*. Finally, this material showed *improved biostability* in comparison with commercially available "biostable" polyurethane under *in vitro* accelerated oxidation test examined by electron spectroscopy for chemical analysis (ESCA).

2.3 Materials and Methods

2.3.1 Materials

Poly (tetramethylene oxide) (PTMO, commercial name: PolyTHF® 1000, Cat. No. 585788) was purchased from BASF Corporation. 4,4'-Methylenebis (phenyl isocyanate) (MDI, Cat. No.

256439-500G) and 1,1,1-Tris (hydroxymethyl) propane (TMP, Cat. No. 93370), phosphate buffered saline (PBS, pH 7.4, Cat. No. P5368-10PAK) were purchased from Sigma-Aldrich. 1,3,5-Tris (6-isocyanatohexyl) biuret (HTI, commercial name: Desmodur N3200, Cat. No. 5288673) was purchased from Bayer Material Science. Uncrosslinked monodisperse 40 µm and 100 µm poly(methyl methacrylate) (PMMA) microspheres were purchased from MICROBEADS (Norway). Pellethane® 2363-80 (Lot. No. 7-20-6R) was purchased from The Upjohn Company (California). HPLC grade N, N-Dimethylacetamide (DMAc, Cat. No. 270555-1L) was purchased from Sigma-Aldrich. Methylene chloride (DCM, Cat. No. D143-4), acetone (Cat. No. A949-4), methanol (Cat. No. A452-4), and 30% hydrogen peroxide (Cat. No. H325-500) were purchased from Fisher Scientific. Anhydrous ethanol (CAS No. 64-17-5) was purchased from Decon Labs. Antibiotic Penicillin Streptomycin (Pen Strep, Ref. No. 15140-122) was purchased from Gibco.

2.3.2 Synthesis of polyurethanes

The polyurethanes were synthesized in a one-step, catalyst-free, solvent-free process. PTMO (Mw=1000), MDI, HTI, and TMP (chemical structures shown in **Fig 2.2)** were heated to 80 °C and mixed in various molar ratios shown in **Table 2.1**. The reaction was completed in 55 °C for 48 hours. Water is a major impurity that competes with the desired reaction. To remove water from the reaction components, PTMO and TMP were first fully mixed then subjected < -30 inch Hg vacuum in a vacuum oven heated to 80 °C for one hour. The vacuum was purged with nitrogen. HTI and MDI were then added and mixed with a stir bar stirring at 250 rpm while maintaining the temperature above 80 °C. Gentle inversion of the reaction vial can help the mixing. Care was taken not to introduce bubbles. Once all the components were well-mixed, the mixtures were immediately pipetted into homemade Teflon molds to form 1 mm-thick sheets of

solid polymers after reaction in 55 °C for 48 hours. Teflon molds were disassembled and separated from polymers.

2.3.3 Fabrications of precision-engineered porous scaffolds in sheet and tube forms

2.3.3.1 Preparation of PMMA sphere templates

To fabricate PMMA sphere templates, PMMA microspheres were poured into homemade molds to assume the desired forms and sintered to form interconnected wholes. For sheets, PMMA microspheres were poured into 1mm × 25mm × 75 mm molds made by sandwiching a 1mm-thick U-shape Teflon spacer between two glass slides. Each mold was held together with 7 small binder clips. Standing upright, every four to five beads-filled molds were loaded into one 500 ml glass beaker against the wall. The centers of the beakers were filled with aluminum foil balls to keep the molds from moving. The beakers were capped with aluminum foil and sonicated for an hour. The sonication allows the beads to pack closely together. While sonicating, a heating/drying oven (BINDER, fan speed at 100%) was preheated to desired sintering temperature. After sonication, the beakers were carefully and quickly transferred into the preheated oven without disturbing the microspheres. The optimal sintering temperature and time for 40 μm microspheres were about 175 °C and 24 hours. The optimal sintering temperature and time for 100 μm microspheres were about 177 °C and 19.5 hours. We found that the exact optimal sintering conditions are dependent on batch, age of microspheres, and other oven conditions. Thus routine quality controls were done by breaking sphere templates in the middle and imaging the breaking edge with SEM. In an optimally sintered template, the diameters of interconnects between the spheres are about one third of the diameters of the spheres. To prepare tube shape PMMA templates, molds were made by holding glass rods with 6 mm diameter and

glass tubes with 8 mm inner diameter concentric with custom-made holders. The rest of the steps are similar to those for sheet PMMA templates. After the tube shape PMMA templates were formed the templates together with the glass rod in the center were taken out of the glass tubes.

2.3.3.2 Fabrication of scaffolds

To fabricate sheets of porous scaffolds, the 1-mm-thick PMMA templates described in **Section 2.3.3.1** were taken out of the molds and submerged in the pre-polymer mixtures described in **Section 2.3.2**. Air in the interstices of the PMMA templates was removed by subjecting the submerged PMMA templates to -25 inch Hg vacuum for 5 minutes in 80 °C. The vacuum was purged by nitrogen to allow the pre-polymers to infiltrate in the interstices of the PMMA templates. This process was repeated once to allow complete air removal and pre-polymers infiltration. The pre-polymer infiltrated PMMA templates were put back into the molds they were made in. The molds were re-assembled with Teflon thin films inserted in between templates and glass slides to prevent adhesion of polymers on glass slides. The molds were then placed in 55 °C ovens with forced convection for 48 hours to allow completion of polymerizations. The polymers were taken out of the molds and the thin nonporous polymer films formed on their surface were scraped off using razor blades. The PMMA templates were removed using organic solvent DCM and acetone. To avoid breakage due to rapid swelling in organic solvent, the polymer sheets were first soaked in 70% ethanol overnight. The 70% ethanol was gradually replaced by acetone (5 ml per time for 2 hours × 3, a third of the solution per time for 2 hours × 3, full acetone change for 2 hours × 3). The gradual change into acetone allows the polymer to slowly swell without breakage. The PMMA templates also started to dissolve in acetone. The scaffolds were then placed in Soxhlet extractors and continuously washed with DCM for 5-7 days. The PMMA templates were completely removed in this process.

The scaffolds were then soaked in acetone for one week with one complete change of fresh acetone. The acetone was gradually replaced by 70 % ethanol (a third of the solution per time for 2 hours × 3, a half of the solution per time for 2 hours × 3, full 70% ethanol change for 2 hours × 3). The 70% ethanol was gradually replaced by DI water in the same manner.

The fabrication processes for tube shape scaffolds from tube shape templates are similar to those for sheet shape scaffolds with a few exceptions. First, after pre-polymer infiltration, the templates together with the glass rods were tightly wrapped with PTFE tapes for polymerization. Second, after the polymerization, the PTFE tapes were taken off and the outer surfaces of the tubes were scraped to remove the nonporous polymer films. Third, the glass rods were removed after the polymers swelled in 70% ethanol overnight or in the process of replacing 70% ethanol with acetone. The tubes detach from the rods when sufficient swelling occurs.

This fabrication process was adapted from the process traditionally termed the "6S" process (**Fig 2.3**). The "6S" process was invented by Andrew Marshall (2008) from the Ratner Lab. Typically, PMMA beads with a broad size distribution were **S**ieved to obtain mono-dispersity. In this case, all the PMMA beads are around 40 μm in diameter. The beads were then loaded into the space between a 6-mm-diameter glass rod and 8-mm-inner-diameter glass tube hold concentric by two Teflon caps at the ends. The beads were **S**haken in a sonicator for 1 hour to obtain close packing and then **S**intered under 175 °C for 20 hours to obtain interconnection between each adjacent bead. The bead cake was taken out from the glass tube submerged in the freshly mixed polyurethane components. The whole mixture was placed in vacuum for 5 minutes for the gas in the bead cake to be sucked out. When the vacuum was purged by nitrogen, the bead cake and its internal space were **S**urrounded by the mixture of the four components. Then the bead cake was taken out of the mixture and wrapped with Teflon films and mixture in the bead cake was

allowed to **S**olidify under 55 °C for two days. After the reaction, the PMMA template was **S**olubilized by organic solvents, leaving behind the precision engineered porous material.

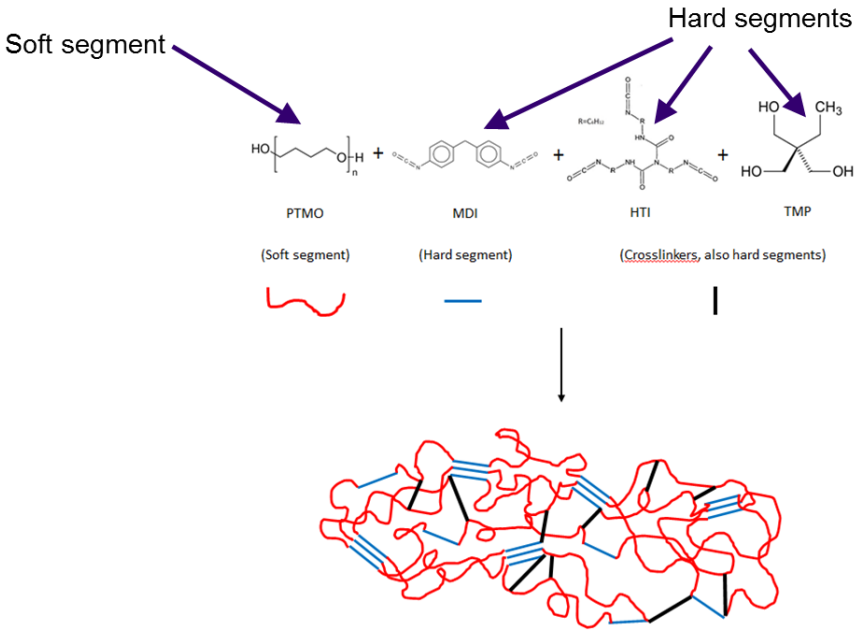

Figure 2.2. Schematic representation of the one-step, catalyst free, solvent free reaction for polyurethane synthesis.

2.3.4 Scanning electron microscopy (SEM)

The microscopic structures of PMMA templates and PU scaffolds were imaged using an FEI Sirion SEM (Hillsboro, OR). Samples were sputter coated with Au/Pd using a SPI-MODULE^{TM} sputter coater at 9 mA for 60 seconds (coating speed 13 nm/min).

2.3.5 Tensile properties measurement

Tensile properties were measured using a 5540 Series Single Column System Instron testing machine (Instron, Norwood, MA) with a 500 N load cell. Materials were punched using a dog-bone shaped steel blade dimensioned per ASTM D-1708-96-MET standard. The nominal sample

length is 35 mm, width 5 mm, and the gauge nominal length is 22 mm. Samples were approximately 1 mm thick. The Bluehill Materials Testing (Instron) software was used to collect data from the tests. The samples were stretched at a constant rate of 10 mm/min, under water at 37 °C using a temperature controlled water bath manufactured by Instron. Data were collected until breakage.

2.3.6 Accelerated oxidation test

2.3.6.1 Sample preparation and hydrogen peroxide treatment

For *in vitro* biostability test, a small piece of non-porous polyurethane (PTMO/MDI/HTI/TMP (molar ratio) = 4/3/4/4, referred to as PU4344) was submerged in 30% hydrogen peroxide under 37 °C for 24 hours then dried under vacuum. A piece of the same material underwent the same treatment except been submerged in DI water served as the control. Commercially available "biostable" polyurethane Pellethane 2363-80A was dissolved in DMF then precipitated in methanol. This process was repeated to remove all the stabilizers in the material. The Pellethane was then dissolved in DMAc in a concentration of 50 mg/ml. The 50 μL of the solution was pipetted on 10-mm micocoverslip and allowed to dry in 55 °C. This process was repeated until the Pellethane film on the coveslip reach 12 mg. Two samples were treated in DI water or in 30% hydrogen peroxide as PU4344 was treated.

2.3.6.2 Electron Spectroscopy for Chemical Analysis (ESCA)

ESCA spectra were taken on a Surface Science Instruments S-Probe photoelectron spectrometer. This instrument has a monochromatized Al K 〈 X-ray source which was operated at 20 mA and 10 kV. X-ray analysis area for these acquisitions was approximately 800 mm across. Pressure in

the analytical chamber during spectral acquisition was less than 5 x 10^{-9} torr. Pass energy for high resolution spectra was 50 eV. Data point spacing was 0.065 eV/step for high resolution spectra. The take-off angle (the angle between the sample normal and the input axis of the energy analyzer) was 0º, (0º take-off angle = 100 Å sampling depth). Service Physics Hawk version 7 data analysis software was used for data analysis.

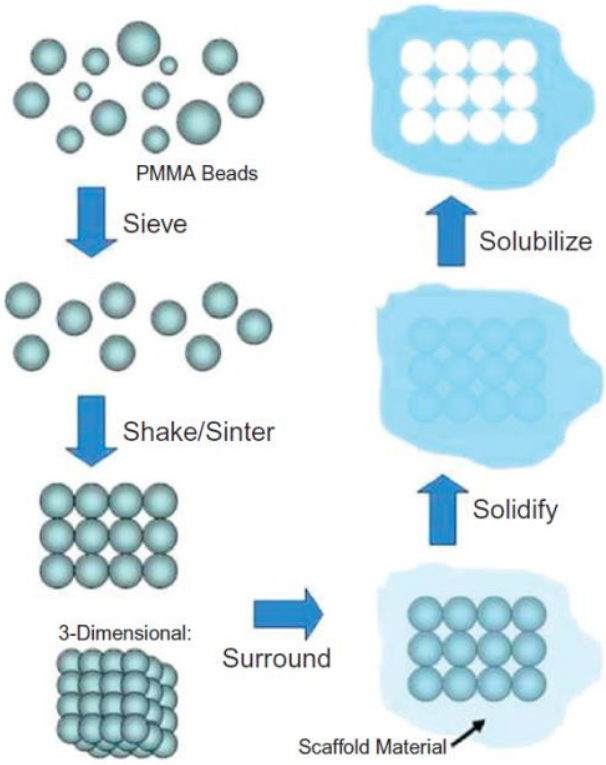

Figure 2.3. Schematic representation of the "6S" manufacture process for the precision-engineered porous material. (Ratner, 2015)

2.4 Results and Discussion

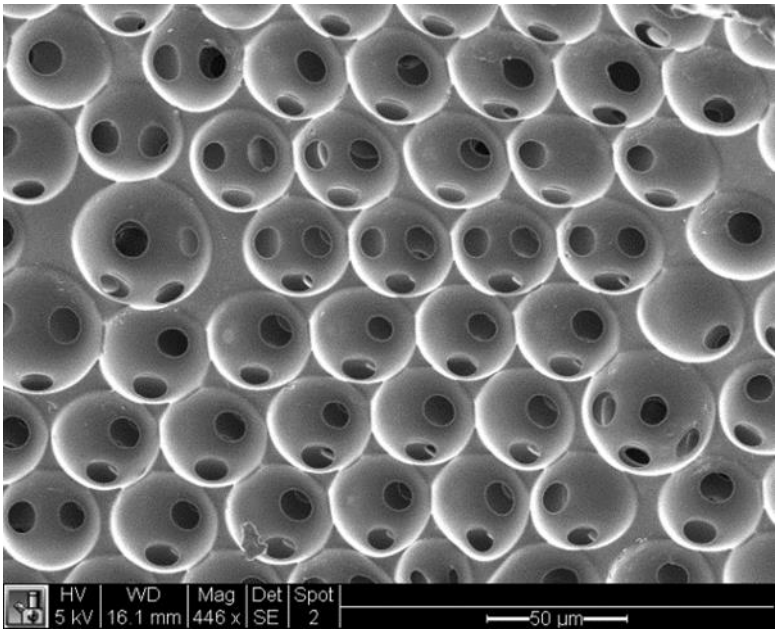

Figure 2.4. SEM image of the precision-engineered porous structure.

Fig. 2.4 shows the precision engineered porous structure of the polyurethane material where spherical pores with a diameter of about 40 µm are interconnected by holes of about 13 µm in diameter. Each pore is interconnected by 10-12 holes, which make the whole material highly interconnected. *In vivo* this structure will quickly be populated by macrophages. The macrophages will attract the endothelial cell ingrowth. Previous study suggests that pores around this size are optimized for endothelial cells ingrowth. (Ratner and Marshall 2008a)

Table 2.1. Compositions and mechanical properties of porous and nonporous polyurethane.

Polymer Code	TMPO/MDI/HTI/TMP molar ratio	Soft segment/hard segments molar ratio	Nonporous Young's Modulus (MPa)	Porous Young's Modulus (MPa)
PU1044	1/0/4/4	0.125	4.99±0.36	0.82±0.05
PU2144	2/1/4/4	0.222	3.90±0.09	0.54±0.06
PU3244	3/2/4/4	0.300	2.81±0.03	0.39±0.08
PU4344	4/3/4/4	0.364	2.36±0.56	0.43±0.02
PU6544	6/5/4/4	0.462	1.93±0.09	0.23±0.02
PU8744	8/7/4/4	0.533	0.85±0.05	0.21±0.03

Table 2.1. (Continued)

Polymer Code	Nonprous ultimate tensile strength (MPa)	Porous ultimate tensile strength (MPa)	Nonporous maximum strain (mm/mm)	Porous maximum strain (mm/mm)
PU1044	0.81±0.19	0.38±0.04	0.172±0.047	0.435±0.020
PU2144	0.77±0.14	0.49±0.10	0.207±0.039	0.814±0.072
PU3244	0.90±0.13	0.48±0.11	0.360±0.073	1.107±0.052
PU4344	0.85±0.04	0.39±0.06	0.422±0.093	0.972±0.141
PU6544	0.66±0.16	0.38±0.10	0.486±0.103	1.715±0.267
PU8744	0.43±0.03	0.33±0.04	0.703±0.039	1.836±0.126

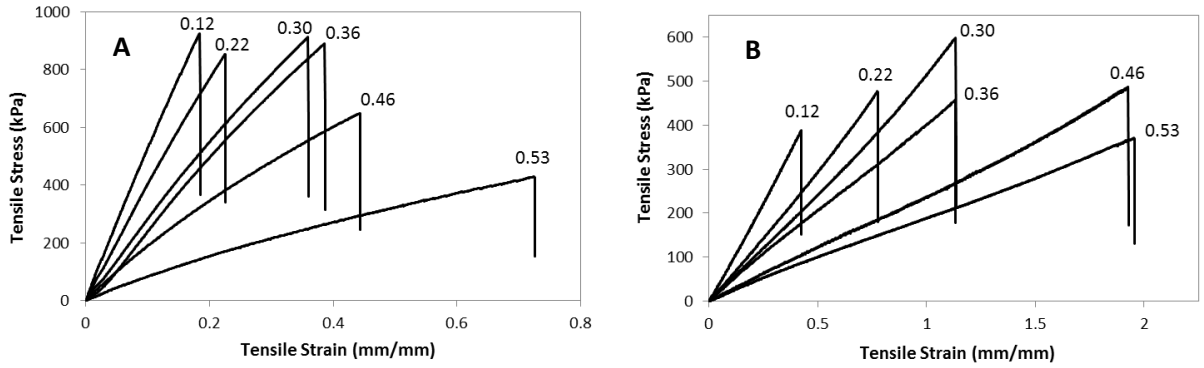

Figure 2.5. Representative stress-strain curves of A) nonporous polyurethane and B)porous polyurethane. (The number above each curve indicates soft segment to hard segment ratio.)

The stress-strain behavior is relatively linear along the whole stress-strain curve for both porous and nonporous polyurethanes. (**Fig 2.5**) This makes the elastic behavior of the material highly predictable. The porous polyurethanes also have much higher elongation and lower apparently Young's modulus compared to the nonporous polyurethanes. This indicates higher macroscopic elasticity. Note that the microscopic mechanical properties are unchanged between the porous and nonporous material when their chemical compositions are identical. The apparent increase of elasticity of the porous polyurethane is attributed to its porous structure.

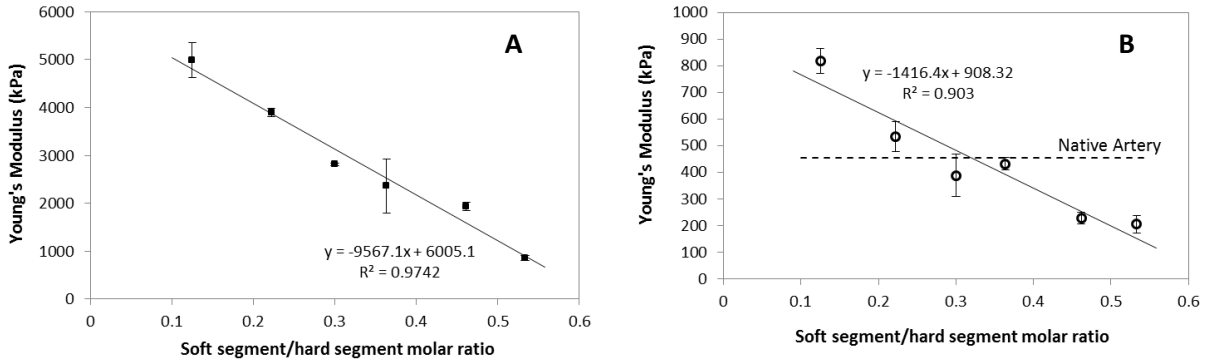

Figure 2.6. Linear relationship between Young's Modulus and soft segment to hard segment ration of A) nonporous polyurethane and B) porous polyurethane.

The Young's Modulus of the material can be fine-tuned by varying the molar ratio of the four components. (**Table 2.1, Fig 2.6**) In the four components used, PTMO is the soft segment, which gives the material elasticity. MDI is the hard segment, which imparts mechanical strength into the material. HTI and TMP are crosslinkers, which hold the material together, preventing it from dissolving during the organic solvent extraction process. HTI and TMP are also hard segments. So it is expected that with the increase of PTMO, the Young's Modulus decreases. This shows that the material is becoming more and more elastic. It is important to note that the Young's modulus decrease linearly with the increase soft segment to hard segment ratio. This

property is highly desirable for quantitative design of elasticity of materials to match that of the native blood vessel. Indeed, **Fig 2.6 B** shows porous PU materials with a range of Young's Modulus span from twice that of the simulated value of native artery (Catto et al. 2014) to half of it. Comparing to experimental results of different types of human blood vessels (Bergel, 1961), PU4344 (432±23kPa) matches thoracic aorta (430 kPa) ; PU1044 (818±48kPa) matches Abdominal aorta (890 kPa); femoral artery (690 kPa) and carotid artery (640 kPa) lie between PU1044 and PU2144. This allows us to design our material to match the elasticity with different types of blood vessels and potentially customize the material for each person. In addition, if the vascular graft becomes more rigid after implantation, we can design the vascular graft to be more elastic than native blood vessels to compensate for this change.

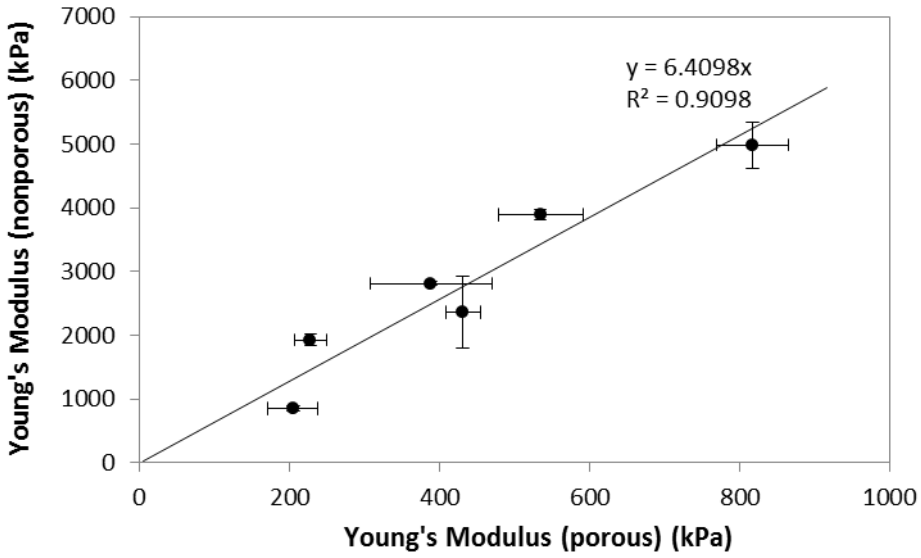

Figure 2.7 The relationship between Young's moduli of porous and nonporous PUs.

The Young's Moduli of the porous PUs linearly correlate to their nonporous counterparts. (**Fig 2.7**) The Young's moduli of the nonporous PU are about 6.4 times that of their porous counterparts. This change of the apparent Young's moduli from nonporous to porous PU is

attributed to the porous structure. The constant ratio between non-porous and porous Young's moduli across all compositions indicates the uniformed porous structure and density ratio (Ashby 2006). This number is useful for the rapid design of porous materials. Since nonporous materials are much easier to make, it is beneficial to test the Young's Moduli of nonporous materials and quickly predict those of the porous ones.

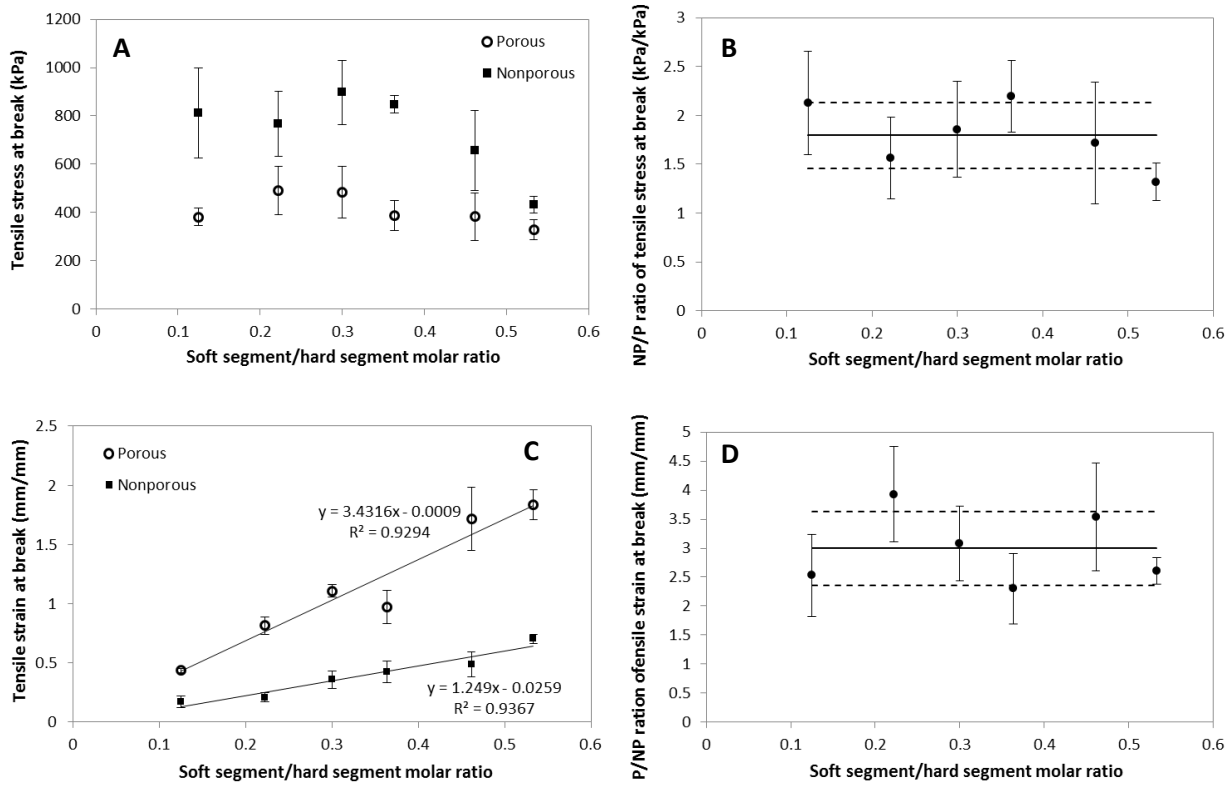

Figure 2.8 Tensile behaviors of porous vs nonporous PUs. A) Ultimate tensile strength (UTS) of nonporous and porous PUs; B) ultimate tensile strength ratios of nonporous/porous PUs; C) tensile strains at break of nonporous and porous PUs; D) porous/nonporous PU tensile strain at break.

The tensile behaviors at breaking point are shown in **Fig 2.8**. The ultimate tensile strength (UTS) remains largely unchanged across the materials, except for those with the highest soft segment to

hard segment ratios. (**Fig 2.8 A**). The UTS's of nonporous PUs are about 1.8 times of those of the porous PUs (**Fig 2.8 B**). The tensile strains at break increase linearly with soft to hard segment ratio. (**Fig 2.8 C**) Porous PUs's tensile strains are about 3 times of those of the nonporous PUs. (**Fig 2.8 D**)

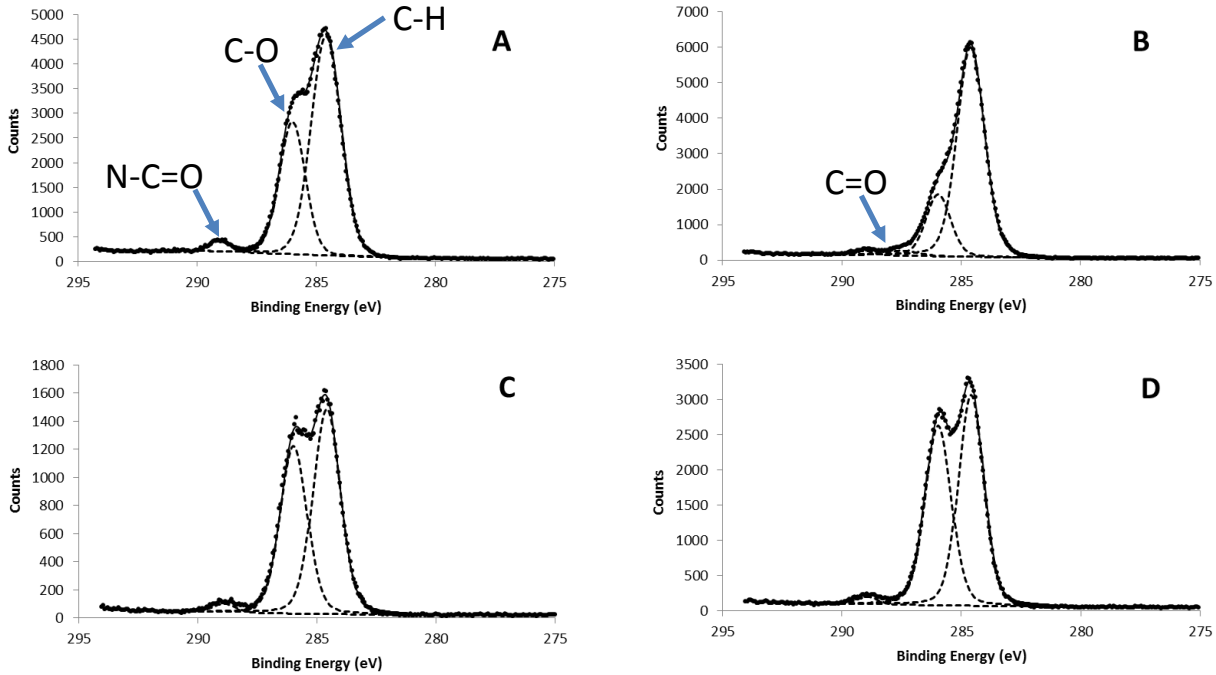

Figure 2.9. High resolution ESCA for C1s peaks of A) Pellethane 2363-80A control; B) Pellethane 2363-80A treated by hydrogen peroxide; C) PU4344 control; D) PU4344 treated by hydrogen peroxide. C-C peak: 284.6 eV, C-O peak: 286 eV, C=O peak:287.5 eV, N-C=O peak: 288.7 eV.

Table 2.2 Composition of different carbon species of control and H_2O_2 treated polyurethanes.

	Pellethane 2363-80A		PU4344	
Carbon spieces	Control	H_2O_2 treated	Control	H_2O_2 treated
C-C (hydrocarbon)	64.227	76.521	52.459	51.769
C-O (ether)	33.713	20.593	44.286	40.884
C=O (carbonyl)	0	0.886	0	4.11
N-C=O (urethane)	2.057	1.991	3.255	3.238

In vivo, macrophages constantly try to attach and break down foreign materials by releasing peroxide species. Hydrogen peroxide treatment has been shown to accurately mimic long term degradation behavior of polyurethane *in vivo*. ESCA probe the outer 10 nm surface of material thus is extremely sensitive to surface change. For these reasons, we chose peroxide treatment examined by ESCA to test the biostability *in vitro*. After hydrogen peroxide treatment, the C-O composition of Pellethane significantly decreases while that of the PU4344 only decreases modestly (**Fig 2.9.** and **Table 2.2**) Both materials show an emerging C=O peak indicating oxidation. The decrease of C-O composition in PU4344 is almost the same as the increase of C=O, indicating a conversion from C-O to C=O through oxidation. However, both carbon and oxygen stay on the surface. On the contrary, in the Pellethane sample, the loss of C-O is replaced by C-C composition. This may indicate that the oxidation was so severe that chains of the C-O rich soft segment was cleaved and escaped from the surface, leaving behind more C-C rich hard segment. Overall, this result indicates better biostability of PU4344 compared to Pellethane 2363-80A.

The biostability of polyurethane is a topic of extensive studies (Ratner, Gladhill, and Horbett 1988; Christenson, Anderson, and Hiltner 2007; Takahara et al. 1991; Wiggins et al. 2004; Zhao et al. 1991; Mathur et al. 1997; Tyler and Ratner 1995; Martin et al. 2000; Stokes, McVenes, and Anderson 1995; Simmons, Hyvarinen, and Poole-Warren 2006; Samterre et al. 2005). Specifically, the oxidative stability is most relevant to the ether-based polyurethane (Kang et al. 2010; Ratner, Gladhill, and Horbett 1988; Tyler and Ratner 1995). We developed a ether-based, highly crosslinked polyurethane that combines precision-porous structure, excellent mechanical property, and good biostability. The biostability can be further improved by switch the ether-

based soft segment (PTMO) to polydimethylsiloxane-based (Martin et al. 2000), polycarbonate-based (Takahara et al. 1991), or polyisobutylene-based (Kang et al. 2010) soft segment. However, these super-stable soft segments may increase the cost and compromise the mechanical property (Wiggins et al. 2004). On the other hand, biodegradable polyurethane may be desirable for tissue engineering (Guelcher 2008). We also developed a biodegradable crosslinked polyurethane for this purpose (Calleros et al. 2020). For the translation of *in situ* tissue engineered graft into human, the answer to the question "how biostable is enough?" is unknown. It depends on how fast human tissue can heal into the graft and whether the healed tissue can ultimately withstand the mechanical loading from the blood. Considering the fact that the population in need of vascular grafts tends to be more senior and have other health complications, we believe a relatively biostable material is a good starting point to accommodate the potentially slow healing rate. The biostability/biodegradability can be further tuned after we gain more knowledge of the healing of the *in situ* tissue engineered graft in human.

2.5 Conclusions

We are able to produce a precision engineered microporous material that matches the Young's Modulus with native blood vessels. The tensile behaviors are highly predictable and can be rationally designed to fit the applications. In addition, this material shows improved biostability compared to commercially available Pellethane 2363-80A. For future study, we will implant this material in mice and examine its biocompatibility.

Chapter 3 A triple-disk model demonstrates an abrupt transition from classic foreign body response to bio-integration depending only on the porous structure of the material

3.1 Abstract

The foreign body response (FBR) leads to the encapsulation of biomedical implants by the foreign body capsule (FBC). Thus FBR affects the performance of most implantable devices, and is the central problem to address in order to improve biocompatibility. In the context of vascular grafts, FBC leads to the constriction of vascular grafts by the peri-graft tissue and exacerbates the problem of intimal hyperplasia (IH). IH is the leading cause of stenosis and vascular grafts failure. Subcutaneous implantation in mice is one of the most common ways for assessing FBR. However, comparing FBR to materials is non-trivial, since FBR is highly sensitive to the location of implant. Migration of implants to different locations under the skin can change the FBR, introducing uncontrolled variables that can overwhelm the FBR to materials. Here, we reported the first triple disk model that incorporates three structures (40 μm porous, nonporous, 100 μm porous) in the same implant. We found that the nonporous part of the implant elicits classic FBR and is encapsulated by dense FBC. The FBC abruptly disappears and transitions into defused extracellular matrix (ECM) once the body encounters the porous part of the material. The 100 μm porous part is mainly invaded by fibrotic tissue, while the 40 μm porous part is integrated with highly cellularized and vascularized tissue. The capillary blood vessels grown into the 40 μm porous part are endothelialized, mature, and perfused. We investigated macrophages responses to the implant and identified a single layer of exclusively M1 (pro-inflammatory) macrophages on the surface of nonporous material, while both porous materials are infiltrated with mixed population of M1 and M2 (pro-healing) macrophages. The 40 μm porous part attracts large amounts of $F4/80^{high}$ macrophages, while the 100 μm porous

part attracts much less macrophage with lower F4/80 expression. These results indicate the amount of macrophage recruited, F4/80 expression, and M1/M2 polarity may all affect FBR and bio-integration.

3.2 Introduction

The Foreign Body Response (FBR) is the body's response to the implantation of foreign materials that ultimately leads to the isolation of the materials from the rest of the body by a dense, avascular collagen "scar" layer called the Foreign Body Capsule (FBC). FBR affects all implantable devices including, but not limited to: sutures (Rossitch, Bullard, and Oakes 1987), wound dressings (Suzuki et al. 1998), surgical meshes (Klinge et al. 1999), hip implants(Maguire Jr, Coscia, and Lynch 1987), intraocular lenses (Sievers and von Domarus 1984), breast implants (Hausner, Schoen, and Pierson 1978), suretac devices (Burkart, Imhoff, and Roscher 2000), bone fracture fixation implants (Bostman et al. 1990), lip augmentation implants (Jesús Fernández-Aceñero, Zamora, and Borbujo 2003), oral implants (Albrektsson et al. 2014), and vascular grafts (Mehta et al. 2011). The lack of integration and vascularization hinders the performance of medical devices and limits the possibility of tissue engineering and regenerative medicine. Thus strategies to reduce FBR is at the core of biomaterial research (Luttikhuizen, Harmsen, and Luyn 2006; Anderson, Rodriguez, and Chang 2008; Sussman et al. 2014; L. Zhang 2013). Here we precision-engineered one of the most widely used class of implantable biomaterials, polyurethanes, with micro-porous structure to combat FBR. The side-by-side comparison of the chemically identical polyurethane with 40 μm pores, no pores, 100 μm pores implanted in the subcutaneous space of mice shows that the material with both porous structure resists FBC formation, but only 40 μm porous structure promote vascularization and tissue integration.

In recent years, the innate immune cells, macrophages, were found to play a central role in orchestrating fibrosis and healing in FBR and diseases (K. Garg et al. 2009; Brown et al. 2009; Salzmann 1997; Bonito et al. 2018; Anghelina et al. 2004; Dick et al. 2019; Spiller et al. 2015; 2014; Roy-Chaudhury et al. 2001). Specifically, macrophages show phenotypic changes in response to the pore structure of materials in vascular grafts (Koyal Garg et al. 2013a; Hibino et al. 2011; Wang et al. 2014). Such phenotypic changes may dictate the success or failure of vascular grafts. Since macrophages are the central players in FBR, we hypothesize that 40 μm porous polyurethane resists FBC formation and promotes vascularization by modulating macrophage response. We tested our hypothesis by immunofluorescence staining with macrophage marker, M1 (pro-inflammatory), and M2 (pro-healing) markers.

3.3 Materials and Methods

The polyurethane material used in this study was synthesis and manufactured with method described in Chapter 2. 8-mm wide discs with a 2-mm wide nonporous stripe in the middle separating two sectors of 40 μm and 100 μm porous structures were implanted in implanted in 8-10 week old 028 BALB/cAnNCrl mice (Charles River Laboratories) subcutaneously for 3 weeks. The disks were harvested with the surrounding tissue, fixed in zinc fixative, embedded in paraffin, and sliced into 6 μm sections. Masson's Trichrome was used to assess FBC. Vascularization was evaluated by immune-enzyme staining with a panendothelial antigen, MECA 32 (BD Pharmingen^{TM}, 550563, 1:30). Immunofluorescence staining was performed to macrophage (stained with F4/80 from eBioscience), and M1 (stained with IL1-RI from R&D), M2 (stained with MMR from R&D).

3.4 Results and Discussions

3.4.1 Precision-engineered triple disk and distinct biological response to each part.

The triple disk consists of three structurally distinct (40 μm porous, nonporous, and 100 μm porous) but chemically identical and continuous parts. (**Fig 3.1 top**) After 3 weeks of subcutaneous implantation, each part elicits distinct biological responses. (**Fig 3.1** bottom) The nonporous part elicits classic FBR that's characterized by the deposition of a dense collagen layer (FBC, dark blue, **Fig 3.2**) around the part. The FBC abruptly disappears and transitions into diffused ECM once the tissue contacts the porous parts of the triple disks. The 100 μm porous part is infiltrated with fibrotic (**Fig 3.1** bottom, light blue), partially cellularized (red) tissues. This is in striking contrast with the 40 μm porous part that's integrated with fully cellularized (red) tissues. This is the first report to show three distinct biological responses on one piece of material.

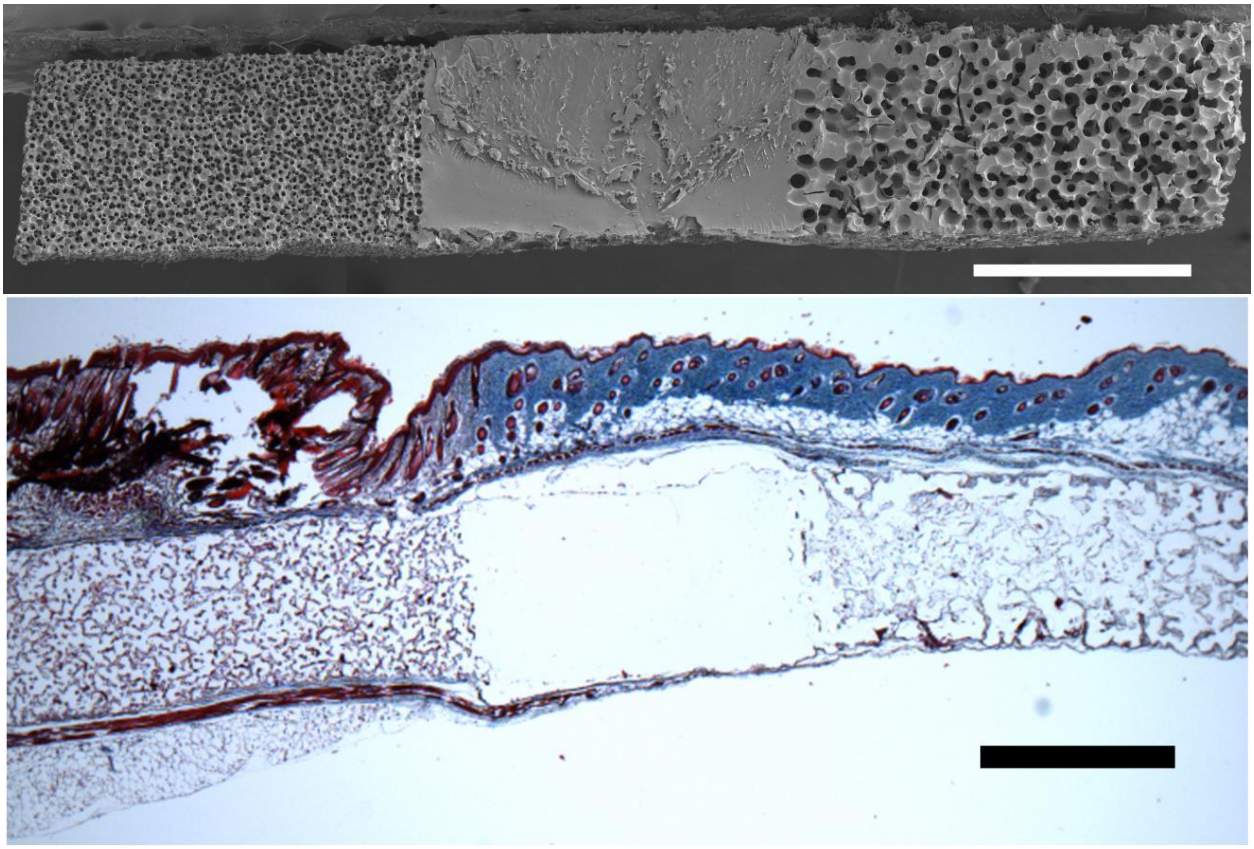

Figure 3.1 A triple disk model for side-by-side comparison of the FBR to chemically identical polyurethane material with different porous structures. The SEM image (top) shows the cross-section of the triple disk with 40 μm pores (left), 100 μm pores (right), and no pore (middle). The Masson's trichrome stain (bottom) shows distinctively different responses to the three structures. Scale bars: 1 mm.

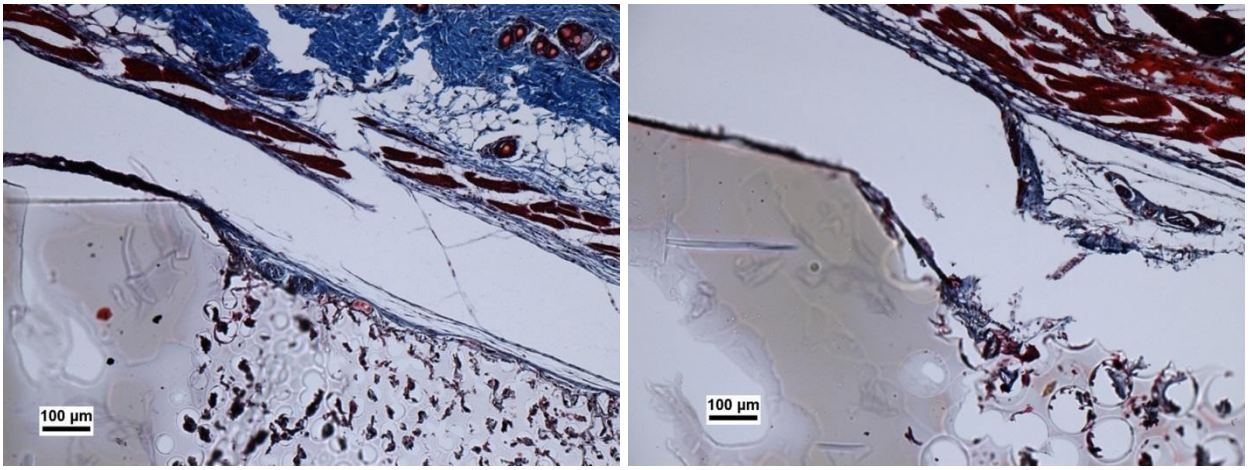

Figure 3.2 Masson's trichrome stain shows an abrupt transition from classic FBC (dark blue) on the non-porous side to diffuse extracellular matrix (light blue) on the porous side.

3.4.2 Pro-angiogenic effect of 40 µm porous PU

The pro-angiogenic effect of porous materials was investigated immunohistochemically with the double staining of MECA 32 (endothelial cell marker) and α-smooth muscle actin (α-SMA, smooth muscle cell marker). (**Fig 3.3 A-C, Fig 3.4 A**) The density of capillary blood vessel profiles in the 40 µm pores is more than 10 times higher than that in the 100 µm pores. (**Fig 3.3 D**) The highly pro-angiogenic nature of 40 µm porous material is consistent with previous observations. (Ratner and Marshall, 2008, Madden et al., 2010, Sussman et al., 2014)

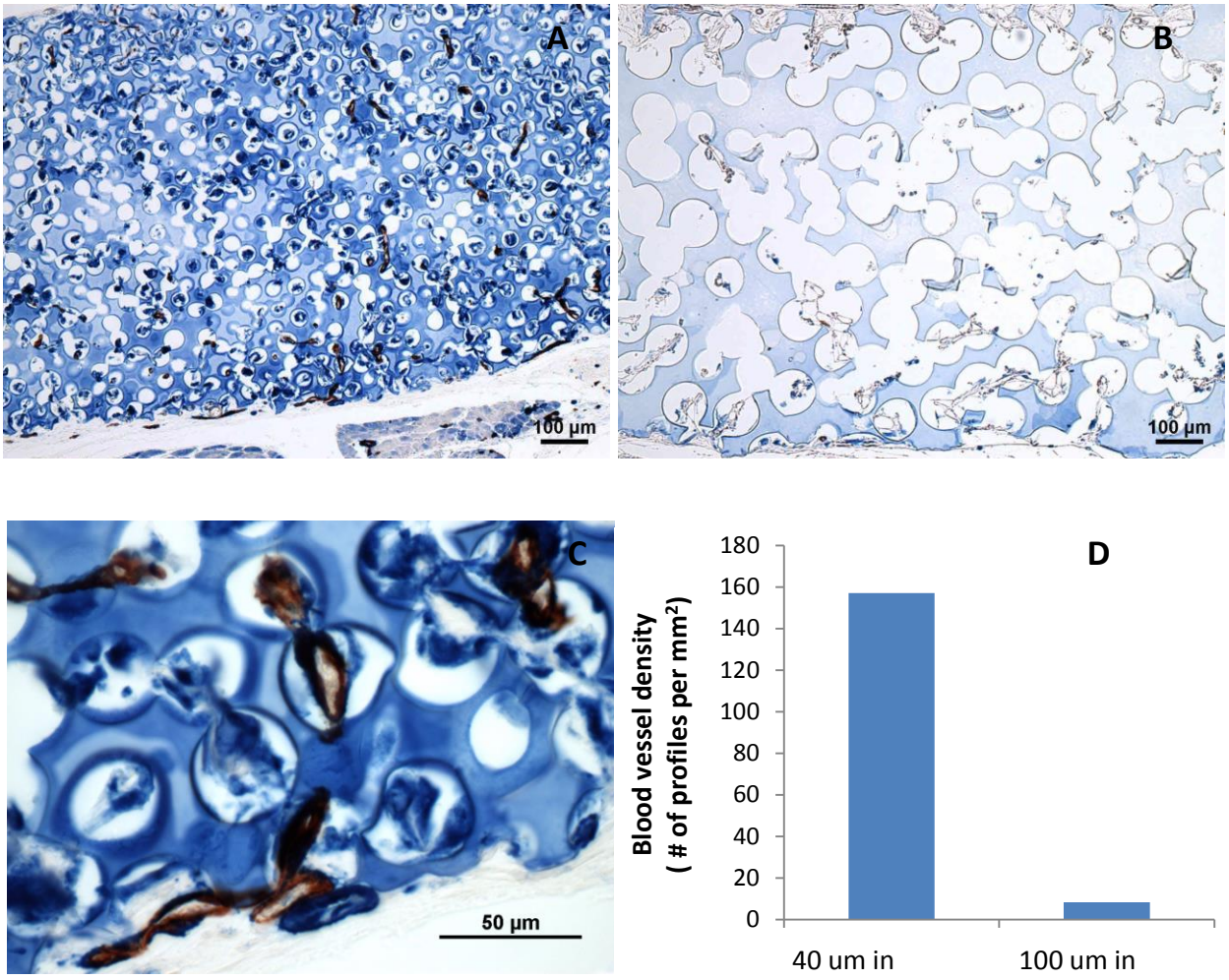

Figure 3.3 Immunohistochemical staining showing vascularization of porous PUs. A) 20X image of 40 µm porous PU; B) 20X image of 100 µm pores PU; C) 60X image of capillaries infiltrating 40 µm porous PU; D) preliminary blood vessel counts in 40 and 100 µm porous PUs. (Red: MECA 32(pan-endothelial cell marker), blue: α-smooth muscle actin (α-SMA, smooth muscle cell marker).)

To examine whether the blood vessels are perfused with blood, serial sections were stained with MECA32 and α-SMA to identify blood vessels (**Fig 3.4 A**) and Masson's trichrome to identify red blood cells (**Fig 3.4 B**). The same blood vessel can be found at the centers of both **Fig 3.4 A** and **Fig 3.4 B**. Large amounts of cells with about 5 μm diameter and without nuclei can be found inside the blood vessels. These are red blood cells in the blood flowing through the mature blood vessels. This provides strong evidence that the blood vessels growing in 40 μm porous PU are mature, perfused and fully functional. Note that, in addition to red blood cells, endothelial cells, and smooth muscle cells, collagen fibers (light blue) and putatively fibroblasts, macrophages (**Fig 3.5**) can also be found in the pores. That completes all the major cell types in a blood vessel.

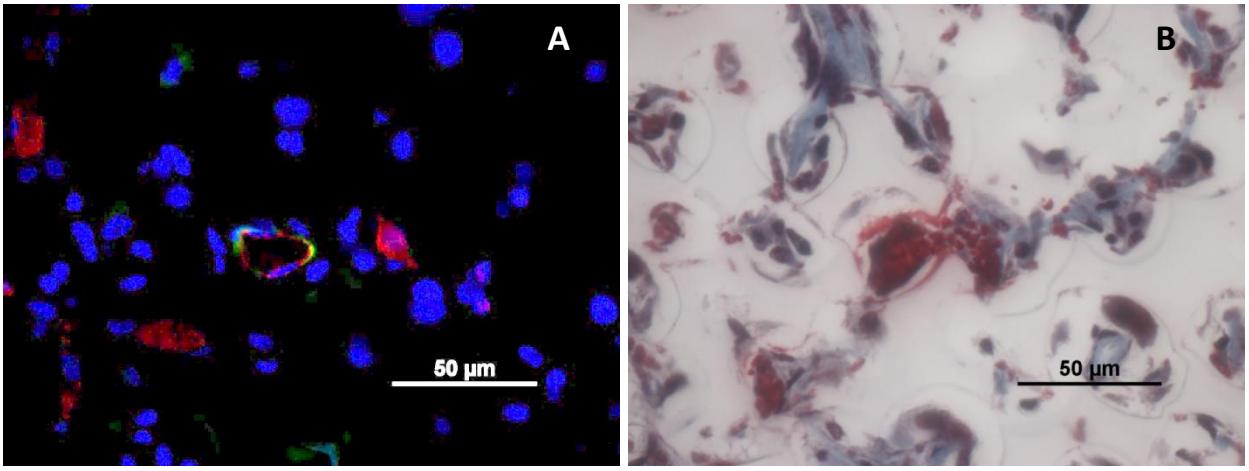

Figure 3.4 Serial sections of blood vessel (center of each image) inside of 40 porous PU stained with A) MECA 32 (endothelial cell marker, red) and α-SMA (smooth muscle cell marker, green), and B) Masson's trichrome.

3.4.3 Immunomodulatory effect of PU with different porous structures

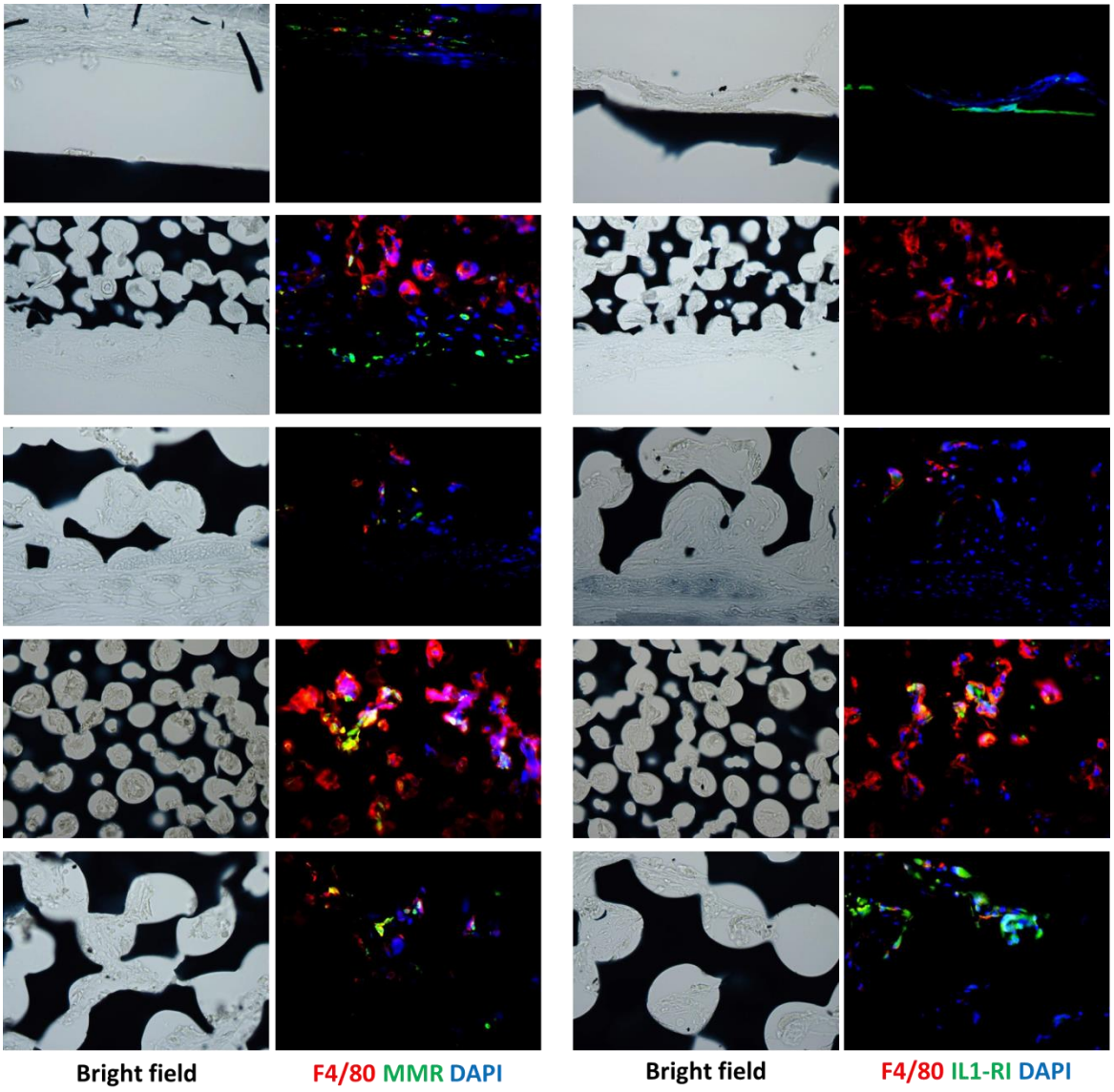

Figure 3.5 Immunofluorescence staining for macrophage polarity (40X micrographs). The sections were double stained with F4/80 (macrophage marker, red) and macrophage mannose receptor (MMR, M2 marker, green), or F4/80 and IL1-RI (M1 marker, green). Nuclei are stained with DAPI (blue). The first and the third columns show the bright field images of the implants. The second and the fourth columns show the corresponding fluorescence images of exactly the same field on their left.

The three parts of the triple disk elicit three distinct macrophage responses to the material. (**Fig 3.5**). A single layer of $F4/80^{low}IL1\text{-}RI^{+}MMR^{-}$ exclusively M1 (pro-inflammatory) macrophages resides on the surface of nonporous PU (**Fig 3.5 top row**), indicating that classic foreign body response is driven by inflammation. The 40 μm porous PU is infiltrated by a large amount of $F4/80^{high}$ macrophages. (**Fig 3.5 second and fourth row**) In comparison, the 100 μm porous PU is infiltrated by much less macrophages, and they may have much lower expression of F4/80. (**Fig 3.5 third and fifth row**) Comparing macrophages inside of 40 μm pores and right outside of it (**Fig 3.5 second row second image**), macrophages inside of pores have much higher expression of F4/80 compared to outside. This indicates that the up-regulation of F4/80 is driven by the 40 μm porous structure. Such up- and down-regulations of F4/80 were also observed in other study (Jenkins et al. 2011), where M1 macrophages had low F4/80 expression while M2 and M0 macrophages had high F4/80 expression. Another relevant observation was made in cancer research, where more mature macrophage expressed higher F4/80 (Tymoszuk et al. 2014). The center of 40 μm porous PU (**Fig 3.5 fourth row second image**) has a higher expression of M2 marker than the edge. The same can be said about M1 marker, although the M1 marker is almost absent on the edge of 40 μm porous PU (**Fig 3.5 second row fourth image**). The M1 marker is much higher inside of 100 μm porous PU (**Fig 3.5 second row fourth image**), despite the overall macrophages are much less compared to 40 μm porous PU. However, M2 marker is also present in 100 μm porous PU. This may explain the reduced FBC around 100 μm porous PU. 40 μm porous PU has increased macrophages recruitment, F4/80 expression, and reduced M1 marker expression. These factors taken together may explain the reduced FBC and increased angiogenesis.

3.5 Conclusions

40 μm porous PU simultaneously reduces FBC and induces angiogenesis. Increased macrophage recruitment, F4/80 expression, and reduced M1 marker expression are indicated as the putative cause of such effects. 40 μm porous PU may be advantageous for the application of vascular grafts.

Chapter 4. Manufacturing of precision-engineered porous elastomer based vascular grafts

4.1 Introduction

40 μm porous PU developed and tested in previous chapter has multiple advantages that include matching mechanical property of native blood vessels, biostability, reduction of FBC, and increased angiogenesis. However, manufacturing vascular grafts with 40 μm porous PU is still challenging. Specifically, two paradoxes need to be solved: 1) the graft needs to be elastic enough to match mechanical properties with native blood vessels, but stiff enough to withstand suturing; 2) the graft need to be porous to allow tissue integration, but nonporous to prevent bleeding. Reinforcement is a commonly used strategy to provide additional strength for elastic grafts (Tai et al. 2000b; Xu et al. 2010; Boretos, Detmer, and Donachy 1971; Xu et al. 2008). Gelatin is a widely used biodegradable sealant for vascular grafts to prevent bleeding and improve blood compatibility(Jonas et al. 1988; Lachapelle, Graham, and Symes 1994; Manju et al. 2011; Drury et al. 1987; Kadoba, Schoen, and Jonas 1992; Bascom 1961; Wissink et al. 2000; Koshiko et al. 2002; Javerliat et al. 2007; Goëau-Brissonnière et al. 1991; Fleckenstein and Werner 1990; Taylor Jr et al. 2003; Goëau-Brissonnière et al. 1994). In light of these research, we solved our two paradoxes by 1) embedding a Dacron mesh as reinforcement in the porous to PU, which maintains the elasticity on the circumferential direction but provide the stiffness on the longitudinal direction to withstand suture; 2) sealing the pores with a fast degradable crosslinked gelatin hydrogel that prevents bleeding but degrades as the tissue heals in, without inducing FBR. In this chapter we present the method of manufacturing this vascular graft.

4.2 Materials and Methods

4.2.1 Manufacturing of precision-engineered porous elastomer based vascular grafts

The vascular graft have three major components (**Fig 4.1**): the majority of the graft is consist of the precision-engineered porous PU described in previous chapters; a polyester mesh (SurgicalMesh^{TM}, PETKM 2008) was embedded in the wall of the graft as reinforcement; the pores were sealed by 5% gelatin (from porcine skin, Type A, Sigma, Cat# 1890-100G) crosslinked with EDC/NHS (5:1 molar ration). The EDC/-COOH (in gelatin) ratio is 2:1 (molar ratio.)

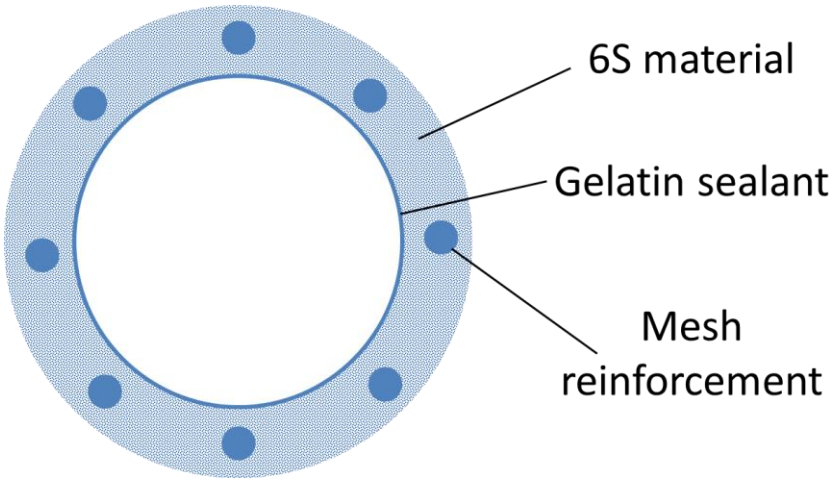

Figure 4.1 The design of the IMPRESSIVE graft.

A modified version of the 6S process was used to create the vascular graft. (Fig 4.2) First the polyester mesh was wrapped around a 6-mm-diameter glass rod twice. Note that the circumferential direction of the wrap was the more elastic direction of the mesh. The wrapped glass rod was then put into an 8-mm-id glass tube. All three parts were sterilized with 70% ethanol, and then dried in an 80 °C oven for two days. The glass rod and glass tube were held concentric by two custom-made Teflon caps. 40 μm PMMA beads were poured into the space

between the glass rod and the class tube and sonicated for 1 hour to allow close packing. Interconnects between PMMA beads were formed by sintering in 177 °C for 28 hours. The glass rod and mesh embedded bead cake were taken out of the class tube and submerged in PU 4344 pre-polymer mixture. The submerged beak cake was subjected to -25 in. Hg for 5 mins. The vacuum was purged with N_2. One more repetition of this vacuum-purge process secured the interstices of the bead cake were completely filled with the pre-polymer mixture. The bead cake was taken out of the pre-polymer mixture and immediately wrapped with low density PTFE tape. Polymerization was completed in 55 °C for 48 hours. The PTFE tape was removed and the nonporous film formed on the surface of the bead cake was scraped off. The glass rod was taken out after soaking in 70% ethanol overnight. The PMMA beads were solubilized and removed by soaking in acetone for 3 days with 1 change per day, then washed DCM for 7 days with 1 change per day, then acetone for 3 days with 1 change per day. The vascular graft was gradually changed into ethanol, then thoroughly washed with DI water and lyophilized overnight. The vascular graft was impregnated with a 5% gelatin solution with the same vacuum-purge process described above for 3 times. The gelatin impregnated graft was refrigerated overnight. The impregnation and refrigeration were repeated one more time. The gelatin was crosslinked with EDC/NHS chemistry (Kuijpers et al. 2000) with gelatin solution/crosslinker solution=1:50 (v/v) for 16 hours in 4 °C. The crosslinking reaction was quenched with ph8.5 PBS for 2 hours then washed with DI water. The gelatin sealed vascular graft was sterilized with 70% ethanol then thoroughly washed with DI water. After lyophilization, the graft was double wrapped and sterilized with ethylene oxide treatment.

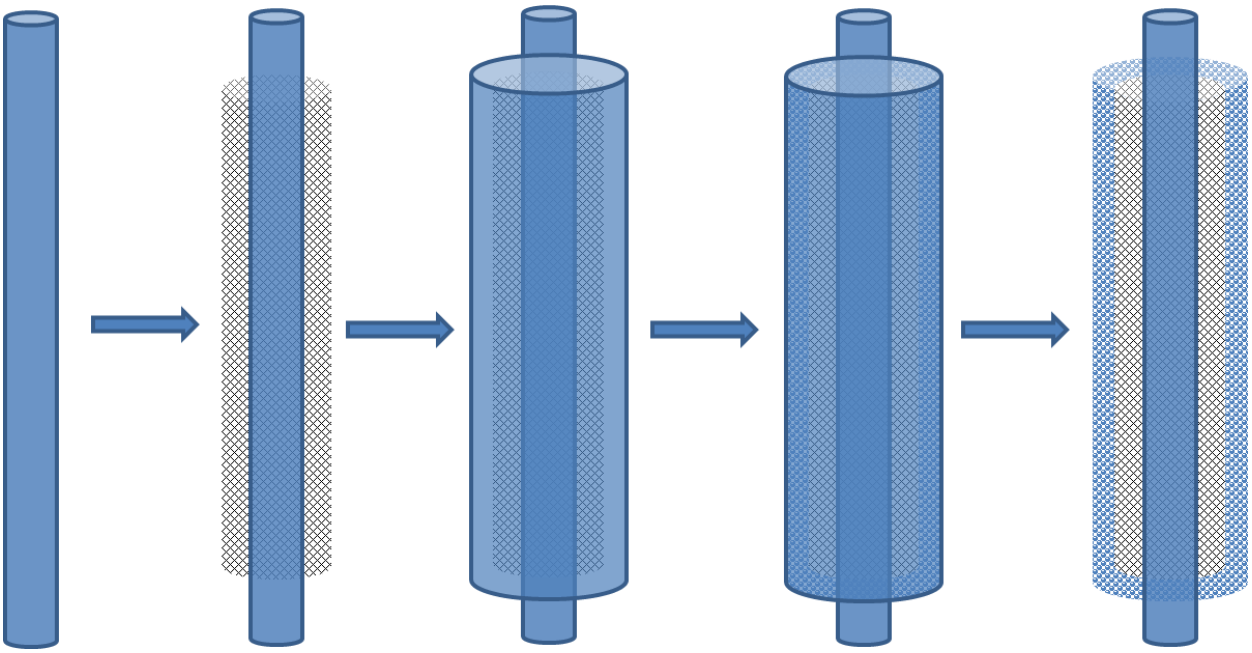

Figure 4.2 The process of creating tubular sphere template for the 6S process.

4.2.2 Structural and mechanical characterization of the vascular graft.

Vascular grafts were cross sectioned. The cross-sections were sputter coated with gold and imaged with SEM.

The suture strength was tested by pulling (2 mm/s) a 6-0 prolene suture (2 mm bite) through a segment of vascular grafts with an Instron machine. The suture strength is the maximum force recorded during the pulling process. Whenever suture strength was measured on a reinforced graft, care was taken to hook polyester mesh with the suture.

Vascular grafts were cut open longitudinally. Dumbbell-shape specimens were cut both along the longitudinal direction and the circumferential direction. Young's modulus was measured in both directions with an Instron machine.

4.2.3 *In vitro* degradation test for gelatin.

Gelatin hydrogels were crosslinked with EDC/NHS chemistry with EDC/-COOH molar ratio= 0.75 (0.75X), 1(1X), 1.2(1.2), 1.4(1.4X), 1.6(1.6X), 1.8(1.8X), 2(2X), and 4(4X). 6mm-diameter disks were punched out of each hydrogel and soaked in 1 ml DMEM buffer supplemented with 10% Calf Serum, 1% L-glutamine, and 1% penicillin-streptomycin (100X) in 6-well tissue culture plate. The plates were incubated at 37 °C with 5% CO_2. The tissue culture media were drawn out periodically, photos of the gel were taken, then new tissue culture media were filled. Each gel was assigned a degradation score at each time point. The meanings of the scores are: 0-no sign of swelling or degradation; 1-slightly swollen; 2-severely swollen; 3-slightly degraded; 4-severely degraded; 5-completely degraded. The tests were done in triplicates.

4.2.4 *In vivo* degradation test for gelatin.

2X gelatin and 4X gelatin were implanted on each side of the upper back of the same 8-10 week old 028 BALB/cAnNCrl mice (Charles Rever Laboratories) subcutaneously for 3 weeks. The disks were harvested with the surrounding tissue, fixed in zinc fixative, embedded in paraffin, and sliced into 6 μm sections. Masson's Trichrome was used to assess FBC.

4.2.5 Histological visualization of gelatin sealed vascular graft.

To visualize the gelatin in the pores of vascular graft, the graft was embedded in paraffin, sliced into 6 μm sections. The sections were stained with Sudan Black B, followed by Masson's trichrome. The sections were cover-slipped with Prolong^{TM} Diamond Antifade Mountant and imaged immediately.

4.2.5 Cytotoxicity evaluation of vascular grafts.

To evaluate cytotoxicity, segments of vascular grafts were incubated in the culture medium (Dulbecco's Modified Eagle Medium supplemented with 10% FBS, 1% L-glutamine, and 1% penicillin streptomycin) at 37 °C for 24 h to extract soluble substances. NIH-3T3 fibroblasts were seeded in multi-well culture plates at 5×10^4 cells per well. After 24 h, the culture medium was replaced with the same amount of the extracting medium from incubated hydrogels and cultured for another 48 h. Then, the attachment and morphology of the cells were assessed using a phase-contrast microscope.

4.3 Results and Discussions

4.3.1 Macroscopic and microscopic structures of vascular grafts

The vascular graft has an inner diameter of 6 mm, outer diameter of 8 mm. (**Fig 4.3 A**) Although the graft shown is about 4 cm long, it can be manufactured in any length by changing the length of the lass rod and glass tube. The polyester mesh embedded doesn't affect the porous structure of the vascular graft. (**Fig 4.3 B**)

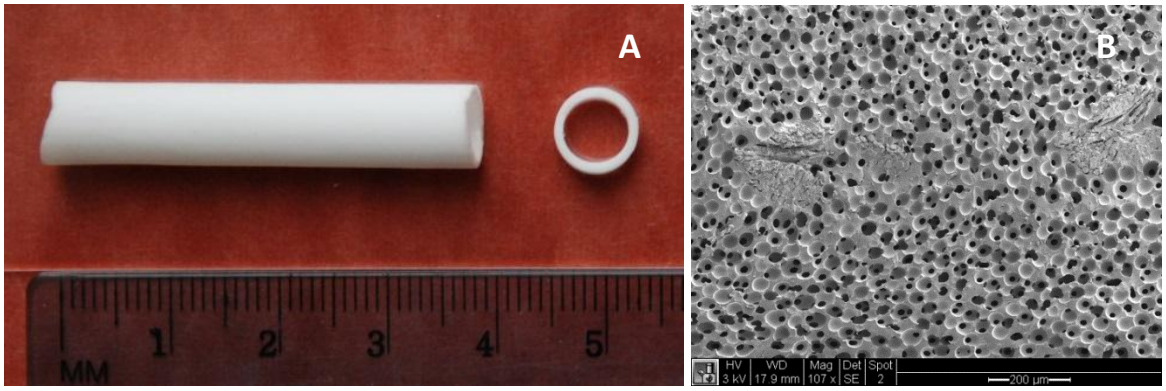

Figure 4.3 Macroscopic and microscopic structures of vascular grafts. A) photograph of the vascular graft; B) SEM micrograph of the cross-section of the vascular graft (nonporous islands are the polyester mesh).

4.3.2 Mechanical properties of vascular grafts

Fig 4.4. shows that, with the reinforcement, the suture strength of the material is 4.77±0.36 N, which is much higher than the suture strength of native blood vessel (~ 2N) (L'Heureux et al. 2006). This indicates that the vascular graft will be strong enough to be sutured to native blood vessels. The Young's Moduli of vascular grafts on the circumferential direction are about 1 MPa, while those on the longitudinal direction are about 9 MPa. Such anisotropic mechanical property allows the vascular graft to have the strength to withstand suturing, while maintaining the elasticity to beat with the blood vessel on the circumferential direction.

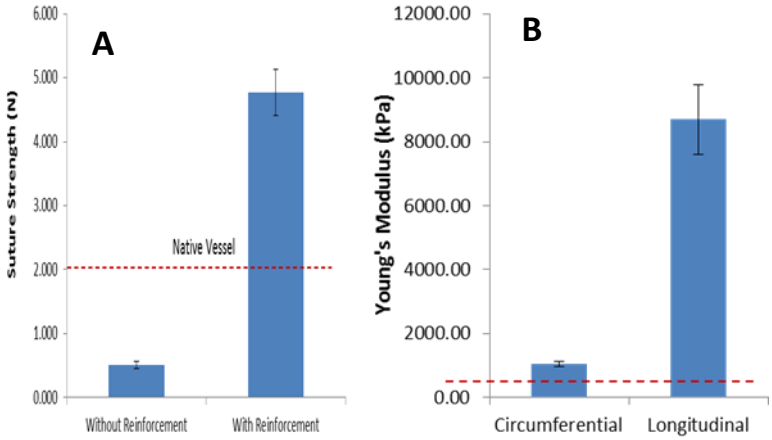

Figure 4.4 Mechanical properties of vascular grafts. A) suture strength without and with re-enforcement; B) the Young's Moduli of vascular grafts on circumferential and longitudinal directions.

4.3.3 *In vitro* and *in vivo* degradation of gelatin hydrogels.

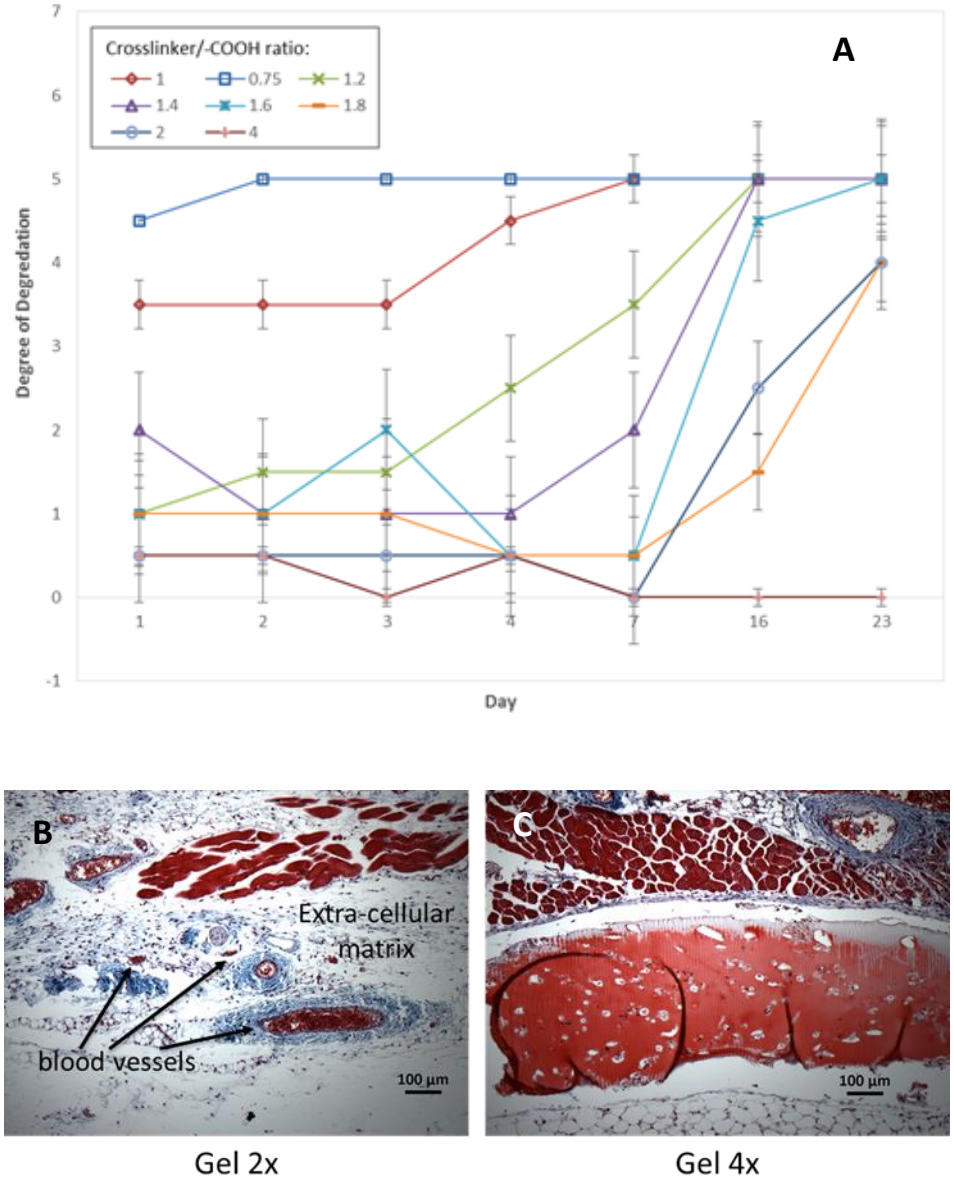

Figure 4.5 *In vitro* and *in vivo* degradation of gelatin hydrogels. **A)** *In vitro* degradation behavior of gelatin hydrogel with different EDC/-COOH molar ratios (0-no sign of swelling or degradation; 1-slightly swollen; 2-severely swollen; 3-slightly degraded; 4-severely degraded; 5-completely degraded) (Data courtesy of Tanmay R. Sapre); **B)** Masson's trichrome staining of

the 2X gelatin hydrogel and surrounding tissue after 3 weeks of subcutaneous implantation; **C)** Masson's trichrome staining of the 4X gelatin hydrogel and surrounding tissue after 3 weeks of subcutaneous implantation.

By simply changing the EDC/-COOH molar ratio, the degradation time in vitro can be fine-tuned to be 2 days (0.75 X), 1 week (1X), 2 weeks (1.2X and 1.4X), 3 weeks (1.6X), and beyond (>1.8 X). (**Fig 4.5 A**) Such fine control of the degradation rate on the fast degrading side is highly desirable because we can match the degradation rate and the rate of healing. This way, the gelatin can block bleeding without blocking healing.

We are targeting the hydrogel to completely degrade in 2-3 weeks, corresponding to the time for the body to integrate with the porous material. Considering cells and matrix metalloproteinases (MMPs) that may accelerate degradation *in vivo*, we chose to implant gelatin 2X (almost finish degrading in 3 weeks *in vitro*), and gelatin 4X (no sign of degradation in 3 weeks *in vitro*, as a control here). The gelatin 2X was completely degraded *in vivo* within 3 weeks. (**Fig 4.5 B**) The space previously occupied by gelatin 2X was filled by ECM. No FBC was formed. Mature blood vessels can be seen growing through the ECM. The gelatin 4X had barely any sign of degradation in 3 weeks. (**Fig 4.5 C**) In addition the hydrogel was surrounded by classic FBC. These observations indicate that the degradation *in vivo* is indeed faster than *in vitro* (gelatin 2X). However, the *in vitro* result is still close enough to predict *in vivo* degradation behavior (gelatin 4X). The gelatin 2X is likely to be the ideal candidate for vascular sealant.

4.3.4 Gelatin 2X as vascular graft sealant

The 5% gelatin solution was able to infiltrate the whole cross-section of the vascular graft and sealed all the porous. (**Fig 4.6**) After being sealed by gelatin 2X, the vascular graft was able to hold water without leaking.

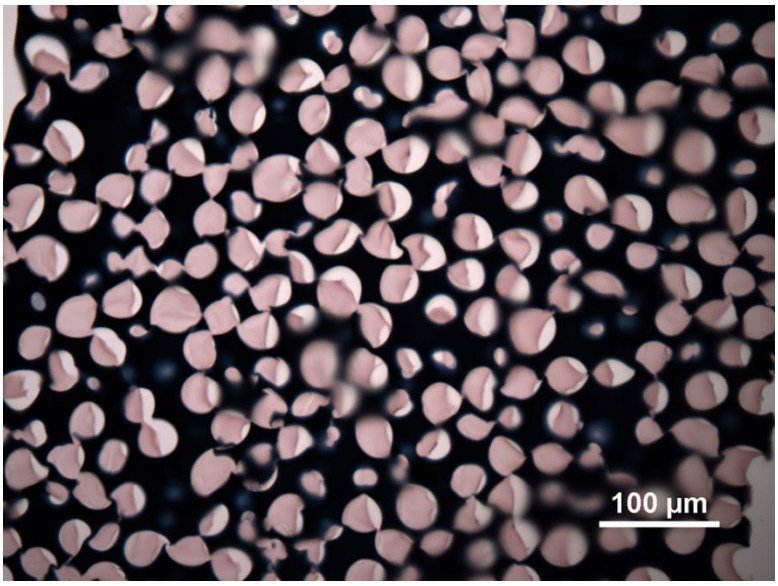

Figure 4.6 A bright-field microscopic image of Sudan Black B and Masson's trichrome stained gelatin sealed vascular graft section.

4.3.4 Cytotoxicity result of the ethylene oxide (EtO) treated vascular graft.

There is no sign of cytotoxicity for both the vascular graft with or without EtO sterilization.

(**Table 4.1**)

Table 4.1 Cytotoxicity scores of Latex, tissue culture polystyrene, ethylene oxide treaded PU grafts, PU grafts without ethylene oxide treatment.

Sample / Time	Latex-1	Latex-2	Latex-3	Tissue culture PS-1	Tissue culture PS-2	Tissue culture PS-3	EO treated PU graft-1	EO treated PU graft-2	EO treated PU graft-3	PU graft-1	PU graft-2	PU graft-3
12 hrs	4	4	4	0	0	0	0	0	0	0	0	0
24 hrs	4	4	4	0	0	0	0	0	0	0	0	0
48 hrs	4	4	4	0	0	0	0	0	0	0	0	0

4.3 Conclusion

We are able to solve both paradoxes in manufacturing the vascular graft: the graft is elastic on the circumferential direction and stiff on the longitudinal direction, thus is able to withstand suturing; the graft is porous to allow healing and sealed with fast-degradable gelatin to prevent excessive bleeding. In addition, the graft passed the cytotoxicity test and can be sterilized by ethylene oxide treatment. In conclusion, the vascular graft is ready for in vivo implantation in relevant animal models (sheep and pigs).

Chapter 5. *In-situ* tissue engineering of vascular grafts in sheep and pigs

5.1 Introduction

Evaluating vascular graft performance in relevant animal models is an indispensable step towards translation. Large animals are favored over small animals because they tend to be hematologically and hemodynamically more similar to human(Byrom et al. 2010). The pig model is popular for evaluating cardiovascular devices because of the overall similarity between pigs and humans (Sauvage and Harkins 1953; 1953; Kelly et al. 2006; Gogolewski, Galletti, and Ussia 1987; Gao et al. 2010; Y. Wang et al. 2008). Sheep is one of the most widely used large animal models in analysis vascular graft performance (Böer et al. 2013; Yavuz et al. 2006; Hoerstrup et al. 2006; Syedain et al. 2014; Soldani et al. 2010; DiVincenti Jr, Westcott, and Lee 2014; Ahmed, Hamilton, and Seifalian 2014; Shofti et al. 2004; Fukunishi et al. 2016). Comparing the two models side-by-side, sheep heals endothelium much slower than pig (Ueberrueck et al. 2005), which makes sheep a more model more similar to human. In addition, sheep develops intimal hyperplasia rapidly (Kohler and Kirkman 1999). In this chapter, we describe preliminary pig and sheep studies.

5.2 Materials and Methods

5.2.1 Sheep surgery

Our surgical team will include Elina Quiroga, M.D.,a board-certified vascular surgeon. At the time of surgery, sedation and general anesthesia will be induced and monitored by DCM VS staff. All administration of anti-stress drugs, anesthetic agents, and post-operative antibiotics will be supervised by attending UW veterinarians. Prior to the first incision an IV bolus dose of 100-150IU/kg of heparin will be given; additional doses of 100IU/kg of heparin will be given at 2

hour intervals until the surgery is completed. A dose of the antibiotic Oxytetracycline will be given. Lidocaine/bupivacaine will be administered SC or IM around the incision site prior to first incision. Additional lidocaine/bupivacaine may be administered during the surgery to provide additional numbing at the site.

5.2.1.1 Interposition implant

In this experiment, each animal will undergo a bilateral interposition bypass of either a PTFE or INT graft placed between the common carotid artery using standard surgical techniques. Right and left side placement of grafts will be randomized. An approximately 7cm in length incision will be made on one side of the neck in order to expose the common carotid artery; the artery will be dissected free from surrounding tissue and encircled with vessel loops. Then a contralateral neck incision will be performed and the contralateral common carotid artery will be exposed in a similar fashion. After clamping the artery, an interposition bypass will be performed using either PTFE or INT graft, 4-6mm ID, 7-10mm OD, and approximately 6-8cm in length. The order and placement of the implanted grafts (PTFE vs INT in the right vs left) will alternate between animals. After implantation of the first graft is completed, the vessel clamps will be released and the patency of the bypass will be confirmed using hand-held Doppler. After the patency of the first graft implant and animal homeostasis is confirmed, the contralateral graft will be performed in a similar fashion. After confirming patency on both sides the wounds will be irrigated with sterile saline and photographed, hemostasis will be confirmed, and a layered closure will be performed. Subcutaneous layers will be closed with re-absorbable suture, continuous pattern. The external skin closure will be done with non-absorbable suture in an interrupted pattern or by use of wound clips. Each complete surgery is expected to take 3-4 hours.

Table 5.1 Plan for short term sheep study.

Experiment	1 month
PTFE vs INTEGRATIVE a-a graft	6 sheep
INTEGRATIVE a-v graft	6 sheep
PTFE a-v graft	6 sheep

5.2.1.2 Arteriovenous implant

Each animal will receive either a PTFE or INT graph be placed connecting the (proximal) right carotid artery (proximal end) to the contralateral external jugular vein (distal end). The grafts will be 4-6mm ID, 7-10mm OD, and approximately 16-18cm in length with a final implant run of 14-16cm. An approximately 5cm incision in length incision will be made on the right side of the neck in order to expose the common carotid artery; the artery will be dissected free from surrounding tissue and encircled with vessel loops. Next, a left side neck incision will be performed and the contralateral jugular vein will be exposed in a similar fashion. The PTFE or INT graft will be tunneled between both incisions in a gentle S-shape. Kinking of the graft can be avoided by placing the grafts low in the neck and making a gentle S-shaped curve from the artery to the vein. An approximately 5-6mm long arteriotomy (longitudinal incision on artery, approximately 5-6mm opening)will be performed and an end-to-side anastomosis between the carotid and INT graft will be performed using absorbable interrupted sutures. Then, an approximately 10-12mm venotomy (longitudinal incision on vein, 10-12mm opening, graft cut on bias to match venotomy dimensions) will be performed in the jugular vein and an end-to-side anastomosis will be constructed using polypropylene sutures. After confirming the patency of the

graft, the artery, the graft, and the vein will be photographed and then the wounds will be irrigated with sterile saline and photographed, hemostasis will be confirmed, and a layered closure will be performed. Subcutaneous layers will be closed with re-absorbable suture, continuous pattern. The external skin closure will be done with non-absorbable suture in an interrupted pattern or by use of wound clips. Each complete surgery is expected to take 2-3 hours.

5.2.2 Pig surgery (plan)

Juvenile Yorkshire crossbred swine, castrated male, 40-50 kg, will be purchased from Steve Thompson farms and kept in standard animal care facilities.

Pigs will be anesthetized and intubated with a combination of Ketamine, xylazine, and atropine Isoflurane was used for maintenance anesthesia. 7-cm-long, 6-mm-ID, straight INTEGRATIVE grafts or PTFE grafts will be placed between the femoral artery and femoral vein using standard surgical techniques. End-to-side anastomosis will be made with an interrupted 6/0 polypropylene suture (surgipro). Special care will be taken to ensure that there are no kinks in the graft and that it will be well placed in a created pocket. The fascia and skin will be closed in layers using 2-0 Maxon for muscle and fascia, and 3-0 vicryl on skin with intradermal pattern. Buprenorphine and carprofen (NSAID) will be used for post-operative analgesia within 72 hrs. All pigs will be administered Aspirin EC 325 ng from day -1 to the time of sacrifice, together with 200IU/kg of heparin before clamping for the first implantation, and repeat the same dose every 2h until all clamps are released. Graft patency will be confirmed immediately after surgery and then every three days by auscultation.

9 healthy pigs will be utilized in this preliminary study and a total of 18 grafts will be placed. Each pig will receive an INTEGRATIVE graft and a PTFE graft (as control). Each pig will

randomly receive an INTEGRATIVE graft that uniquely combines one of the reinforcement strategies (PETKM2006, PETKM2008, or PETKM 3002) and one of the sealing strategies (no sealant, sealed with gelatin (2X), or sealed with gelatin (2X) and heparin). In addition, 2 uremic pigs will be used to study the effect of uremia on gelatin degradation. Each uremic pigs will receive two INTEGRATIVE graft with gelatin sealant of different crosslinking densities (2X, 2.5X, 3X, and 4X). Post-op follow up will be done at day 7, day 14, day 21, and day 28 by ultrasound evaluation. Study end MRI will be done on day 21. All pigs will be sacrificed on day 28. All pigs will be injected with bromodeoxyuridine (BrDU; 50mg/kg) IP 24 hours prior to the sacrifice at day 28. If failure occurs before the sacrifice, the vascular grafts should still be harvested if possible, and the modes of failure (bursting, kinking, clotting, intimal hyperplasia) should be assessed to guide improvement of the graft design. At the time of sacrifice the animals will be anesthetized as above, and the graft will be carefully dissected out. Following a lethal injection of sodium pentothal, the entire graft together with attached artery and vein will be removed. The graft will be cut 1 cm above the arterial and venous anastomoses, following which it will be fixed in 4% paraformaldehyde and trimmed. Paraffin embedded sections will be used for histological, morphometric and immunohistochemical analyses.

5.2.3 Histology (plan)

The histological methods relevant to this study are listed in Table 5.2.

Table 5.2 Histological stains relevant to vascular graft study.

Histological staining	Function	Reference
H & E	Basic histology	
Masson's Trichrome	Foreign body response	(Madden et al., 2010)
Picrosirius Red	Organized collagen fibers	(Ahmed et al., 2014)
Russell-Movat pentachrome	All connective tissue	(Dekker et al., 2018)
Von Kossa staining	Calcification	(Soldani et al., 2010)

5.2.4 Immunohistochemistry (plan)

The sheep specific antibodies relevant to this study are listed in Table 5.3. (Dekker et al. 2018)

Table 5.3 Sheep specific antibodies relevant to vascular graft study.

Targets	Sheep specific antibodies
ECM	Collagen type I Collagen type III
elastin	(Tropo)elastin
Smooth Muscle Cells	a-SMA Vimentin SM22 Calponin Cadherin-11 SMemB
Endothelial Cells	CD31 (PECAM-1) CD34 VE-Cadherin von Willebrand factor
Proliferation	Ki-67
Apoptosis	Cas3
T cells	CD45 CD3
Macrophage	CD64 EMR-1
M1 polarization	iNOS CCR7 (CD197) TNF-a
M2 polarization	CD163 CD200R Arginase-1 IL-10
Foreign Body Giant Cells	CD44

5.3 Results and Discussions

5.3.1 Pilot study on arteriovenous graft in pig

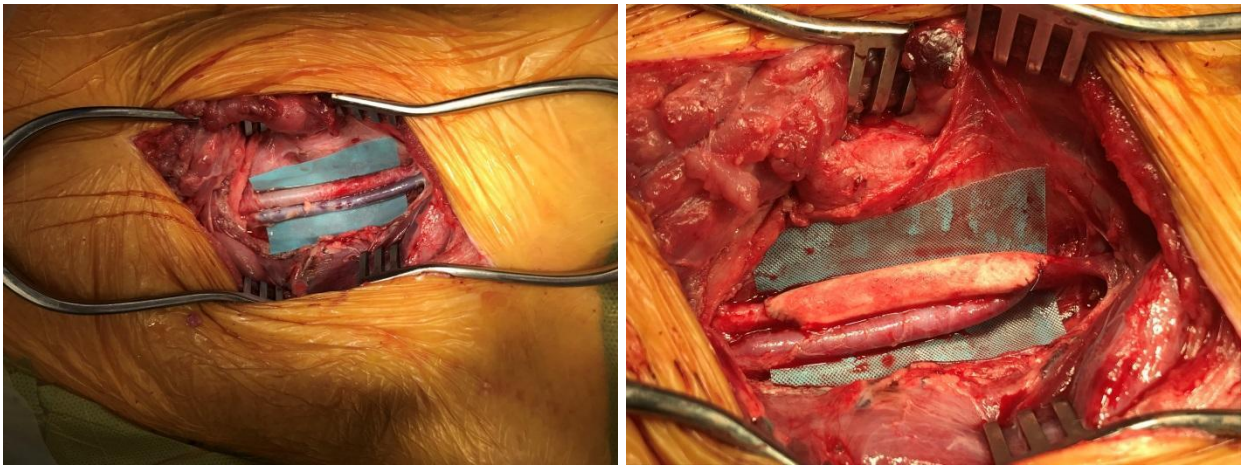

Figure 5.1 Photographs from the first pig arteriovenous implant study. Left) Native blood vessels at the carotid implant site: carotid artery (CA, top) and internal jugular (IJ, bottom); Right) the vascular graft we produced connecting the CA and the IJ.

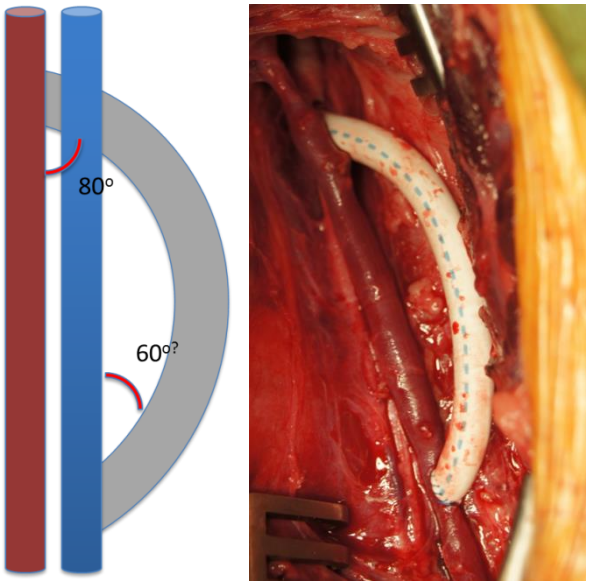

Figure 5.2 The ideal configuration of AV graft in the carotid position. Left) illustration of ideal AV graft configuration; Right) an ePTFE graft as AV graft at the carotid position.

An 8-cm-long vascular graft was successfully sutured to the carotid artery (CA) and the internal jugular (IJ). (**Fig 5.1 Right**). The handling and hemostasis of the material were excellent. However, the inability of the material to bend led to the bending of the IJ. This may increase the chance of clotting. To achieve the ideal configuration of AV graft (**Fig 5.2**), we are going to manufacture our vascular graft in "C" shape as illustrated.

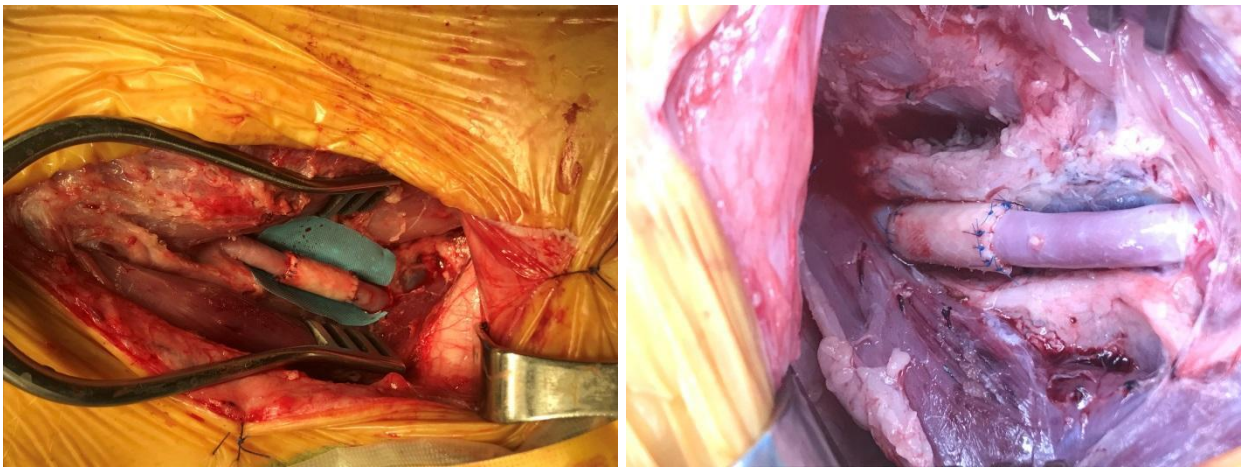

Figure 5.3 Interposition vascular grafts implanted in the femoral arteries in the groins. Left) graft implanted in the left femoral artery; right) graft implanted in the right femoral artery.

Our vascular grafts appeared perfect for interposition grafts. (**Fig 5.3**) Notably, the grafts were able to beat with the native femoral arteries. This indicates a close match of mechanical

property.

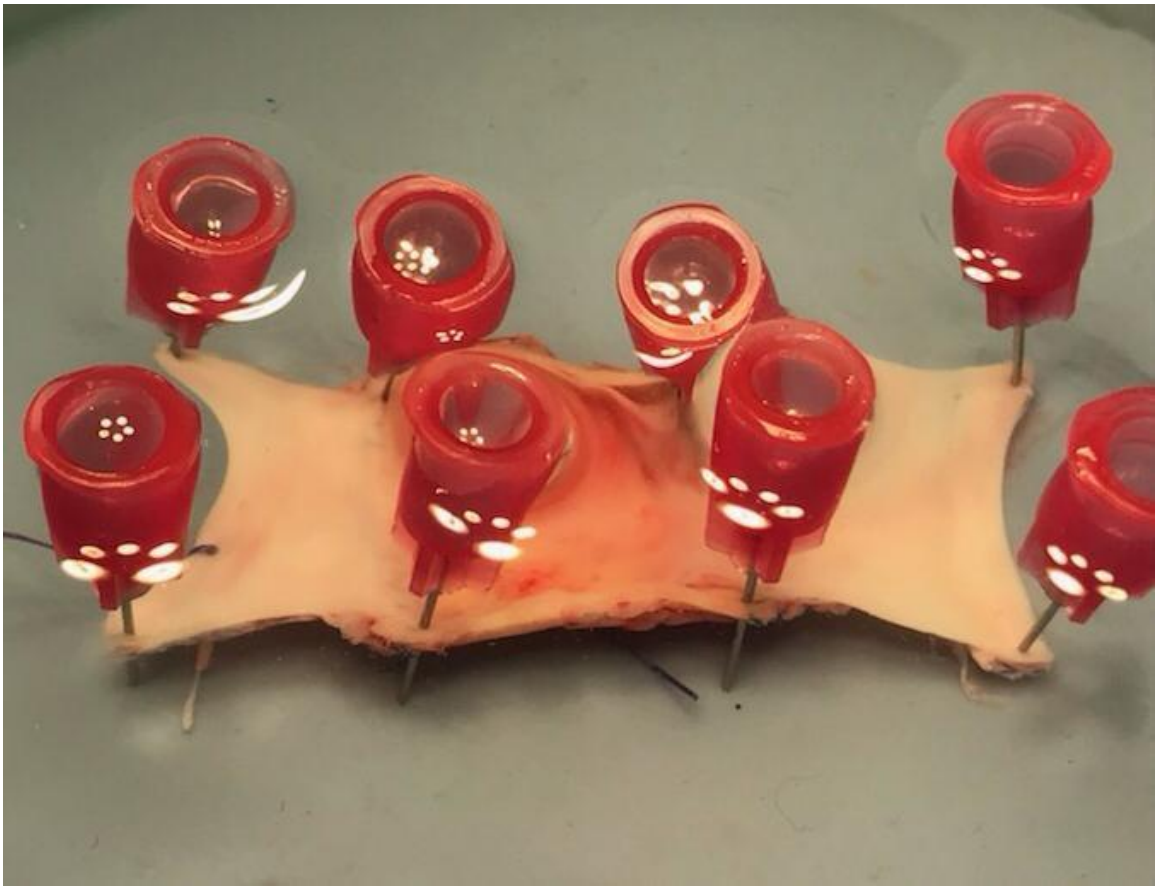

Figure 5.4 Photograph of the luminal surface of an IMPRESSIVE graft after implantation into the femoral artery of a pig for 4 weeks. The four pins in the center mark the boundaries between grafts and native blood vessels.

After 4 weeks of implantation in the femoral artery of a pig, the luminal surface of an IMPRESSIVE graft appeared to be almost indistinguishable from native artery (**Figure 5.4**). This indicates excellent integration of the pig's tissue with the graft. Histological examination shows that the graft wall, as well as the luminal surface was completely infiltrated by cells (**Figure 5.5**). Importantly, endothelial cells infiltrate the porous graft wall, and start to cover the luminal surface from the anastomosis (**Figure 5.5 Bottom**).

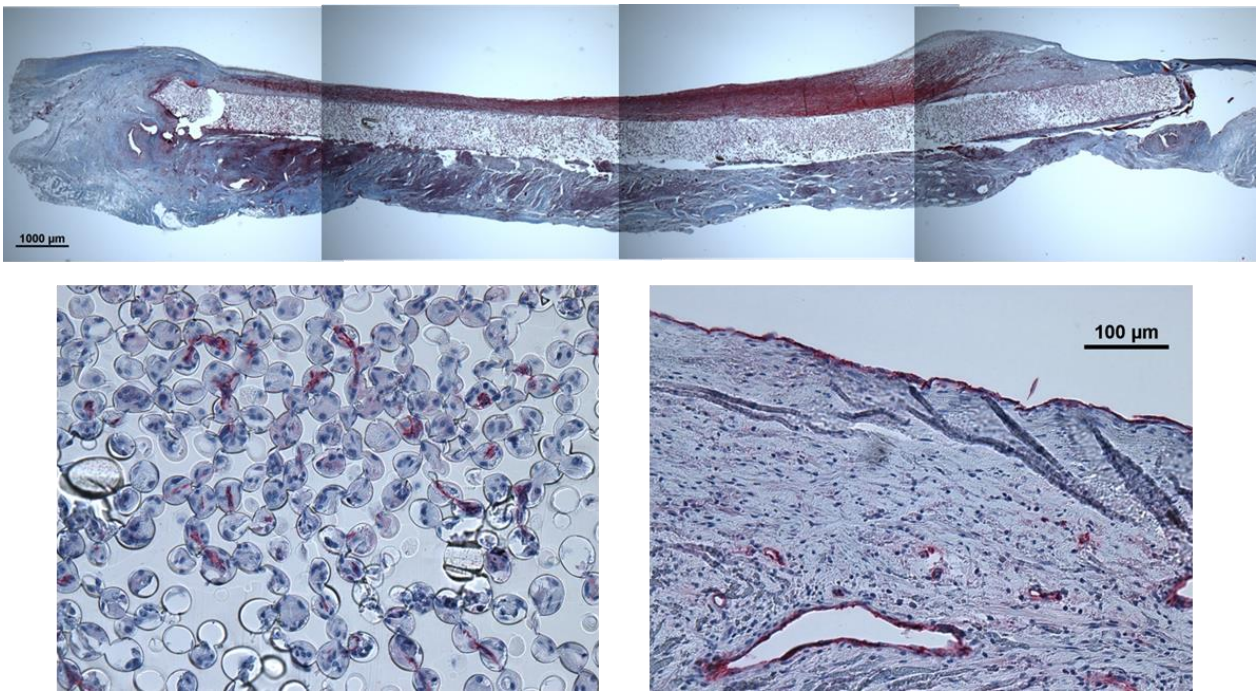

Figure 5.5 Histological images of an IMPRESSIVE graft after 4 weeks of implantation the femoral artery of a pig. **Top)** Masson's trichrome staining of the entire cross-section of the graft on the longitudinal direction; **Bottom Left)** CD31 (endothelial cell marker, in red) stained section (inside the porous structure); **Bottom Right)** CD31 (endothelial cell marker, in red) stained section (luminal surface near anastomosis).

The preliminary results from pig demonstrate early feasibility of using IMPRESSIVE grafts as vascular prosthesis. The complete coverage of luminal surface by pig cells, the intense endothelial cells infiltration, and the beginning of endothelialization in the lumen are indications of the highly pro-healing effect of the IMPRESSIVE graft. However, we need to take caution in translating such promising results in predicting performance in humans, since pigs are much more potent in healing compared to humans. The results should be considered the best case scenario in predicting vascular graft healing in humans.

5.3.2 Preliminary results from sheep study

In contrast to pig, sheep is a much slower healing species, and the most relevant in predicting performance in humans. For this reason, we focus on establishing sheep models in both arterial system and arteriovenous setting. The preliminary results are discussed.

5.3.2.1 IMPRESSIVE grafts as arterial prosthesis

IMPRESSIVE and ePTFE grafts were implanted in each side of the carotid arteries in the same sheep for 4 weeks. A total of six sheep received both grafts. All grafts remained patent at the end point. All IMPRESSIVE grafts are free of infection. One ePTFE graft failed due to infection. **Figure 5.6** shows the dramatic difference in luminal surface at the time of explanation. All ePTFE grafts are almost completely covered with red clots, while all IMPRESSIVE grafts show few spots of clots covered surface.

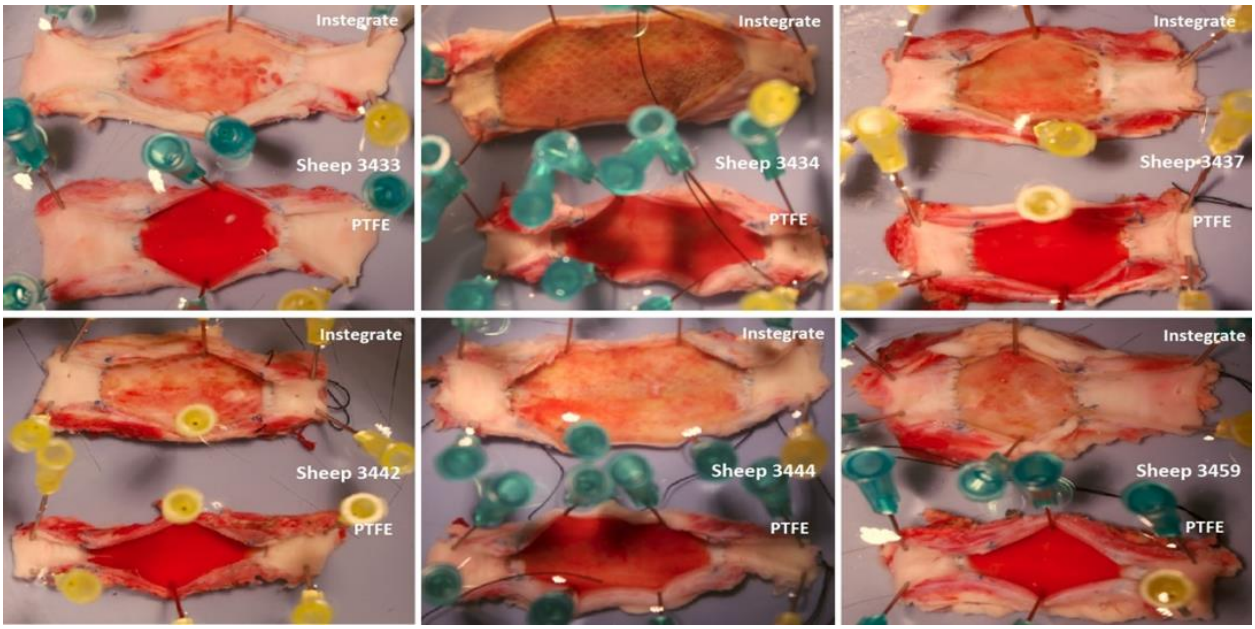

Figure 5.6. Photographs of the luminal surfaces of all 12 grafts implanted as interposition grafts in sheep model for 4 weeks. Each photograph shows the side-by-side comparison of IMPRESSIVE (top) and PTFE graft (bottom) implanted in the same sheep.

To examine whether IMPRESSIVE can guide the surrounding tissue to heal through the graft wall, we double-stained an IMPRESSIVE explant with CD 31 (endothelial cell marker, red stain, red arrows) and smoothelin (smooth muscle cell marker, brown stain) (**Figure 5.7**). The porous structure was completely infiltrated by cells (rich in endothelial cells) both near the anastomosis (**Figure 5.7A**), and in the mid-graft area (**Figure 5.7B**). The luminal surfaces in both areas are coved by smooth muscle cells. The area near the anastomosis is endothelialized.

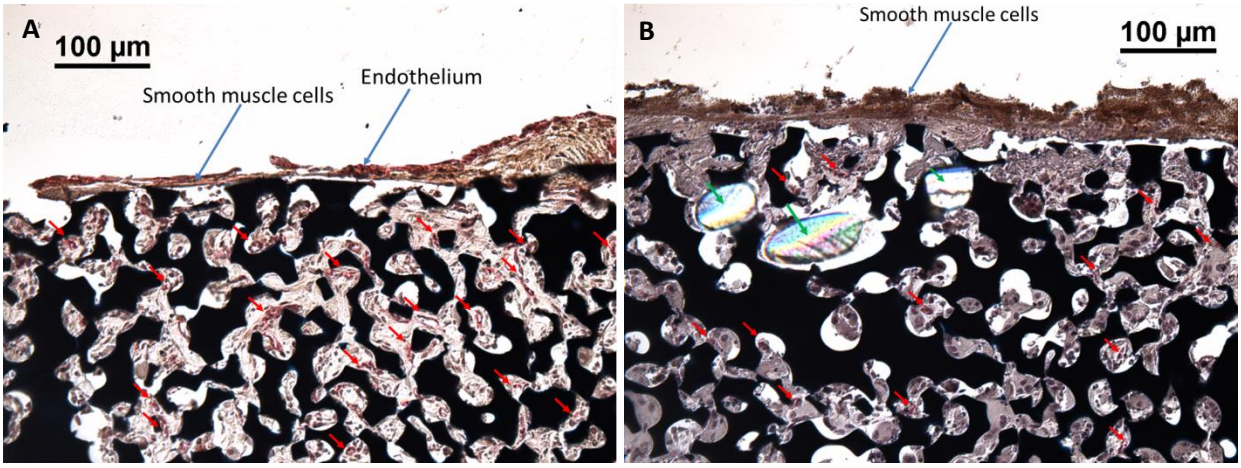

Figure 5.7 CD 31 and smoothelin double staining of IMPRESSIVE grafts after 4 weeks implantation. **A)** Area near the anastomosis; **B)** mid-graft area. Red: CD31, endothelial cell marker; brown: smoothelin, healthy smooth muscle cell marker; blue: nuclei; black: graft wall material. Red arrows point to the capillaries in the porous structure. Green arrows point to the reinforcement mesh.

5.3.2.2 IMPRESSIVE grafts as arterial-venous (AV) grafts

IMPRESSIVE and ePTFE grafts were implanted in the neck connecting carotid arteries to the contralateral external jugular vein (one graft per sheep) for 4 weeks in sheep. Three ePTFE graft and one IMPRESSIVE were implanted. The IMPRESSIVE graft remained patent at the end point. One ePTFE graft failed due to suture failure and hemorrhage after one week. The luminal surface of IMPRESSIVE at explant was free of thrombotic material in contrast to fully clot-covered surfaces of ePTFE graft (**Figure 5.8**).

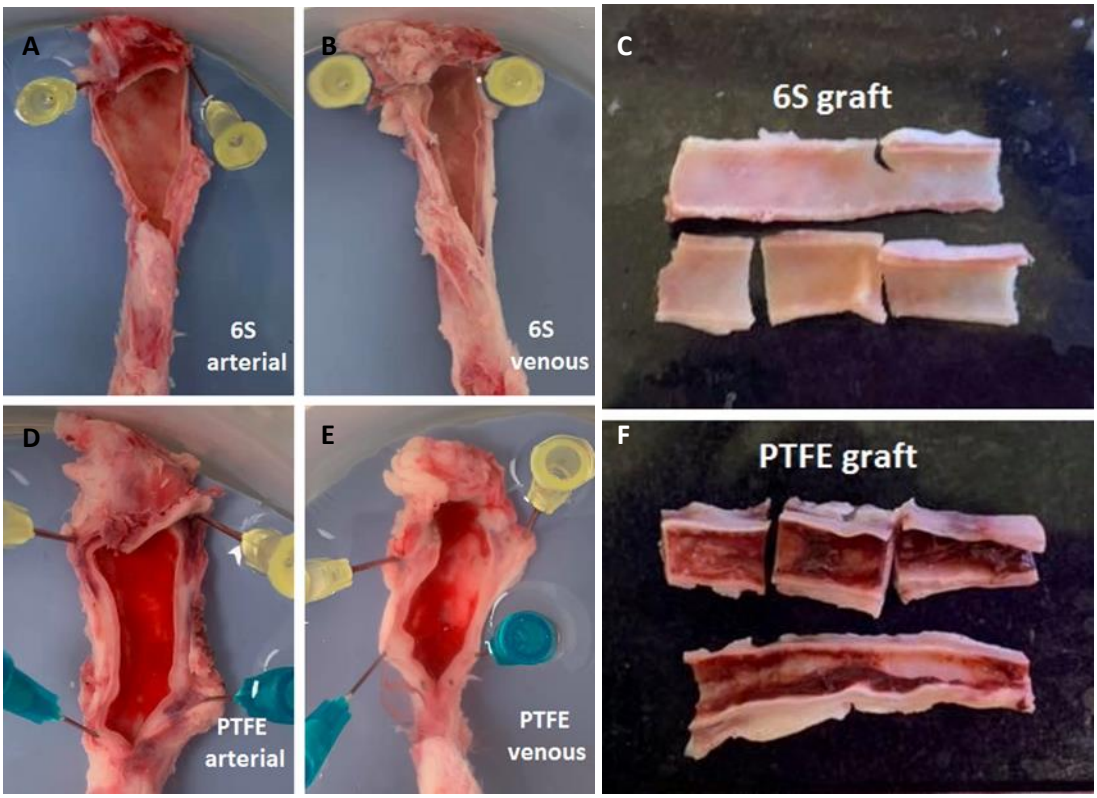

Figure 5.8 Photographs of luminal surfaces of AV grafts after 4 weeks implantation in sheep. **A)** Arterial end of the IMPRESSIVE graft; **B)** Venous end of the IMPRESSIVE graft; **C)** Mid-graft section of the IMPRESSIVE graft; **D)** Arterial end of ePTFE graft; **E)** Venous end of ePTFE graft; **F)** Mid-graft section of ePTFE graft.

In addition, ultrasound imaging revealed that IMPRESSIVE maintains the pulsatile motion after 4 weeks of implantation. The pulsatile motion resembles the contractile motion a native artery has.

By gross appearance of the luminal surfaces, IMPRESSIVE grafts consistently demonstrate better blood compatibility compared to the commercially available ePTFE grafts. This is likely due to improved healing in the IMPRESSIVE grafts. All IMPRESSIVE grafts implanted were mostly covered by tissue. And any tissue coverage provides better blood contacting surface compared to bare PTFE surfaces.

Immunohistochemistry analysis revealed that, tissue covering the inner surfaces consist of endothelial cells and smooth muscle cells. While the lumen near the anastomosis was covered by endothelial cells with smooth muscle cells beneath, the mid-graft section was covered by only smooth muscle cells. This is consistent with the traditional paradigm of trans-anastomosis endothelium healing. Whether the IMPRESSIVE grafts can be completely endothelialized will likely be revealed in longer term studies (90 days, 180 days).

The coverage by smooth muscle cells appeared to improve blood compatibility. An important function of smooth muscle cells is to contract when bleeding happens. For arteriovenous grafts that are designed to be punctured repeatedly by needles for blood access, the smooth muscle cells coverage may have a significant function in sealing the holes after punctures. On the other hand, smooth muscle cells proliferation is a hallmark of intimal hyperplasia, a major failure mechanism for vascular access. Smooth muscle cells proliferation can be assessed by double staining with smoothelin (smooth muscle cells marker) and Ki67 (proliferation marker). While early smooth muscle cell proliferation may help to cover the whole graft surface with cells, long-term

proliferation may lead to graft failure through exacerbating intimal hyperplasia. Thus the overall effect of smooth muscle cell coverage remains to be elucidated through long-term studies (90 days, 180 days).

5.4 Conclusion

The preliminary pig and sheep study demonstrate early feasibility for using IMPRESSIVE grafts as vascular prosthesis. Our vascular grafts were able to be sutured to blood vessels. The grafts had excellent handling and hemostasis properties. The elasticity of the grafts was closely matching that of the artery. IMPRESSIVE grafts maintain the pulsatile motion after 4 weeks of implantation. All IMPRESSIVE grafts demonstrate better healing and better blood compatibility compared to ePTFE grafts. All IMPRESSIVE grafts are completely covered by tissue from the host animals. The tissue is consists of endothelial cells and smooth muscles, the major cell types in native blood vessel. All these results appeared promising in terms of a short term study. Whether these results confer long-term benefits will be determined by long-term studies (90 days, 180 days implantation studies) in the future.

Chapter 6. The translational pathway towards first in human clinical trial (future directions)

6. 1. Goal

We had a highly informative discussion with the FDA on 10/18/2019. Based on the constructive feedback, we would like to focus our current discussion on the list of experiments needed and the standards applied to these experiments to support the investigational device exemption (IDE) application for early feasibility clinical study. Once the agreement is reached we will further discuss the details of each experiment through pre-submission supplements.

Specifically we would like to discuss the following questions.

1. We have proposed the list of standard tests and modifications in **Section 6.4.1** to justify an early feasibility trial. We believe the tests we proposed are sufficient to justify an early feasibility trial.

2. We have proposed the list of standard tests and modifications in **Section 6.4.1** to justify an early feasibility trial. We believe the standards the tests are based on are appropriate.

3. We proposed implant study in 6 sheep for 90 days to justify an early feasibility trail. We believe the number of animal and duration of the study is sufficient to justify early feasibility trial.

4. We list the attributes of the device in **Table 6.8**. We believe these attributes listed are appropriate.

6. 2. Indications for Use

The IMPRESSIVE Arteriovenous Graft is indicated for use in creating hemodialysis access for end stage renal disease (ESRD) patients.

6.3. Clinical and Device Development Background and Device Design Concept

6.3.1 Clinical Background

A blood access needs to be surgically created for ESRD patients to initiate hemodialysis. Currently, the standard of care includes three options: 1) AV fistula; 2) AV graft; 3) catheter. **Table 6.1** compares the benefits and risks associated with these current access options.

Table 6.1. *Benefits and risks associated with current options for hemodialysis access.*

Type	Configuration	Chance of maturation	Maturation time	Major risks	Failure rate
Catheter	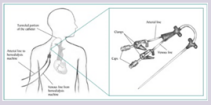	High (~100%)	Short (immediate use)	Infection	High
AV graft	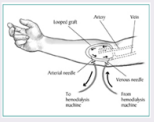	High (~100%)	Medium (2-3 weeks)	Intimal hyperplasia, thrombosis, infection	Medium
AV fistula	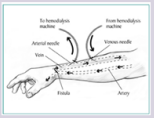	Low (64.1%)	Long (2-3 months)	Intimal hyperplasia, aneurysm	Low

Catheter can be surgically inserted and used immediately after surgery. However, the percutaneous device is associated with the highest infection risks. This is normally not considered a long-term option.

AV fistula can be created by suturing the artery and vein in the lower arm together. The vein can gradually mature under increased blood flow over 2-3 months. The matured vein can be used as blood access. Once matured the AV fistula has the lowest rate of failure. However, for about one third of ESRD patients, AV fistula never matures enough to be used.

A blood access can also be created by connecting the artery and the vein with a synthetic AV graft (most commonly, PTFE graft). After a short maturation time (2-3 weeks), the AV graft can be used to access the blood. The AV graft is considered a long term option. However, due to mechanical mismatch, poor blood compatibility, and foreign body response, currently AV grafts are subjected major risks including intimal hyperplasia, thrombosis, and infection. As the result, current AV grafts have a 50% failure rate within the first year of implantation.

6.3.2 Device Development Background

The Ratner Lab invented a new class of materials whose microporous structure and pore size can be precisely controlled through the "6S" process. We discovered that maximum vascularization and minimum foreign body capsule formation are achieved when the pore size is between 30-40 μm. (Ratner and Marshall 2008; Madden et al. 2010; Sussman et al. 2013) Based on this invention, we developed elastic, biostable, polyurethane based vascular graft with the precision-engineered porous structure. We anticipate such design will guide the surrounding tissue from the patient to heal through the graft wall and ultimately form a semi-living blood vessel *in situ*. (Preliminary data shown in **Section 3.2.3**).

6.3.2.1 Evolution of the device design

We have developed two generations of the device designs: 1) the first generation (1G) design consists of the precision-engineered polyurethane graft wall, and a gelatin film sealing the inner surface of the graft; 2) the second generation (2G) design consists of the precision-engineered polyurethane graft wall, a gelatin sealant sealing all the pores, and a surgical mesh reinforcement embedded within the graft wall. The 2G design provide sufficient suture strength and good reproducibility in sealing the graft.

6.3.2.2 Features retained in the latest design

The latest design has three features: 1) polyurethane graft wall with precision-engineered porous structure; 2) gelatin sealant sealing all the pores; 3) surgical mesh reinforcement embedded within the graft wall.

6.3.2.3 Preliminary animal testing

We implanted IMPRESSIVE grafts with the latest design features in two sheep models: 1) as arterial interposition grafts; 2) as arterial-venous (AV) grafts. Both showed promising results (See **Chapter 5**).

6.3.2.4 Lessons learned from the preliminary evaluation

Through the preliminary studies presented above, we have deepened our understanding on the limitations and benefits of our graft design, the animal model, its applicability, and attributes it cannot predict.

6.3.2.4.1 Limitations and benefits of the device design

The major limitation of the device design is its tendency to kink while bended. Several slight kinks were observed while the graft was implanted as AV graft in sheep. Surprisingly, no adverse effect associated with kinks was observed: the graft remained open with excellent blood compatibility. The elasticity and pro-healing property of the graft may have overcome the effect of slight kinks. The limitation of kinking can be circumvent by implant in sites where straight graft is required (brachial artery to axillary vein) or manufacturing grafts in the shapes needed (U shape, C shape).

Major benefits learned from the preliminary evaluation are: 1) IMPRESSIVE demonstrates superior blood compatibility to the ePTFE graft; 2) IMPRESSIVE is able to guide surrounding tissue to heal into the graft (the healing on the luminal surface is likely the reason for superior blood compatibility); 3) IMPRESSIVE is more compliance and maintains its compliance after implantation. We believe that the benefits clearly overwhelm the limitation.

6.3.2.4.2 Limitations and benefits of the test model

The major limitation of the sheep model is its high cost. This has prompted the early discussion with the FDA to maximize the use of each sheep to facilitate translation.

As the large animal model of choice for vascular graft research, the sheep model has many benefits: 1) its slow healing and rapid development of stenosis resembles human the most (Kohler and Kirkman 1999); 2) it has comparable hemodynamic and hematology properties to human (Byrom et al. 2010); 3) AV graft can be easily inserted in the neck and can be readily accessed; 4) sheep are relatively easy to work with. The benefits of the test model also outweigh its limitation.

6.3.2.4.3 Applicability of nonclinical or animal testing to predict clinical performance

Based on the analysis above, we believe that the sheep model is the most applicable animal model to predict clinical performance.

6.3.2.4.4 Device attributes that could not be appropriately evaluated with nonclinical or animal studies

Although the sheep model is the best model currently available to predict clinical performance, the device attribute to guide the tissue integration could not be appropriately evaluated with animal studies. Specifically, how age, the ESRD, and routine dialysis would affect the guided healing can be most appropriately evaluated in clinical trial. A clinical trial on vascular access is most convenient for such evaluation, since medical interventions are routinely performed and sections of grafts can be easily retrieved without jeopardizing the lives of patients.

6.3.3 Device Design Concept

6.3.3.1 Device description

The IMPRESSIVE Arteriovenous Graft is an elastic, pro-healing vascular prosthesis comprised precision-engineered porous polyurethane graft wall (**Figure 6.1A, B, C**), polyethylene terephthalate (Dacron) reinforcement mesh embedded within the graft wall (**Figure 6.1 A & B**), and gelatin sealant sealing all the pores (**Figure 6.1 A & C**). The IMPRESSIVE Arteriovenous Graft can be used to connect an artery and a vain through standard surgical procedure for dialysis access. The graft has an inner diameter of 6 mm and length as needed (e.g. 15 cm). Details of materials of construction are shown in **Table 6.2**.

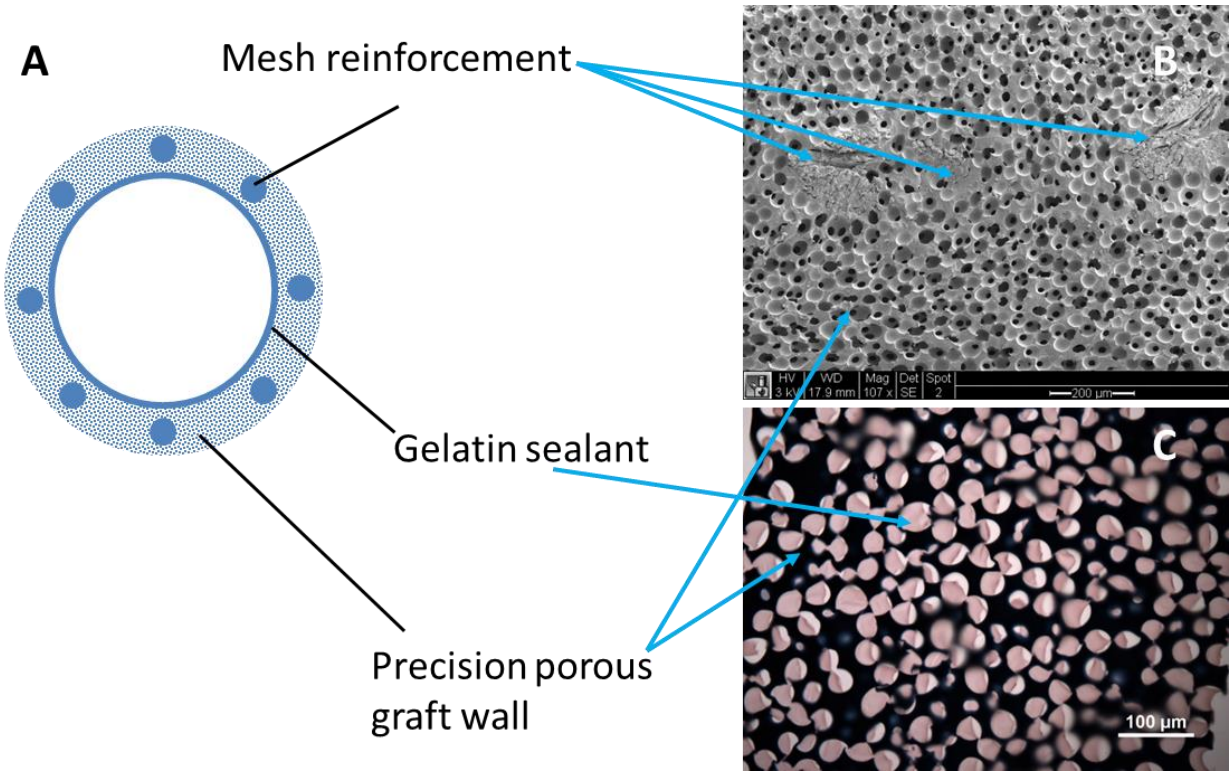

Figure 6.1. Key parts of IMPRESSIVE grafts. **A)** Illustration of key parts of IMPRESSIVE: precision-engineered porous graft wall, polyester (Dacron) surgical mesh reinforcement, and gelatin sealant; **B)** SEM image of the cross section of IMPRESSIVE (without gelatin sealant); **C)** microscopic image of cross section IMPRESSIVE stained with Masson's trichrome and Sudan Black B (pink: gelatin, black: polyurethane graft wall).

Table 6.2. *Materials for constructing IMPRESSIVE grafts*

Material of Construction	**Chemical Name**	**Trade Name**	**Supplier**	**Contact Type**
[Vascular graft (implant)]				
[Part: Polyurethane graft wall]				
Polyurethane	Polyurethane	N/A (synthesized in house)	N/A	permanent blood contact

[Part: Gelatin sealant]				
Gelatin	Gelatin	Gelatin	Sigma	prolonged blood contact
[Part: Surgical mesh reinforcement]				
Polyester surgical mesh	Polyethylene terephthalate	Dacron	Surgicalmesh^{TM}	permanent tissue contact

The three key parts showed in **Table 6.2** have crucial functions.

The presicion-engineer porous polyurethane graft wall guides and maintains the pulsatile blood flow from the artery to the vein, and guides the surrounding tissue to heal into the graft. Polyurethane graft wall guides and maintains the pulsatile blood flow by having good compliance. The presicion-engineered porous structure guides healing through recruiting macrophages locally and modulating them towards a pro-healing phenotype. Pro-healing macrophages in turn orchestrate the healing of endothelial cells and other cells. (Madden et al. 2010; Sussman et al. 2013)

The gelatin sealant provides short term hemostasis for the vascular graft by sealing all the pores (**Figure 6.1C**). And it degrades in a rate that's commensurate with the rate of healing. Our preliminary results show that the gelatin is completely replaced by tissue after 4 weeks of implantation (**Chapter 5**). Out of all seven IMPRESSIVE grafts we implanted, none shows any leakage problem.

The polyester (Dacron) surgical mesh provides sufficient suture strength and long-term stability for the vascular graft. When sutures are tied to the surgical mesh during the suture, the mesh

becomes to weight-bearing part to the force from the suture. We have never experience any suture failure after implantation in all our preliminary experiments on IMPRESSIVE. Dacron is also a widely used material for vascular graft and is known to have good long-term stability.

6.3.3.2 Intended clinical use

IMPRESSIVE is intended for creating hemodialysis access for ESRD patients. There are seven anatomical locations IMPRESSIVE could be implanted to: four of them are in the upper extremity: **1)** straight forearm arteriovenous graft from the radial artery at the wrist to the antecubital fossa in the elbow (**Figure 6.2 A**); **2)** looped forearm arteriovenous graft from the brachial or radial artery to the antecubital fossa in the elbow(**Figure 6.2 B**); **3)** straight upper arm arteriovenous graft from the brachial or radial artery to the axillary vein (**Figure 6.2 C**); **4)** looped upper arm arteriovenous graft from the axillary artery to the axillary vein (**Figure 6.2 E**); three of them are for the thorax and lower extremity: **5)** necklace graft from the subclavian artery on one side to the subclavian vein on the other side (**Figure 6.2 E**); **6)** straight graft from the axillary artery to the femoral vein (**Figure 6.2 F**); **7)** straight and looped prosthetic graft configuration in the lower extremity (**Figure 6.2 G**). (Bode and Tordoir 2012) Currently, the main limitation is that the straight IMPRESSIVE grafts cannot be applied to the looped configurations because of high risk of kinking. This limitation can be overcome by manufacturing the graft in a looped shape. We can directly apply IMPRESSIVE grafts to all the straight configurations. The most likely anatomic location for the early feasibility trial (first in human) is **3)** straight upper arm arteriovenous graft from brachial artery to axillary vein. This is the most widely used anatomic location for first in human trial because of its straight

configuration, common practice, and easy access. We will further discuss this anatomic location in ***In Vivo*** **Environment**.

6.3.3.3 Description of device use and procedural steps

The IMPRESSIVE Arteriovenous Graft will be used to create hemodialysis access through standard procedure. Briefly, taking brachial artery to axillary vein (**Figure 5C**) as an example, after anesthesia and antibiotics administration, two incisions will be made to expose the artery and the vein. A superficial tunnel connecting the two incisions will be created by using a bi-directional tunneling device. The IMPRESSIVE grafts will be placed in the tunnel and the ends will be sewn to the blood vessels in an end-to-side fashion.

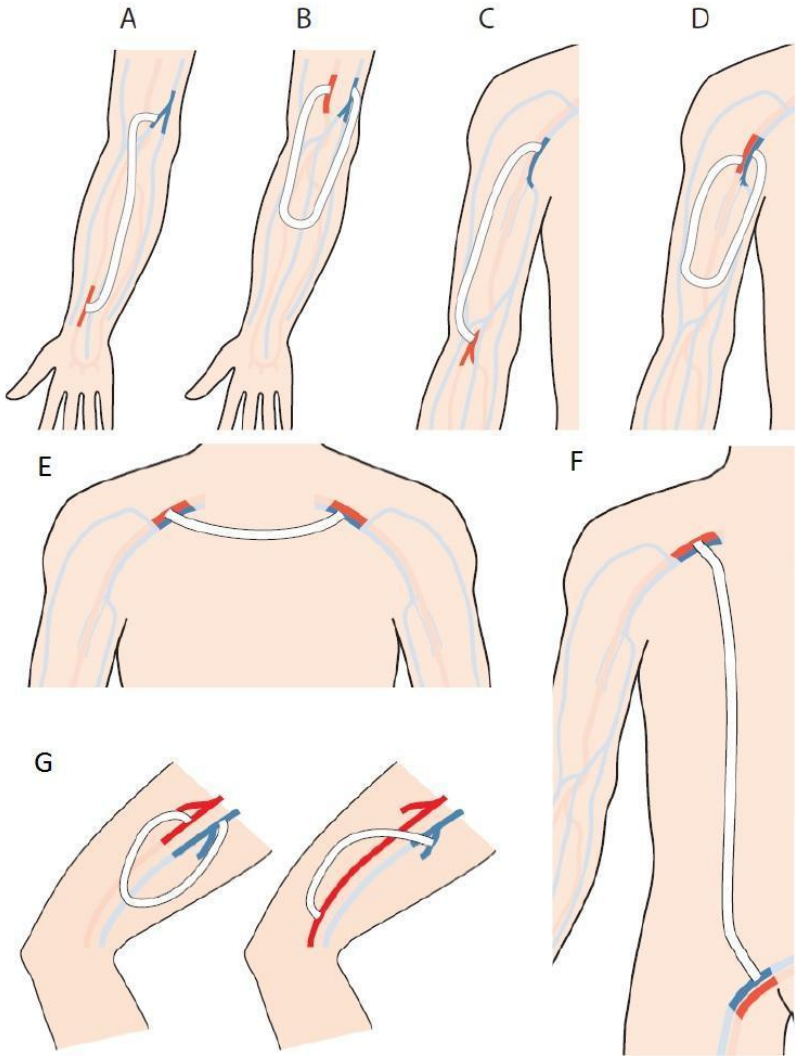

Figure 6.2 Potential anatomical locations and configurations for surgical placement of IMPRESSIVE Arteriovenous Grafts. **A)** straight forearm arteriovenous graft from the radial artery at the wrist to the antecubital fossa in the elbow; **B)** looped forearm arteriovenous graft from the brachial or radial artery to the antecubital fossa in the elbow; **C)** straight upper arm arteriovenous graft from the brachial or radial artery to the axillary vein; **D)** looped upper arm arteriovenous graft from the axillary artery to the axillary vein); **E)** necklace graft from the subclavian artery on one side to the subclavian vein on the other side; **F)** straight graft from the axillary artery to the femoral vein; **G)** straight and looped prosthetic graft configuration in the lower extremity. (Figure was adapted from Bode and Tordoir 2012.)

Two surgical details specific to IMPRESSIVE grafts will be incorporated to enhance the performance: 1) to prevent acute thrombosis, Instegrate will be soaked in heparinized saline for

at least 30 minutes before implantation; 2) To maintain the compliance of IMPRESSIVE grafts, interrupted suture technique will be used instead of running suture technique. Interrupted suture technique is known to lead to better compliance at the anastomosis (Klein et al. 1982). We hypothesize these two surgical details will enhance the performance of IMPRESSIVE grafts, however, they are not absolutely necessary for the graft to function normally.

6.3.3.4 Conditions of Use/In Vivo Environment

Table 6.3 lists aspects of the *In vivo* environment that can be readily described, observed, and/or quantified. The aspects whose effects are complex and difficult to describe are not listed. For example, how the ESRD condition will affect graft performance are difficult to describe and can only be assessed in clinical trial. The aspects listed are mainly mechanical and can be addressed readily with mechanical testing and preclinical animal studies.

Table 6.3. *Effects of the In Vivo Environment on the Device Evaluation*

Unique Aspects of the Intended Use	***In Vivo* Parameters**			**Potentially Affected Parts of the Device**
List each unique aspect associated with	Important Parameter	Qualitative or Quantitative Description	Rationale for Addressing	List each part of the device that could be

the intended use (e.g., implant location, disease state, lesion type) that may be important in assessing device performance.	Identify each in vivo parameter that could be affected by the unique aspect. Examples of in vivo parameters include blood vessel sizes, angulation, external forces, pulsatile loading, tortuosity, compliance, and flow characteristics.	Provide anticipated qualitative or quantitative description of the parameter and the basis for the estimate.	For each in vivo parameter identified, explain why it is important to consider (e.g., identify each procedure-related function or performance-related function that could be affected by the parameter).	affected by the in vivo parameter.
Implant Location (upper arm: Brachial artery to Axillary vein*)	Blood vessel sizes	Axillary vein ≥ 7 mm in diameter; brachial artery ≥ 4 mm in diameter.	This is the factor that determines the size of the vascular graft.	Graft wall: the inner diameter of the graft is about 6 mm.
	Suture strength	≥ 2 N	The vascular graft needs sufficient suture strength to withstand suture.	Reinforcement: the reinforcement provides more than twice the suture strength needed (4.77±0.36 N).
	Angulation	Small/straight	Our graft will be manufactured with the angulation needed in each site.	Graft wall: the vascular graft is straight.

	Pulsatile loading	Systolic blood pressure: 140-162 mmHg (Keuter et al., 2008)	Grafts will need to be able to withstand the pulsatile loading	Graft wall and reinforcement: the vascular graft needs to withstand the blood pressure in vivo.
	Compliance	6%/100 mmHg	Better match of compliance between grafts and blood vessels reduce the chance of intimal hyperplasia	Graft wall and reinforcement: the vascular graft needs to have compliance close to the native blood vessels
	Blood flow rate	>600 ml/min	The blood flow rate influence vascular graft performance in many ways (neointima growth, platelet adhesion). A closer match of blood flow in animal model is preferred.	Graft wall and gelatin sealant: the vascular graft needs to withstand such high blood flow without significant bleeding.

*This implant location is used as an example because it is the most likely location for the first in human study. Other possible locations are described in **Section 6.3.3.3**. The many aspects of the *in vivo* environment are similar across the locations.

6.3.3.5 Minimum design-life of the device

Based on the clinical observation that most AV grafts fail within the first two years of use, we targets the minimum design-life of the device to be two years. The actual life of the device can only be estimated by clinical trial and it may extend much longer than two years.

6.4. Device Evaluation Strategy

To address biocompatibility evaluation, non-clinical bench testing, and device-specific evaluation, we are developing our device evaluation strategy (DES) based on ISO 10993, ISO 7198,Guidance for Industry and FDA Staff-General Considerations for Animal Studies for Cardiovascular Devices, and Investigational Device Exemptions (IDEs) for Early Feasibility Medical Device Clinical Studies, Including Certain First in Human (FIH) Studies.

We would like to separate the discussion in at least two parts: 1) DES for FIH; 2) DES for pivotal clinical trial. The DES for FIH will focus on the evaluations that are indispensable for the safety of the device. It will be done, mostly, without GLP, but with the highest possible standard we can achieve in an academic research setting. FDA guidance document states that "non-GLP study data may be used to support an early feasibility study IDE application only if the deviations from GLP are identified and justified and do not compromise the validity of the study results". We would like to work with the FDA to reach agreement on practices needed for using non-GLP data to justify FIH. The FDA guidance document also stated that "short-term animal studies may be adequate for the initiation of an early feasibility study". We would like to use 90 days study in sheep to justify the initiation of FIH. In contrast, DES for pivotal clinical trial will be done mostly with GLP, and includes sheep study of 30 days, 90 days, and 180 days. For this pre-submission meeting, we would like to focus on the DES for FIH.

In general the DES for FIH focuses on the tests most essential to address the risks associated with the device. Tests that are good to run but not essential are not included. The DES will start with leachable analysis to confirm no leachable chemicals from the grafts that are outside the allowable limit. Then, we will conduct bench tests to address potential modes of mechanical

failure. This will be followed by *in vitro* biocompatibility tests. Finally, we will conduct *in vivo* tests to address biocompatibility. Based on the "3R" principles (reduce, replace, refine), we proposed to replace biocompatibility tests that used to be done in multiple animal models (rodent, rabbit, dog) with our sheep model. We believe this will not only reduce the cost and animal use, but more importantly, generate more clinically relevant results. This requires simple incorporation of multiple tests into the sheep study. The only biocompatibility test not replaced by the sheep study is the sensitization test with Guinea pig because the problem addressed is very specific and difficult to incorporate into the sheep study.

6.4.1 Standard Device Evaluation

Standard device evaluations involve biocompatibility evaluations based on ISO 10993, and nonclinical bench testing based on ISO 7198.

6.4.1.1 Biocompatibility Evaluation

Biocompatibility evaluations for justifying FIH trial of Instegrate are listed in **Table 6.4**. These tests will be done without GLP, but with the highest standard possible in our academic setting. All the protocols will be available. All animal studies will be IACUC approved. All raw data, electronic images, histology blocks, and histology slides will be retained for seven years and (2) standard fixed tissues for two years. Whenever possible, assessment (for example histology scoring) will be made by professionals independent of the project management. If the FDA feels necessary, we can have the report audited.

For justifying FIH trial, we will focus on the biocompatibility tests most relevant to the safety of the device. For example, we do not believe most of the detailed blood compatibility tests are

necessary, because 1) blood compatibility is only minor factor contributing the failure of medium diameter vascular graft; 2) our preliminary data (**Chapter 5**) has clearly demonstrated superior blood compatibility compared to standard ePTFE grafts. Thus we don't believe that blood compatibility will likely be a major contribution to the risk of our device.

Many biocompatibility endpoints are going to be addressed by a sheep implant study for 90 days. Hemolysis will be addressed by monitoring the hemoglobin level of sheep during implantation. Pyrogenicity will be addressed by monitoring the body temperature of sheep during implantation. Systemic toxicity will be addressed by histological observation of the kidney and lung of one randomly selected animal after sacrifice.

After 90 days of implantation, the graft, surrounding tissue and adjacent blood vessels will be harvested and detail histological and immunohistological studies will be conducted. Based on the FDA guidance document: *General Considerations for Animal Studies for Cardiovascular Devices (2010)*, the following aspects will be assessed:

- Endothelialization;
- mural injury;
- inflammation;
- vascularization;
- intimal fibrin;
- intimal and medial smooth muscle cell proliferation;
- adventitial fibrosis;

- the integrity of the internal and external elastic laminae.

Chronic toxicity, carcinogenicity, and genotoxicity will be addressed by leachable tests (**Table 6.6**). We will make sure that no leachables from the proposed material are outside the allowable limits.

If we can reach agreement with the FDA on the principle of these tests, we will further develop the detailed protocols and submit them through pre-submission supplements for further feedback before we finish the tests.

Table 6.4. *Biocompatibility Evaluation for Blood-Contacting, Permanent Implant Component (for FIH)*

Biocompatibility Endpoint	How the Endpoint will be Addressed	Test Article Description	Extraction Ratio (cm2/mL), Extraction Medium, & Conditions	Method	Acceptance Criteria
Cytotoxicity	conducting testing on the device to be used in the clinical study	finished device that is intended to be used in the clinical study	3, DMEM plus 1 v% L-glutamine, 1 v% antibiotic, and 10 v% fetal bovine serum, 37 °C, 24 hours	ISO 10993 Part 5	≤ 2

Sensitization	using data from an in vivo animal study	finished device that is intended to be used in the clinical study	3, saline and corn oil (separately), 37 °C, 72 hours	Guinea Pig Maximization Test based on ISO 10993 Part 10 (Note that sensitization test will be conducted without ethylene oxide sterilization, because ethylene oxide may cause false positive result)	Magnusson and Kligman grades < 1
Hemocompatibility					
Hemolysis (Direct and Indirect Contact)	using data from an in vivo animal study	finished device that is intended to be used in the clinical study	N/A	In vitro hemolysis test will be replaced by evaluating haemoglobin (Hb) concentrations in sheep implant study according to ISO 10993 Part 4	Haemoglobin elevation similar to or lower than, control PTFE grafts
C3a Complement Activation	not needed because SC5b-9 is generally considered a more important marker representative				

	of the full extent of complement activation according to ISO 10993 Part 4				
SC5b9 Complement Activation	will be valuable to know for pivotal trial, but not needed for early feasibility trial.	finished device that is intended to be used in the clinical study	N/A	In vitro test with human blood or, if possible, replace in vitro test with in vivo test in sheep implant study. ELISA kits will be used to determine SC5b9 level according to ISO 10993 Part 4	Complement activation level similar to or lower than control PTFE graft
In vivo thrombogenicity (e.g., leveraged from GLP study, canine NAVI)	will be valuable to know for pivotal trial, but not needed for early feasibility trial.	finished device that is intended to be used in the clinical study	N/A	Canine NAVI test will be replaced by sheep study in relevant implant site with methods suggested in C2 section in Annex C of ISO10993-4. This method is a better choice compared to the canine NAVI test according	Thrombogenicity similar to or lower than control PTFE graft

				to ISO10993-4.	
Partial Thromboplastin Time	will be valuable to know for pivotal trial, but not needed for early feasibility trial.	finished device that is intended to be used in the clinical study	N/A	ISO10993-4 and ASTM 2382	PTT longer than or similar to control PTFE graft
Platelet/Leukocyte Count	will be valuable to know for pivotal trial, but not needed for early feasibility trial.	finished device that is intended to be used in the clinical study	N/A	In vitro test will be replaced by in vivo test in sheep implant model based on the recommendation of Table 1. of ISO 10993-4.	Similar or higher platelet in blood, similar or less platelet counts and/or activation, similar or less leukocyte in blood, compared to PTFE graft

Material-Mediated Pyrogenicity	conducting testing on the device to be used in the clinical study, and using data from an in vivo animal study	finished device that is intended to be used in the clinical study	(for endotoxin test) 3, endotoxin-free water, 1 hr, under vigorous agitation	The Rabbit Pyrogen test will be replaced by the combination of LAL test and monitoring body temperature of sheep during implant study. Endotoxin level will be tested using chromogenic technique based on the United States Pharmacopeial Convention (<85> Bacterial Endotoxins Test). Body temperature of sheep will be monitored during implant study.	similar or less body temperature increase compared to PTFE graft
Implantation					
Systemic Toxicity	using data from an in vivo animal study	finished device that is intended to be used in the clinical study	N/A	Kidneys and lungs will be collected and evaluated for systemic toxicity in sheep implant study according to ISO 10993	No sign of systemic toxicity

				Part 11	
Acute Systemic Toxicity	Not needed because longer term toxicity will be studied				
Sub-Chronic Toxicity	will be valuable to know for pivotal trial, but not needed for early feasibility trial. Systemic toxicity study on sheep is sufficient	finished device that is intended to be used in the clinical study	N/A	Will be evaluated in rabbit implant study according to ISO 10993 Part 6 & Part 11	No sign of systemic toxicity
Chronic Toxicity	conducting testing on the device to be used in the clinical study	finished device that is intended to be used in the clinical study	(For exhaustive extraction) 3, Hexane, 2-propanol, water (separately), incubator shaker 50 °C/72 hours, exhaustive extraction is	Will be replaced by extractable Leachable Profile with Toxicologist Risk Assessment based on ISO 10993 part 18 & ISO/TS21726	No leachables from the proposed material are outside the allowable limits.

			performed by solvent replacement until >90% extractables is obtained.		
Carcinogenicity	conducting testing on the device to be used in the clinical study	finished device that is intended to be used in the clinical study	(For exhaustive extraction) 3, Hexane, 2-propanol, water (separately), incubator shaker 50 °C/72 hours, exhaustive extraction is performed by solvent replacement until >90% extractables is obtained.	Will be replaced by extractable Leachable Profile with Toxicologist Risk Assessment based on ISO 10993 part 18 & ISO/TS21726	No leachables from the proposed material are outside the allowable limits.
Genotoxicity					

Bacterial Mutagenicity Test – Ames Assay	May not be needed depending on the results of Leachable Profile with Toxicologist Risk Assessment	finished device that is intended to be used in the clinical study		Follow ISO 10993 Part 3 if needed	
In Vitro Mouse Lymphoma Assay	May not be needed depending on the results of Leachable Profile with Toxicologist Risk Assessment	finished device that is intended to be used in the clinical study		Follow ISO 10993 Part 3 if needed	
In Vitro Chromosome Aberration Assay	not needed because it's equivalent to in vitro mouse lymphoma assay	finished device that is intended to be used in the clinical study		Follow ISO 10993 Part 3 if needed	
In Vivo Mouse Micronucleus Assay	May not be needed depending on the results of Leachable Profile with Toxicologist Risk Assessment	finished device that is intended to be used in the clinical study		Follow ISO 10993 Part 3 if needed	

After potentially multiple rounds of early feasibility trials and the design of the device refined to its mature state, we will conduct much more thorough biocompatibility evaluations under GLP to justify pivotal trial (**Table 6.5**). Also the full sheep implant studies will include 30 days, 90 days, and 180 days as the FDA suggested in our last pre-sub meeting.

Table 6.5. *Biocompatibility Evaluation for Blood-Contacting, Permanent Implant Component (for pivotal trial)*

Biocompatibility Endpoint	How the Endpoint will be Addressed	Test Article Description	Extraction Ratio (cm2/mL), Extraction Medium, & Conditions	Method	Acceptance Criteria
Cytotoxicity	conducting testing on the device to be used in the clinical study	finished device that is intended to be used in the clinical study	3, DMEM plus 1 v% L-glutamine, 1 v% antibiotic, and 10 v% fetal bovine serum, 37 °C, 24 hours	ISO 10993 Part 5	≤ 2
Sensitization	using data from an in vivo animal study	finished device that is intended to be used in the clinical study	3, saline and corn oil (separately), 37 °C, 72 hours	Guinea Pig Maximization Test based on ISO 10993 Part 10 (Note that sensitization test will be conducted without ethylene oxide sterilization,	Magnusson and Kligman grades < 1

				because ethylene oxide may cause false positive result)	
Hemocompatibility					
Hemolysis (Direct and Indirect Contact)	using data from an in vivo animal study	finished device that is intended to be used in the clinical study	N/A	In vitro hemolysis test will be replaced by evaluating haemoglobin (Hb) concentrations in sheep implant study according to ISO 10993 Part 4	Haemoglobin elevation similar or lower than, control PTFE grafts
C3a Complement Activation	not needed because SC5b-9 is generally considered a more important marker representative of the full extent of complement activation according to ISO 10993 Part 4				

SC5b9 Complement Activation	conducting testing on the device to be used in the clinical study	finished device that is intended to be used in the clinical study	N/A	In vitro test with human blood or, if possible, replace in vitro test with in vivo test in sheep implant study. ELISA kits will be used to determine SC5b9 level according to ISO 10993 Part 4	Complement activation level similar to or lower than control PTFE graft
In vivo thrombogenicity (e.g., leveraged from GLP study, canine NAVI)	using data from an in vivo animal study	finished device that is intended to be used in the clinical study	N/A	Canine NAVI test will be replaced by sheep study in relevant implant site with methods suggested in C2 section in Annex C of ISO10993-4. This method is better choice compared to the canine NAVI test according to ISO10993-4.	Thrombogenicity similar to or lower than control PTFE graft
Partial Thromboplastin Time	conducting testing on the device to be used in the clinical study	finished device that is intended to be used in the clinical	N/A	ISO10993-4 and ASTM 2382	PTT longer than or similar to control PTFE

		study			graft
Platelet/Leukocyte Count	conducting testing on the device to be used in the clinical study	finished device that is intended to be used in the clinical study	N/A	In vitro test will be replaced by in vivo test in sheep implant model based on the recommendation of Table 1. of ISO 10993-4.	Similar or higher platelet in blood, similar or less platelet counts and/or activation, similar or less leukocyte in blood, compared to PTFE graft
Material-Mediated Pyrogenicity	conducting testing on the device to be used in the clinical study, and using data from an in vivo animal study	finished device that is intended to be used in the clinical study	(for endotoxin test) 3, endotoxin-free water, 1 hr, under vigorous agitation	The Rabbit Pyrogen test will be replaced by the combination of LAL test and monitoring body temperature of sheep during implant study. Endotoxin level will be tested using chromogenic technique based on the United States	similar or less body temperature increase compared to PTFE graft

				Pharmacopeial Convention (<85> Bacterial Endotoxins Test). Body temperature of sheep will be monitored during implant study.	
Implantation					
Systemic Toxicity	using data from an in vivo animal study	finished device that is intended to be used in the clinical study	N/A	Kidneys and lungs will be collected and evaluated for systemic toxicity in sheep implant study according to ISO 10993 Part 11	No sign of systemic toxicity
Acute Systemic Toxicity	Not needed because longer term toxicity will be studied				
Sub-Chronic Toxicity	using data from an in vivo animal study	finished device that is intended to be used in the clinical study	N/A	Will be evaluated in rabbit implant study according to ISO 10993 Part 6 & Part 11	No sign of systemic toxicity

Chronic Toxicity	conducting testing on the device to be used in the clinical study	finished device that is intended to be used in the clinical study	(For exhaustive extraction) 3, Hexane, 2-propanol, water (separately), incubator shaker 50 °C/72 hours, exhaustive extraction is performed by solvent replacement until >90% extractables is obtained.	Will be replaced by extractable Leachable Profile with Toxicologist Risk Assessment based on ISO 10993 part 18 & ISO/TS21726	No leachables from the proposed material are outside the allowable limits.
Carcinogenicity	conducting testing on the device to be used in the clinical study	finished device that is intended to be used in the clinical study	(For exhaustive extraction) 3, Hexane, 2-propanol, water (separately), incubator shaker 50 °C/72 hours, exhaustive extraction is performed by solvent replacement until	Will be replaced by extractable Leachable Profile with Toxicologist Risk Assessment based on ISO 10993 part 18 & ISO/TS21726	No leachables from the proposed material are outside the allowable limits.

			>90% extractables is obtained.		
Genotoxicity					
Bacterial Mutagenicity Test – Ames Assay	May not be needed depending on the results of Leachable Profile with Toxicologist Risk Assessment	finished device that is intended to be used in the clinical study		Follow ISO 10993 Part 3 if needed	
In Vitro Mouse Lymphoma Assay	May not be needed depending on the results of Leachable Profile with Toxicologist Risk Assessment	finished device that is intended to be used in the clinical study		Follow ISO 10993 Part 3 if needed	

In Vitro Chromosome Aberration Assay	not needed because it's equivalent to in vitro mouse lymphoma assay	finished device that is intended to be used in the clinical study		Follow ISO 10993 Part 3 if needed	
In Vivo Mouse Micronucleus Assay	May not be needed depending on the results of Leachable Profile with Toxicologist Risk Assessment	finished device that is intended to be used in the clinical study		Follow ISO 10993 Part 3 if needed	

Table 6.6. *Planned Chemical Characterization*

Analysis Method	Test Article Used for Extractions	Extraction Solvent	# Samples per Solvent	Temperature (°C)	Time (per Iteration) (hour)	Extraction Ratio (cm^3/ml)
HPLC	finished device that is intended to be used in the clinical study	Hexane	3	50	72	3
HPLC	finished device that is intended to be used in the clinical study	2-Propanol	3	50	72	3
HPLC	finished device that is intended to be used in the clinical study	Water	3	50	72	3

6.4.1.2 Nonclinical Bench Testing

Nonclinical bench tests from ISO 7198 are listed in **Table 6.7**. Note that in the most recent version of ISO 7198 (2016 edition), acceptance criteria are not listed. Most tests only need to be tested to generate results for labelling purpose. Thus we only select the tests that are most relevant to the *in vivo* environment (**Table 6.3**) and device or procedure attribute (**Table 6.8**) to justify the early feasibility trial. Although strength after repeated puncture seems relevant, it does not capture the effect of healing on strengthening the graft after puncture *in vivo*. We suggest including this assessment in the 90-day sheep implant study: after 3 weeks of implantation, start puncturing the graft with needles 3 times per week. And study whether this operation contribute to failures.

Table 6.7. *Standard Testing from ISO 7198*

Test	Purpose of Test	Applicability to Device/Device Parts	Impacted by Device Design or Use or In Vivo Conditions	Effect of Device Design or Use or In Vivo Conditions on the Acceptance Criteria	Necessity for justifying early feasibility trial

List the tests that are provided in the standard or FDA guidance document.	State the purpose of each test.	For Option 1 – Indicate whether the test is applicable and if so, to which part(s) of the device, the combination of the parts, or the whole device. If the test is not applicable, explain why. For Option 2 – Indicate which part(s) of the device, the combination of the parts or the whole device	Discuss if the protocol for each test will be modified to incorporate the device design or use or in vivo conditions.	Discuss how the acceptance criteria may need to address the device design or use or in vivo conditions.	
Permeability					
Porosity (non-textile materials)	Determine the porosity of a tubular vascular graft constructed of synthetic, non-textile materials.	Applicable to the graft without sealant	N/A	N/A	No
Water entry pressure	Determine the pressure required to force water through a synthetic non-textile tubular vascular graft	Applicable to the whole graft	N/A	N/A	No

Water permeability	Determine the rate of water flow through the graft wall of a tubular vascular graft constructed with a water permeable material.	Not applicable because this test is for textile materials			No
Strength					
Circumferential tensile strength	Determine the circumferential tensile strength of the tubular vascular graft in its tubular form	Applicable to the whole graft	N/A	N/A	No
Diaphragm pressurized burst strength	Determine the burst strength of the tubular vascular graft in a flat form.	Not applicable because pressurized burst strength is more appropriate			No
Longitudinal tensile strength	Determine the longitudinal tensile strength of the tubular vascular graft in tubular form		N/A	N/A	No
Pressurized burst strength	Determine the pressurized burst strength of the tubular vascular graft in its tubular form	Applicable to the whole graft	N/A	> 300 mm Hg (about twice the highest pressure experience by the graft in vivo)	Yes

Probe burst strength	Determine the probe burst strength of the tubular vascular graft in flat form	Not applicable because pressurized burst strength is more appropriate			No
Strength after repeated puncture	Determine the strength of the tubular vascular graft following repeated dialysis-needle punctures	Applicable to the whole graft	N/A	N/A	No
Length	Determine the usable length of the tubular vascular graft.	Applicable to the whole graft	N/A	> 15 cm	Yes
Relaxed internal diameter	Determine the relaxed internal diameter of the tubular vascular graft	Applicable to the whole graft	N/A	6 ± 0.5 cm	Yes
Pressurized internal diameter	Determine the pressurized internal diameter of the tubular vascular graft under clinical conditions, if applicable.	Applicable to the whole graft	Will be tested under 120 mm Hg	N/A	No
Wall thickness	Determine the wall thickness of the tubular vascular graft.	Applicable to the whole graft	N/A	N/A	Yes
Suture retention strength	Suture retention strength	Applicable to the whole graft	Suture will need to be tied to the	> 2 N	Yes

			reinforcement mesh		
Kink diameter/radius	Determine the radius of curvature required to kink a tubular vascular graft	Not applicable because this graft is not designed to bend	N/A	N/A	No
Dynamic radial compliance	Determine the dynamic radial compliance of a tubular vascular graft constructed of an elastomeric material (e.g. polyurethane)	Applicable to the whole graft	N/A	N/A	Yes

6.4.2 Device-Specific Evaluation

Based on the Attachment 4 of last FDA feedback document, we populated Column 1 and Column 2 of **Table 6.8**. We listed several device or procedure attributes and would like to obtain feedback from the FDA before populating the rest of the table.

Table 6.8. *Device-Specific Evaluation*

Column 1	Column 2	Column 3	Column 4	Column 5	Column 6	Column 7	Column 8
Device or Procedure-Related Attribute	Potential Failure Modes	Potential Device Effects of Failure	Potential Clinical Effects of Failure	Leveraged Nonclinical Information	Supportive Clinical Information	Noncli-nical Device Testing	Clinical Study Mitigat-ion Strateg-ies

Each procedure-related function or performance-related function required for the device to achieve the desired performance.	For each Attribute, the types of problems or failures that might occur and could result in consequences to the device or study subject if the function or feature is not attained.	The potential effect(s) of the failure mode on the device.	The potential effect(s) of the failure mode on the study subject.	Non-clinical information leveraged from internal or external sources to support the assertions that the Device Attribute will be attained; and/or the Potential Failure Mode will not likely occur or will not be catastrophic to the patient if it does occur. For example, data from testing of a prototype device.	Relevant clinical experience obtained from internal or external sources for a similar device or indication to support the assertions that the Device Attribute will be attained; and/or the Potential Failure Mode will not likely occur or will not be catastrophic to the patient if it does occur.	The bench, laboratory, analytical, and/or animal testing of the study device (i.e., the device that will be used in the clinical study) to complete the evaluation of the Device Attribute and the Potential Failure Mode(s).	For each Potential Clinical Effect of Failure, the mitigation strategies included in the clinical protocol intended to minimize the frequency or severity of the potential clinical effects resulting from a failure to attain the attribute.

[Device] IMPRESSIVE vascular graft							
[Key Part or Feature and Purpose] Polyurethane graft wall							
Guide tissue integration	Inability to guide tissue integration						
Compliance	Lack of compliance						
[Key Part or Feature and Purpose] Surgical mesh reinforcement							
Provide suture strength	Failure to withstand suture						
Ensure long term stability	Lack of long term stability						
[Key Part or Feature and Purpose] Gelatin Sealant							
Hemostasis	Inability to seal the graft						
Appropriate degradation rate	Degrade too fast: blood leakage; Degrade too slow: foreign body capsule formation.						
[Combination of Specific Parts of the Component] Polyurethane graft all & surgical mesh reinforcement							
Implant integrity	breakage						
Whole Device							

Device deployment	Failure to be deployed to the desired location by surgery						
Device patency	Failure to remain patent						
Biocompatibility	Non-biocompatibility						

Chapter 7. Pushing the boundary of small diameter vascular grafts (future directions)

7.1 Introduction

This Chapter is sharply focused on rapidly bringing an immunomodulatory, *in situ* tissue engineered vascular prosthesis (IMPRESSIVE) (Ratner et al. 2018) to clinical trial. The *objective* of this project is to solve the 70-year unsolved problem of small diameter vascular prostheses by bringing together the regenerative, anti-scarring, precision porous scaffold (Lauran R. Madden et al. 2010) and the *de novo* designed immune cytokine technology (Silva et al. 2019).

The foreign material induced, *inflammation driven*, chronic fibrosis (foreign body response, FBR) results in the isolation of all FDA approved long-term implantable devices (including vascular prostheses) from the rest of the body by a dense, stiff, avascular, collagenous scar layer (foreign body capsule, FBC). Our *long-term goal* is to improve bio-integration and eliminate FBR associated with implantable devices and tissue engineering. Specific to current vascular prostheses, FBR intensifies the already intense mechanical mismatch between grafts and native blood vessels, which is hypothesized to lead to intimal hyperplasia. FBR inhibits the transmural healing of the endothelium that mitigates the long-term risks of thrombosis. FBR also isolates grafts of the body's immune defense system, creating an ideal location for infection. As the result, there are no FDA-approved grafts with inner diameters less than 5mm. Dialysis access AV grafts have a 1 yr. 50% failure rate. There are 1 million lower limb amputations globally, many attributed to the lack of a functional small-diameter graft. There are no prosthetic grafts suitable for the coronary artery (200,000/yr in the US).

In vitro tissue engineered vascular grafts has the potential to circumvent FBR by using human cells to construct vascular grafts free of foreign materials (Kirkton et al. 2019; Syedain et al. 2017). However, this approach is intrinsically complex, time-consuming, and expensive. We propose the simple, instantaneous, and affordable *in situ* tissue engineering approach using the pro-angiogenic, anti-scarring, precision porous "6S" material (Ratner and Marshall 2008a). This material has demonstrated seamless integration into bone (Osathanon et al. 2008), heart stroma (Madden et al. 2010), skin (Fleckman et al. 2012), and sclera (Teng et al. 2014). This material has received a CE mark for ophthalmic implants. And 6S material coated ePTFE grafts are currently in clinical trial in the US. We recently invented a complete 6S vascular graft that matches the mechanical property with native blood vessels (Ratner et al. 2018). *In side-by-side comparisons with ePTFE grafts in sheep models, 6S grafts demonstrated superior performance in terms of compliance, blood compatibility, and bio-integration.*

We found that the 6S material mitigate FBR and improve bio-integration by locally drives macrophages to an M2 (pro-regenerative) polarization (Sussman et al. 2014). This is highly consistent with the recent discoveries that type 2 inflammation, involving M2 macrophages (Brown et al. 2009), N2 neutrophils (Lin et al. 2017), and Th2 T cells (Sadtler et al. 2016), drives the bio-integration with biomaterials. Interleukin 4 (IL-4) is the cytokine that orchestrates type 2 inflammation. The short-term delivery of IL-4 reduces FBR (Hachim et al. 2017). However, native IL-4 may not be suitable for addressing FBR in the long term due to its intrinsic instability. In collaboration with the Baker Lab, we *de novo* designed a super-stable IL-4 mimic (Neo-4). Based on these observations and our preliminary data, our *central hypothesis* is that *vascular graft associated inflammation can be driven towards type 2 by matching mechanical property, pro-healing porous structure, and timely delivery of Neo-4 to enable the FBC-free and*

complete bio-integration in small diameter vascular prostheses. The *rationale* is that, *in situ* immunomodulatory approaches for enhancing bio-integration, once developed, can be readily generalized to improve implantable devices, tissue engineering, and regenerative medicine. Specific aims to test the central hypothesis and achieve our objective are:

1. Co-optimize the porous structure and mechanical properties of the IMPRESSIVE vascular grafts, and study their impacts on healing and immune responses of macrophages, neutrophils and T cells over time.

2. Optimize the timing and method for local delivery of de novo designed IL-4 mimic in IMPRESSIVE and PTFE grafts, and study how they impact inflammation, driving it in a regenerative manner.

3. Optimize small diameter vascular grafts (SDVG) designed for long term implantation by combining 6S regenerative scaffolds and de novo designed IL-4 mimic delivery strategies.

The sheep model is predictive of graft performance (i.e., pre-clinical evaluation). This model is expensive under GLP protocols, but provides meaningful data for the FDA. Strong preliminary results encourage us to request NIH funding to address FDA criteria leading to clinical trials.

7.2. Proposed Approach

7.2.1 Aim 1: Co-optimize the porous structure and mechanical properties of the IMPRESSIVE vascular grafts, and study their impacts on healing and immune responses of macrophages, neutrophils and T cells over time.

Introduction: Two factors hypothesized to be important for the patency of vascular grafts are: a porous structure that allows healing (Voorhees, Jaretzki, and Blakemore 1952; White et al. 1981; Clowes, Kirkman, and Reidy 1986), and matching mechanical properties of the graft and artery to minimize flow disturbances (Kidson 1983; Abbott et al. 1987). However, the co-optimization of both factors has not been achieved, especially in a relevant animal model. In addition, how these factors impact healing and fibrosis, and the underlying macrophages, neutrophils, and T cell responses have been incompletely examined. The *objective of this aim* is to co-optimize the porous structure and mechanical properties of the IMPRESSIVE graft in a sheep model, and direct the immunomodulatory effects of both factors to a non-fibrotic, pro-healing state. Our *working hypothesis* is that grafts with uniform 40 μm pores and mechanical properties matched with native blood vessels will maximize healing and mitigate intimal hyperplasia by driving the inflammation towards type 2 (pro-healing). Our *approach* to test this hypothesis is to assess the patency, histology, and immune cell phenotypes of grafts with different mechanical properties (stiff, matching, and soft, **SA1.1**) and porous structure (40 μm, 100 μm, and 40 μm externally wrapped, **SA1.2**). The optimized characteristics will be combined in the final grafts, which will be compared side-by-side with commercially available PTFE grafts in both AV and AA graft models (6-mm i.d.) from 1 week to 8 weeks. (**SA1.3**) The *rationale for this aim* is that co-optimization of both mechanical properties and the porous structure is the key to improving vascular graft performance. The understanding of how these factors modulate immune response, which in turn dictates healing, will lead to a rethinking of the design of implantable devices and

engineered tissues. Our *expectation* is that the optimized synthetic graft will heal into a living, beating blood vessel *in vivo* (*in situ* tissue engineering), and achieve scar-free, complication-free, and long-lasting symbiosis with native blood vessels. The *importance* of achieving this aim is that it paves the way for long-term and small-diameter grafts studies in sheep (**Aim 3**), which will justify future clinical trials.

Justification, feasibility, and preliminary data: There have been many attempts to optimize the porous structure of vascular grafts. The difficulty in reaching conclusions about the significance of porosity lies in the *inability of manufacturing grafts with a uniform porous structure*. (Clowes, Kirkman, and Reidy 1986; Wang et al. 2014) One group capable of manufacturing uniform porous structure concluded that large pores (>100 μm) are optimal based on reduced macrophage infiltration. (Bezuidenhout, Davies, and Zilla 2002) This reflects the difficulties in *properly understanding inflammatory responses*. In our lab, in ~30 studies, 100 μm pores always produce heavy fibrosis while 40 μm pores lead to vascularization and little fibrosis. The function of alternatively activated macrophages (M2) in orchestrating healing was not widely understood in 2002. *We invented the "6S" process* (Ratner and Marshall 2008a) that produces biomaterials with highly uniform pore structure (**Figure 7.1**). With this platform technology, we discovered that vascularization and minimal fibrosis are achieved when the pore are between 30-40 μm (Lauran R. Madden et al. 2010; Sussman et al. 2013). Materials with many different chemical compositions but the same porous structure have demonstrated seamless integration into bone (Osathanon et al. 2008), heart stroma (Madden et al. 2010), skin (Fleckman et al. 2012), and sclera (Teng et al. 2014). Based on these observations, *we hypothesize that a pore size of 40 μm is also optimal for healing in vascular sites*.

Mechanically matching vascular grafts to blood vessels has been explored. However, most studies rely on complex, bio-derived materials for generating these grafts presenting a significant barrier for translation. (Wise et al. 2011; Syedain et al. 2014) In addition, the premature degradation of bio-derived grafts is a major safety concern in clinical translation.

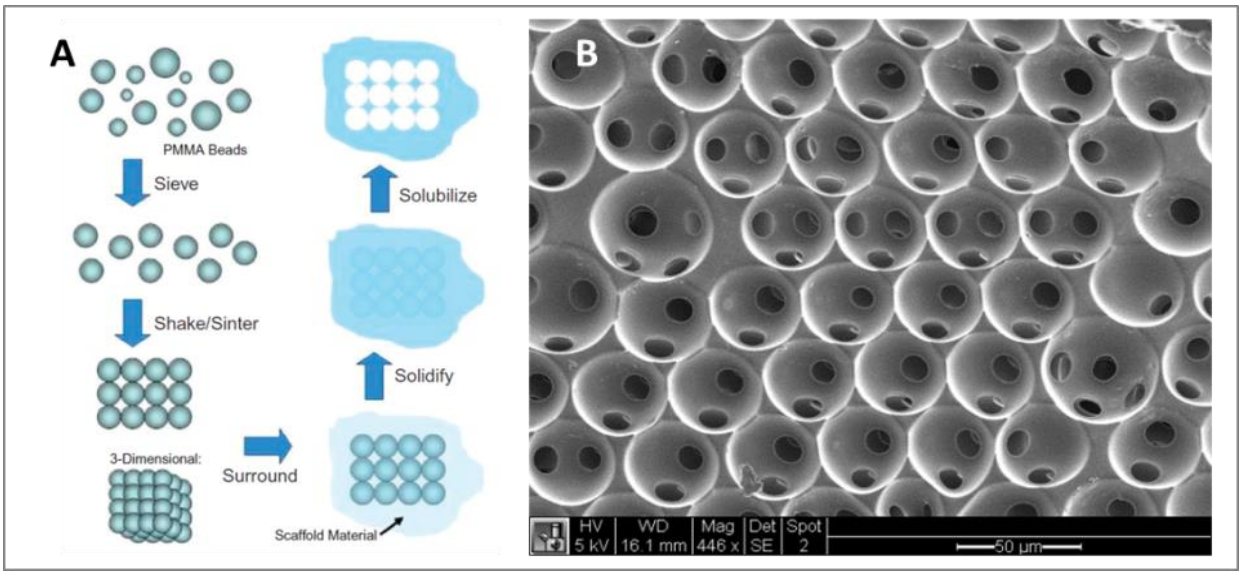

Figure 7.1. The "6S" process produces uniform porous structures. **A)** The *"6S" process:* PMMA beads were **s**ieved to uniform size, **s**haken until close-packed, **s**intered to create interconnectivity, and then **s**urrounded by monomer solution. The monomers were **s**olidified to form crosslinked polymer. The uniform porous scaffolds were generated by **s**olubilizing the PMMA beads. **B)** Scanning electron micrograph of the porous structure. Small black holes are interconnects.

Synthetic grafts mechanically matched to blood vessels also have been made. However, the FBR tough capsule leads to loss of compliance over time (White, Klein, and Shors 1986). We invented a synthetic, inexpensive, and biostable polyurethane material whose mechanical property can be tuned to match that of the native blood vessel (**Figure 7.2**). This material is compatible with the "6S" process and has been made into vascular grafts from 2 mm to 6 mm i.d. (Ratner et al. 2018). *This novel graft will simultaneously match the initial compliance and*

maintain the long-term compliance by mitigating fibrosis. In fact, 6S materials have such a significant effect on fibrosis reduction that the patency of PTFE grafts can be improved by simply coating their outer surfaces with 6S material. Healionics, a spinout from the Ratner Lab, is currently spearheading the clinical trial of a silicone-based 6S material-coated PTFE graft.

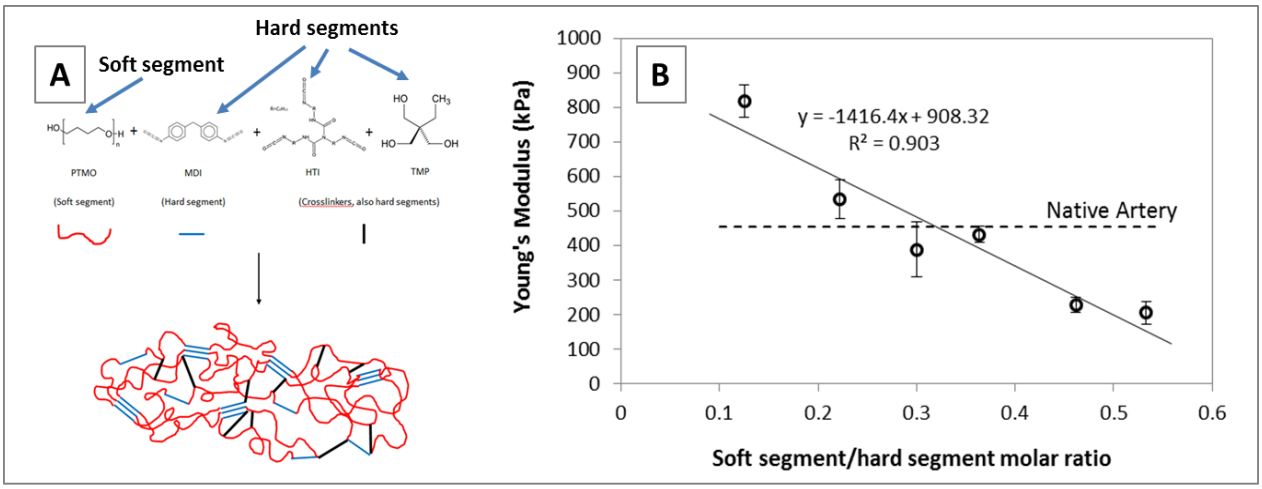

Figure 7.2. The biostable polyurethane (PU) material with tunable mechanical property. **A)** Chemical composition of the PU and its crosslinked, semi-crystalline structure; **B)** The mechanical property of the PU can be tuned to match that of the native blood vessel. *Method:* the PU was synthesized with one-step, catalyst-free, solvent-free method. Poly (tetramethylene oxide) (PTMO, Mw=1000, elastic soft segment), methylene diphenyl diisocyanate (MDI, crystalline hard segment), Desmodur N3200 (HTI, crosslinking hard segment), and 1,1,1-Tris(hydroxymethyl) propane (TMP, crosslinking hard segment) were mixed and reacted in 55 °C to form elastic PU.

We believe that we can further improve vascular graft patency by addressing two issues the Healionics approach does not: 1) although the stiffening effect from the FBR is mitigated, the mechanical mismatch between native blood vessel and PTFE is still large; 2) peri-vascular tissue still cannot integrate with the PTFE layer, thus the luminal surface is never healed. Our *goal* is to use a mechanically and structurally optimized 6S graft as an *in situ* tissue engineering scaffold to guide the regeneration of blood vessels. To achieve this goal, we have implanted 6S grafts with

40 μm pores and tuned mechanical properties as an A-A graft replacing the carotid artery (CA) and as an A-V graft in sheep for 4 weeks. Comparing side-by-side with standard PTFE grafts, every 6S grafts showed superior performance in terms of maintenance of pulsatile motion (**Supplement Video 1**), blood compatibility, and tissue integration (**Figure 7.3**). In both A-A and A-V graft models, the luminal surfaces of 6S grafts were almost completely cellularized, while PTFE grafts were almost complete covered by thrombi. (**Figure 7.3A & B**) Immunohistochemistry shows that the luminal surface of 6S grafts are partially covered by endothelial cells and healthy smooth muscle cells organized in a way similar to that of the native blood vessel. (**Figure 7.3C**) Note that the pores of the 6S material (stained black by Sudan Black B) were infiltrated by large blood vessel structures resembling the *vasa vasorum* in the wall of native artery. Based on these observations, *we hypothesize* that *endothelialization of the luminal surface will occur when endothelial cells from the peri-graft tissue infiltrate the graft wall (transmural ingrowth) and reach the luminal surface*. We will test this hypothesis by comparing 40 μm 6S grafts with externally wrapped 6S grafts. (**SA 1.2**)

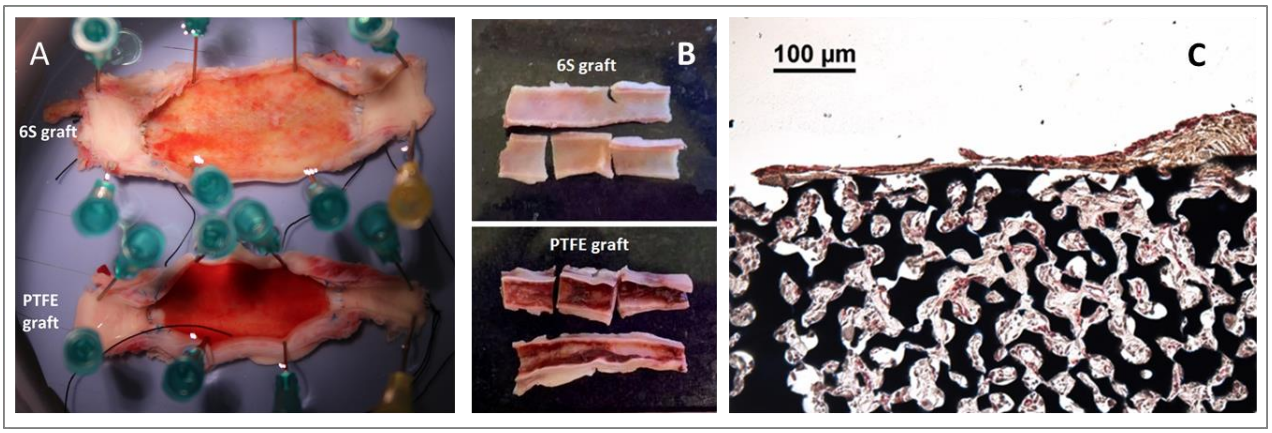

Figure 7.3 6S grafts outperform PTFE grafts in sheep models. A) Luminal surfaces of a 6S graft and a PTFE graft after 4 weeks grafted in each side of the carotid arteries in the same sheep; B) Luminal surfaces of a 6S graft and a PTFE graft after 4 weeks of implantation as AV grafts in two sheep; C) Double staining of endothelial cell marker CD 31 (red) and smooth muscle cell marker smoothelin (brown) on the luminal side of explanted 6S grafts. Note: All grafts were

opened in the longitudinal direction and vigorously rinsed with heparinized saline immediately after explant to remove loosely attached material.

Research design: The general strategies of Aim 1 are first to optimize the mechanical properties (1.1) and porous structure (1.2), then compare the optimal 6S grafts side-by-side with PTFE grafts and study their inflammatory responses over time (1.3). Our laboratory has been involved in vascular graft research for more than 40 years. The PI is a leading scientist on immunomodulatory and regenerative biomaterials. The laboratory has published multiple high impact papers on the subject (Madden et al. 2010; Sussman et al. 2013; Zhang 2013). All the essential techniques to achieve this aim, including polymer chemistry, precision polymer processing, clinically relevant sheep vascular graft models, histology, and immunohistochemistry are well-established in our laboratory.

The FDA guidance document and ISO 7198: 2016 state that "each type of vascular prosthesis shall be tested by implantation at the intended, or an analogous, vascular site in a reasonable number of animals (i.e. at *least six*)". Considering the high cost of the sheep model, we will do 6 biological replicates for each experimental group. We expect this to provide sufficient statistical power to answer the scientific questions. Whenever appropriate, we will implant two grafts from different groups in one sheep to minimize animal usage.

7.2.1.1 Optimize the mechanical property of 6S grafts

Preliminary data (**Figure 3B**) demonstrate that we can fine tune the mechanical properties of our material to match 2X stiffer, and 2X softer then the native blood vessel by changing the soft

segment/hard segment ratio. To maximize the chance of eliciting significant differences in the *in vivo* model, we will develop materials even softer and even stiffer by changing the molecular weight (Mw) of the soft segment. Higher Mw will make a softer material and lower Mw will make a stiffer material. To monitor the Mw of the soft segment, we are requesting funding for purchasing a gel permeation chromatography (GPC) apparatus, standard equipment for this kind of work. After we produce appropriate soft and stiff materials, we will make 6S grafts with 40 μm pores. We will implant these three groups with 12 cm long grafts as AV grafts in 6 sheep per group for 2 months. The compliance of each graft will be measured *in vitro* before implant an*d again once harvested* after 2 months of implantation (Klein et al. 1982). The sheep AV graft model is selected for this aim because intimal hyperplasia is the primary failure mode for AV grafts (Swedberg et al. 1989) and mechanical mismatch is widely hypothesized to cause of intimal hyperplasia (Trubel et al. 1995). The two month time point is established considering the stiffening from the FBR that is thought stabilize by two months (White, Klein, and Shors 1986). Patency of the grafts will be monitored and recorded daily by finger palpation, and every two weeks by ultrasound. Upon sacrifice, all grafts will be harvested with surrounding tissue. Half of each graft, including the arterial anastomosis, the venous anastomosis, and the mid graft section beyond 2 cm from both anastomoses, will be fixed and processed for histology and immunohistochemistry. FBR, cellular integration, and inflammatory responses will be examined. The other half will be immediately frozen in 10% DMSO for other tests. Aim 1.1 will use 18 sheep.

7.2.1.2 Optimize the porous structure of 6S grafts and identify the source of healing

One of the advantages of the 6S process (**Figures 7.1**) is that we can easily and precisely manufacture porous materials of different pore sizes with narrow pore size distributions. We have published multiple papers detailing the effect of pore size on healing and the FBR in mice and rats (Sussman et al. 2013; Madden et al. 2010). However, it is well-known that mice and rats heal much faster and develop less fibrosis than humans. Thus, *it is both novel and significant to study the clinical relevance of the sheep model*. In the context of vascular graft research, endothelialization is a controversial subject. Three possible sources of endothelial cells are transanastomosis ingrowth, transmural ingrowth and/or progenitor cells from blood. Transanastomotic ingrowth is not seen in humans beyond 1 cm from the anastomosis (Berger et al. 1972). Clowes et al. (1986) demonstrated the significant role of transmural healing. However, the same group also showed the possibility of progenitor cells using an externally wrapped graft model (Shi et al. 1994). By wrapping the outer surface of the porous vascular graft with an impermeable silicone layer, this model is able to isolate the contribution of progenitor cells to healing. This model can shed new light into the recent explosion of research on tissue resident versus blood monocyte derived macrophages. Macrophages were previously perceived as terminally differentiated and their accumulation in the inflammation site was thought to be solely due to blood monocyte recruitment. A landmark paper challenged this view by discovering that tissue resident macrophages, driven by IL-4, can proliferate in type 2 inflammation (Jenkins et al. 2011). This new knowledge is highly significant to tissue engineering and regenerative medicine, considering the crucial role of type 2 inflammation in regeneration. However, this research was done in mice, thus its clinical relevance is unclear. Given the sophisticated genetic manipulation normally required for cell fate mapping, it is extremely difficult to verify this study in clinically relevant animal models. Our proposed vascular graft study can answer this question.

Consider that outside of the graft is tissue, and inside the graft is blood. Once the external surface is made impermeable, the impact of blood recruited macrophages will be clarified. A nuance in the 6S fabrication process is that it naturally generates an impermeable thin film on the outer surface (we routinely peel off this skin layer to generate an open porous structure to allow cell infiltration from surrounding tissue). In Aim 1.2, we intentionally include a group prepared without the scraping process (40 μm externally wrapped) to isolate the effect of blood-origin cells on healing. *This is significant because it offers a simple yet effective model to answer the question of the contributions of blood-origin and tissue resident macrophage on healing.* In the case of a mixed population of blood-derived and tissue resident macrophages in open pore grafts, CCR2 and TIMD4 antibodies can be used to distinguish the two types of macrophages (Dick et al. 2019).

For this aim we will use the carotid artery AA graft model in sheep, in which two grafts can be implanted in one sheep. Thus, we only need 9 sheep for all three groups (40 μm, 100 μm, 40 μm externally wrapped) for replicates of 6. Sheep will be sacrificed at 1 week, 2 weeks, 4 weeks, and 8 weeks. Detailed histology will be conducted to examine healing, fibrosis, and inflammatory responses. Aim 1.2 will use 36 sheep.

7.2.1.3 Compare the performance and inflammatory responses of optimized 6S and PTFE grafts

The 6S grafts with optimal mechanical properties and porous structure identified in 1.1 and 1.2 will be compared with ePTFE grafts, side-by-side, as both AA grafts (6mm) and AV grafts (6mm) in the sheep model. *The significance of this aim is twofold: 1) generate short-term to mid-term efficacy data with the goal of translation; 2) provide insight into the differences in inflammatory responses of pro-healing versus pro-fibrotic materials*. One 6S graft and one PTFE

graft will be implanted in each side of the carotid artery in the AA graft model, thus it takes 6 sheep to compare the two groups. In the AV graft model, one graft can be implanted in each sheep, so 12 sheep are required to compare the two groups. Sheep will be sacrificed at 1 week, 2 weeks, 4 weeks, and 8 weeks. A total of 72 sheep are needed for this aim. Upon sacrifice, grafts will be harvested and processed as described in 1.1 and 1.2. Detailed histology will be performed to quantify tissue integration, fibrosis, and intimal hyperplasia. Types 1 and 2 inflammation will be quantified by immunohistochemistry staining of N1 ($Ly6G^+CD54^+$) and N2 ($Ly6G^+IL\text{-}4^+$) neutrophils (Lin et al. 2017), M1 ($CD64^+CCR7^+$) and M2 ($CD64^+CD206^+$) macrophages (Dekker et al. 2018) and Th1 ($CD3^+$ $IFN\gamma^+$) and Th2 ($CD3^+IL\text{-}4^+$) T helper cells (Sadtler et al. 2016). Multiple markers will be used to corroborate the findings. We chose immunohistochemistry as the primary quantification because: 1) the bio-stable synthetic scaffold cannot be solubilized, thus cells cannot be taken out of the graft for flow cytometry; 2) we found that inflammatory responses to biomaterials are highly location dependent (inside the pores, at the interface, and tens of microns away from the material all have different responses) (Sussman et al. 2013). Such spatial dependence cannot be captured by PCR and other DNA/RNA analysis. We have verified 10 essential antibodies for the sheep study. All slides will be scanned, and quantified in blinded studies in the UW histology core. These analyses will also be applied to other aims proposed.

Expected outcomes: The objective of this aim is to co-optimize the mechanical property and porous structure of 6S grafts based on performance (patency) and histology (fibrosis, bio-integration, intimal hyperplasia) outcomes, and then study the detailed inflammatory responses to a pro-healing material (6S) and a pro-fibrotic material (PTFE). We expect to conclusively identify optimal mechanical properties (1.1), optimal pore structure and origin of pro-healing

cells (1.2). We expect to gain a detailed understanding of inflammatory responses to pro-healing and pro-fibrotic materials (1.3). *This aim will facilitate clinical translation of in situ tissue engineering grafts and advance clinical interventions to inhibit fibrosis and promote healing*.

Potential pitfalls and alternative approaches: Our working hypothesis of this aim is that optimal mechanical property and porous structure will improve graft performance, bio-integration, and reduce fibrosis by driving the inflammatory response towards type 2. Although the view that type 2 inflammation promotes healing is strongly supported by the literature (Brown et al. 2009; Sadtler et al. 2016; Lin et al. 2017), there is a possibility that type 1 inflammation, especially in the acute phase, also contributes to healing (Spiller et al. 2015). A strength of our approach is that we do not depend on the type 2 inflammation hypothesis to achieve our aim. All optimization will be done based on the graft performance outcomes (patency, bio-integration, fibrosis, and intimal hyperplasia) that can be unambiguously assessed. Thus, we will establish the association between inflammatory responses and desirable outcomes. Regardless of the type of inflammation observed and how it will associate with outcomes, such observation will be significant in guiding the improvement of graft designs. Another potential pitfall could be the equipment used might not be sensitive enough to accurately measure compliance after *in vivo* experiments. Were this problem to arise, we would use the frozen half of the AV graft for highly sensitive *in vitro* compliance measurements.

7.2.2 Aim 2: Optimize the timing and local delivery of de novo designed IL-4 mimic in IMPRESSIVE and PTFE grafts, and study how they impact inflammation, driving it in a regenerative manner.

Introduction: Type 2 inflammation including M2 macrophages (Brown et al. 2009), N2 neutrophils (Lin et al. 2017), and Th2 T cells (Sadtler et al. 2016) are widely recognized as

central to biomaterial bio-integration. IL-4, a cytokine directing type 2 inflammation, is the logical choice for enhancing bio-integration. Short-term, local delivery of IL-4 has been demonstrated to improve bio-integration (Hachim et al. 2017). Sequential delivery of INFγ and IL-4 also has been shown to promote angiogenesis (Spiller et al. 2015). However, these short-term delivery approaches may not address the chronic fibrosis in long-term implants. To date, long-term IL-4 delivery or permanent IL-4 immobilization on biomaterials has not been explored. Three potential roadblocks to such an approach are: 1) IL-4 lacks long-term stability; 2) there is no convenient way to site-specifically immobilize IL-4, and random immobilization can inactivate it; 3) IL-4 might be associated with fibrosis through pleiotropy. David Baker's lab at the UW developed the first *de novo* designed highly stable cytokine, an IL-2 mimic that resists boiling and is more effective and selective than its native counterpart (Silva et al. 2019). In collaboration with the Baker Lab, we developed the second *de novo* designed stable cytokine, an IL-4 mimic (Neo-4). *We propose that the immobilization of Neo-4 has the potential to overcome all three roadblocks and achieve bio-integration in a long-term implant.* Our *objective* is to mitigate fibrosis and promote healing in both PTFE and 6S grafts by timely and local delivery of Neo-4. The *working hypothesis* is that site-specific, permanent immobilization of Neo-4 is optimal for bio-integration. To test this hypothesis, we devised a three-step *approach*: 1) obtain the appropriate version of Neo-4 and develop delivery strategies using sheep macrophages *in vitro* (**SA 2.1**); 2) optimize Neo-4 delivery strategies with PTFE grafts in a sheep model (**SA 2.2**); 3) study the effects that optimal Neo-4 delivery has on graft performance and inflammatory responses in both 6S and PTFE grafts (**SA 2.3**). Our *rationale* for this aim is to bring about a generalizable strategy to reduce fibrosis and promote healing. We *expect* that the optimized Neo-4 delivery strategy will enhance the performance of both 6S and PTFE grafts. The *significance* of

achieving this aim is that this strategy can be applied to many implantable devices, tissue engineering and anti-inflammation therapies.

Justification, feasibility, and preliminary data: Type 2 inflammation orchestrates bio-integration into regenerative biomaterials (Brown et al. 2009; Sadtler et al. 2016; Lin et al. 2017). Although involving multiple cell types (macrophages, neutrophils, T cells), type 2 responses converge on the indispensable role of IL-4. Indeed, short-term IL-4 delivery improves bio-integration (Hachim et al. 2017), however, it's not sufficient to mitigate chronic fibrosis in long-term implants. The oriented and permanent immobilization of stable Neo-4 has potential in achieving long-term bio-integration. Although persistent IL-4 expression is sometimes associated with fibrosis (Huaux et al. 2003), only IL-13 knock-out mice, not IL-4 knock-out mice, showed reduction of fibrosis (Kolodsick et al. 2004). IL-4 is probably associated with fibrosis through cross-reacting the IL-13 receptor and only in combination with TNF-α (Fichtner-Feigl et al. 2006). It is unlikely that IL-4 alone is the culprit for fibrosis. Our preliminary data strongly suggest that type 1 inflammation, instead of type 2 inflammation is associated with biomaterial-induced fibrosis (**Figure 7.4**).

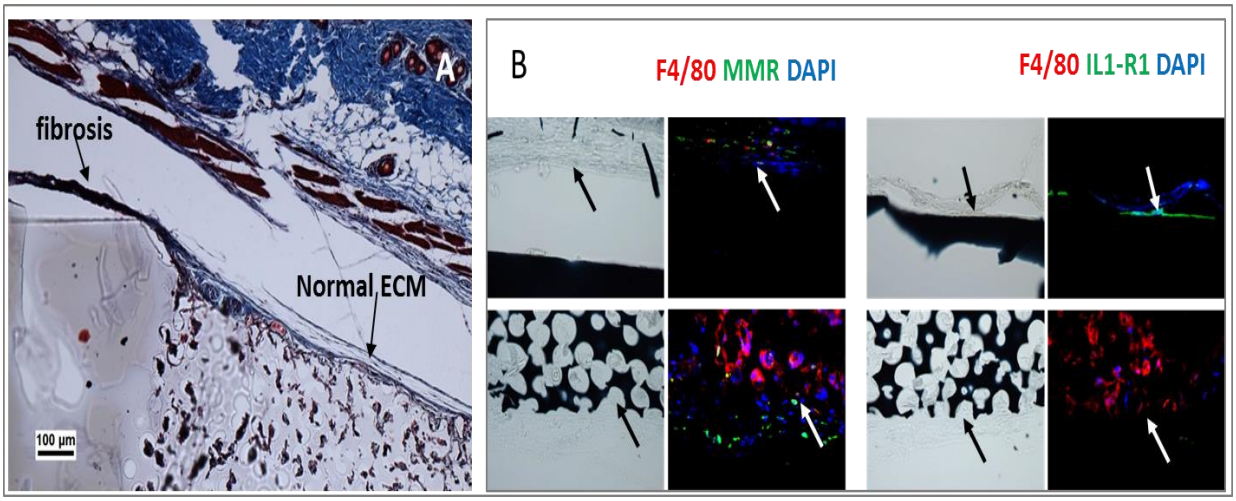

Figure 7.4 Type 1 inflammation is associated with biomaterial induced fibrosis. A) Masson's trichrome staining of a 3-week subcutaneous mouse implant of a single piece of PU material containing a nonporous part (left) and a 40 μm porous part (right). The nonporous part was encapsulated by dense, fibrotic scar, while the 40 μm porous part was surrounded by diffuse, normal extracellular matrix. B) Immunofluorescence staining of M1 (F4/80+IL1-R1) and M2 (F4/80+MMR) macrophage responses to nonporous and 40 μm porous PU. To aid the visualization of tissue and PU material (stained black by Sudan Black B), the corresponding bright field image is shown on the left of each IF image. Arrows are pointing at the interfaces between tissue and PU material. Note that a single layer of M1 macrophages is seen at the surface of nonporous material, co-localizing with dense fibrotic scar. M1 macrophages are absent, and M2 macrophages are present on the surface of 40 μm porous PU.

The first *de novo* designed cytokine, the IL-2 mimic, is revolutionary, because it not only enhances the therapeutic effect for cancer treatment, but also reduces the side-effects by eliminating the cross-reactivity with CD25, a receptor associated with toxicity (Silva et al. 2019). By applying the same designing principle, Dr. Umut Ulge is able to create the second *de novo* designed cytokine, Neo-4. **Figure 7.5A** shows Neo-4 binding to IL-4Rα and γ_C, the receptors that trigger type 2 inflammation. Neo-4 shows comparable efficiency to IL-4 in activating STAT6, the transcriptional factor required for type 2 inflammation (**Figure 7.5B**). In addition, the super-stable structure of Neo-4 is unaffected by heating up to 95 °C (**Figure 7.5C**). We have developed two versions of Neo-4 for both human and mice. Based on these promising data, we strongly believe that permanent immobilization of Neo-4 on a biomaterial surface will elicit sustained type 2 inflammation. Such type 2 inflammation can shut off the type 1 inflammation seen on the surfaces pro-fibrotic materials.

Research design: Our strategy for this aim is first to verify the effectiveness of Neo-4 and immobilization techniques on sheep cells *in vitro* (2.1), then to optimize the method and timing

of delivery with PTFE grafts in sheep (2.2), and finally to compare the effect of the optimized Neo-4 delivery on 6S and PTFE grafts (2.3).

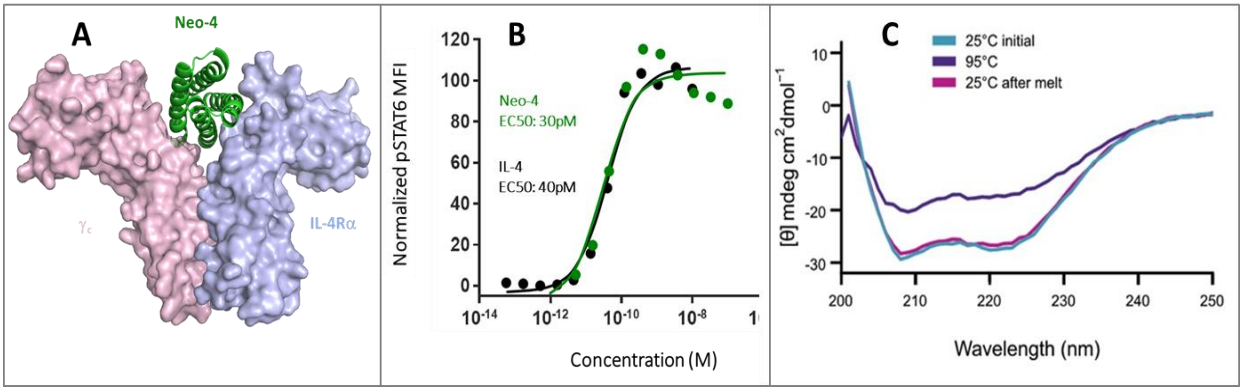

Figure 7.5. The *de novo* designed Neo-4. **A)** Model of Neo-4 bound to IL-4Rα and γ_C. **B)** STAT6 phosphorylation in human Ramos 2G6 cells (Courtesy Dr. Jamie Spangler, Johns Hopkins University). **C)** The thermostability of the protein is seen in its circular dichroism ellipticity spectra before, during and after heating to 95°C. The ellipticity of an unstructured protein would be zero at all wavelengths. The alpha-helical structure of Neo-4 causes the characteristic curve seen in the initial spectrum at 25°C. Heating to 95°C only partially reduces the alpha helical signal, and this change is complete reversed by cooling back to 25°C. (Courtesy Dr. Umut Ulge, University of Washington)

7.2.2.1 Obtain the appropriate version of Neo-4 and develop delivery strategies in vitro

We have successfully produced both human and mouse Neo-4. The first question we need to answer is whether the human Neo-4 will cross-react with the sheep receptor. The sequences of IL4 in human and sheep are more similar than human and mouse, which supports that sheep is a more clinically relevant model. There are only 4 amino acid differences in sheep IL-4 that contact IL-4Rα and that are accommodated by compensatory mutations in the receptor, thus it is possible that human Neo-4 will cross-react with sheep receptor. This is the ideal scenario. We will verify the cross-reactivity by exposing sheep blood derived macrophages to human Neo-4 *in*

vitro. The result will be quantified with flow cytometry and PCR. If human Neo-4 is proven to cross-react with sheep receptor, we will proceed to immobilization. If human Neo-4 does not react with sheep receptor, a sheep Neo-4 will be generated by modifying its IL-4Ra interface to resemble the sheep IL-4 sequence, similarly to how mouse Neo-4 was made. (Note that any protein development work is not within the scope of funding requested by this grant. This aspect of the research is fully funded internally by Neoleukin Therapeutics, Inc. All the rights to developed proteins belong to Neoleukin Therapeutics.)

The next step is to immobilize Neo-4 on the surface of PTFE. For *permanent immobilization*, we will introduce OH groups on the surface using well-established plasma deposition of relatively intact poly (2-hydroxyethyl methacrylate) (pHEMA), pioneered by our lab (Lopez et al. 1993). This method is applicable to any surface. Then, a double bond is grafted onto the OH group by reaction with 2-isocyanatoethyl methacrylate. Finally, click-chemistry (Li et al. 2010) will be use to form covalent bonds between the double bond and primary thiol group on Neo-4. Note that a thiol group is site-specifically engineered in the sequence of Neo-4 away from the receptor interface. This allows us to control the orientation of immobilized Neo-4 for optimal activity. Because the structure of Neo-4 is vastly different from IL-4, IL-4 antibody does not recognize Neo-4. To allow the detection of Neo-4, a terminal myc polypeptide tag can be added to Neo-4 to render it readily detectable by anti-myc antibody. The immobilization will first be verified by staining with anti-myc antibody. The binding of Neo-4 will be confirmed by FC tagged IL-4 receptor and staining with FC antibody. Finally the immunomodulatory effect of the immobilized Neo-4 will be verified in a sheep macrophage seeding study. To create a *transient immobilization* Neo-4, PTFE will be impregnated with gelatin. The gelatin will be crosslinked adequately to cause degradation to occur over about two weeks *in vivo;* Neo-4 will be released as

the gelatin degrades. This technique is well-established in our lab. Since 2-Isocyanatoethyl methacrylate readily reacts with the amine and carboxyl groups of proteins, Neo-4 can be immobilized on the gelatin with the same click chemistry. Finally, to test whether initial type 1 inflammation improves bio-integration, the PTFE can be soaked in IFN-γ for its immediate release.

7.2.2.2 Optimize Neo-4 delivery strategies with PTFE grafts in sheep model

Five PTFE treatment groups (transient Neo-4, permanent Neo-4, transient + permanent Neo-4, immediate IFN-γ + transient Neo-4, immediate IFN-γ + transient Neo-4 + permanent Neo-4) will be implanted as AA grafts in carotid arteries in sheep for 2 months. Since we are implanting two grafts in one sheep, it will require only 15 sheep to achieve six biological replicates for all five groups. The five groups cover all the major hypotheses proposed in the literature. Two months is chosen to allow full release of transiently immobilized cytokine. This way we can assess whether short-term release can affect long-term outcomes. We chose PTFE instead of 6S grafts for optimization because 6S grafts are already very pro-regenerative, so any pro-regenerative effects of Neo-4 delivery may be more difficult to detect using the 6S material. Based on our preliminary data (**Figure 4**), we hypothesize that transient Neo-4 + permanent Neo-4 will produce the optimal results.

7.2.2.3 Study the effects that the optimal Neo-4 delivery strategy has on both 6S and PTFE grafts

The optimized Neo-4 delivery method will be applied to both 6S and PTFE grafts. The two kinds of grafts will be implanted side-by-side in the same sheep in carotid arteries. Thus, it only

takes 6 sheep to achieve biological replicates for both groups. Sheep will be sacrificed at 1 week, 2 weeks, 4 weeks, and 8 weeks. Patency, fibrosis, intimal hyperplasia and bio-integration will be examined as described earlier. Detailed inflammatory responses will be studied. This sub-aim will provide short-term to mid-term efficacy data to inform a long-term study.

Expected outcomes: Our objective for this aim is to optimize the method and timing of Neo-4 delivery to improve vascular performance. We expect to develop immediate, short term, and long term delivery strategies for immunomodulatory cytokines (2.1) and identify the strategy or combinations of strategies for optimal vascular grafts performance (2.2). Then, we will study the detailed immune reposes to the optimal strategies and how they affect performance (2.3). This is the first proposed research to apply a *de novo* designed cytokine to improve bio-integration. This approach can be applied to many implantable device and tissue engineering. The achievement of this aim will justify a long term study aimed at translation.

Potential pitfalls and alternative approaches: Based on the strong consensus in the literature and our preliminary data, we believe our hypothesis that long-term Neo-4 signal delivery improves bio-integration is justified. We recognize the alternative hypothesis that long-term Neo-4 could promote fibrosis through IL-13 cross-reactivity. Should this result arise, we would request a version of Neo-4 that does not cross-react with IL-13 receptor. Neoleukin Therapeutics has demonstrated the capability to generate such protein (Silva et al. 2019). Another potential pitfall is that Neo-4 might be unable to bind its receptor due to steric hindrance from the biomaterial surface. In this case, we would request a version of Neo4 that includes a peptide linker between the thiol group and the body of the protein; the added steric flexibility should solve the problem.

7.2.3 Aim 3: Optimize small diameter vascular grafts (SDVG) designed for long term implantation by combining 6S regenerative scaffolds and de novo designed IL-4 mimic delivery strategies.

Introduction: Currently, there is no FDA approved vascular prosthesis under 5 mm inner diameter. FDA approved PTFE access grafts for hemodialysis has a failure rate of 50% after one year of implantation. *In vitro* tissue engineered grafts will be too complex and expensive to manufacture. There is an urgent need to bring new, affordable, high performance vascular grafts to clinical trial. We believe that the IMPRESSIVE graft offers such an opportunity. All approvals for clinical trials require long-term data in a clinically relevant animal model performed under GLP protocols. The FDA requires at least 5 months study to justify clinical trials. Our *objective* is to generate the long-term data to justify clinical trials in both medium diameter grafts and small diameter grafts. Our *working hypothesis* is that the IMPRESSIVE grafts will demonstrate superior performance compared to PTFE grafts as a medium diameter vascular prosthesis, and the optimized IMPRESSIVE grafts will be able to function long-term as a SDVG. Our *approach* for achieving this aim is to first conduct a long term study comparing first generation IMPRESSIVE grafts with PTFE grafts (**3.1**), and then to perform a long term study on 4mm grafts with the optimal design identified in previous aims (**3.2**). Finally, we will explore 2 mm grafts with the optimal IMPRESSIVE design (**3.3**). Our *rationale* for this aim is to maximize clinical translation of cutting edge technology to life-saving devices. We *expect* to spin out one or more clinical trials from this aim. The *significance* of this aim is that it has a potential to positively impact millions of patients, if a functional SDVG were to exist.

Justification, feasibility, and preliminary data: We have implanted the IMPRESSIVE grafts both as AA grafts (6 mm) and AV grafts (6 mm) side-by-side with PTFE in 10 sheep. In every

case, the IMPRESSIVE demonstrates superior performance compared to PTFE grafts. These preliminary data can justify a long-term study on the first generation IMPRESSIVE graft (40 μm pores, matching mechanical properties, no Neo-4). Through Aim 1 and Aim 2 of this grant, we will develop an optimized version of the IMPRESSIVE graft. The second generation IMPRESSIVE grafts will be studied long-term in a 4 mm i.d. configuration, and then a 2 mm configuration.

Research design: Our strategy is to immediately start the long term study on first generation IMPRESSIVE medium diameter AA and AV grafts with the aim of rapidly bringing this technology to clinical trial. If optimized IMPRESSIVE grafts demonstrate significant improvement in performance, a long-term study on second generation IMPRESSIVE will also be conducted (3.1). With the information learned from 3.1 and aims 1 and 2, we will conduct a long term study on 4 mm AA grafts (3.2). Building on all the lessons learned from previous aims, we will conduct a long term study on 2 mm coronary bypass grafts (3.3). We have chosen American Preclinical Services to conduct the long-term sheep study. This research organization is responsible for bringing other grafts to clinical trial and is highly competent in conducting FDA recognized preclinical research under GLP.

7.2.3.1 Optimize long-term performance of 6 mm IMPRESSIVE grafts as both AA and AV grafts.

We will start the long term study on first-generation IMPRESSIVE grafts (6 mm i.d., 40 μm pores, matching mechanical properties, no Neo-4) as both AA grafts and AV grafts immediately after the funding is granted. Standard PTFE grafts will be used as the control. A total of 18 sheep will be used in the 5 month implantation study. All the results will be analyzed, compiled, and presented to the FDA by the end of the second year. This will open the way for a first clinical

trial at the 3rd year of this project (not funded by this research effort). If the optimization in Aim 1 and Aim 2 generates a significantly better version of IMPRESSIVE, we will perform a long-term study on the second-generation IMPRESSIVE later into the project. Since we will already have well-established PTFE data by this point, the second round of long term studies will only take 12 sheep.

7.2.3.2 Optimize the performance of 4 mm IMPRESSIVE grafts as femoral bypass grafts.

We will use optimized IMPRESSIVE 4 mm grafts. We have examined the vascular bed of the sheep model and found the femoral artery can receive such grafts as long as 6 cm. Two grafts can be implanted in sheep. Since standard PTFE grafts are not approved for such application, we will not use them as the control. Instead, we will use the optimized PTFE grafts identified in Aim 2 as the control. We will first conduct a 4-week study with optimized IMPRESSIVE and optimized PTFE implanted side-by-side. If the optimized PTFE performs poorly in the short term study and is unlikely to last to 5 months, we will implant optimized IMPRESSIVE on both sides for the long term study. If the optimized PTFE performs well in the short term study, we will simply repeat the study for long term. We expect this aim to take 12 sheep.

7.2.3.3 Optimize the performance of 2 mm IMPRESSIVE grafts as coronary bypass grafts.

Optimized IMPRESSIVE will be used for the 2 mm coronary bypass graft study. Since no synthetic graft is approved for this use, no control will be included. A 4-week short term study will be conducted first to identify potential problems. If no concerns are observed, we will conduct the long term study. We expect this aim to use 12 sheep.

Expected outcomes: We expect to demonstrate high patency in the long term for medium diameter AA and AV grafts (3.1), small diameter femoral bypass grafts (3.2) and even coronary bypass graft (3.3). These results can lead to multiple clinical trials of high performance, medium and small diameter vascular grafts.

Potential pitfalls and alternative approaches: One potential concern for small diameter grafts might be acute thrombosis. Given the excellent blood compatibility IMPRESSIVE has demonstrated in the preliminary data (**Figure 3**), we do not expect thrombotic occlusion to occur. Should this problem arise, we would incorporate anticoagulants in the graft design and develop better anticoagulation regimes for the sheep.

7.3 Timeline

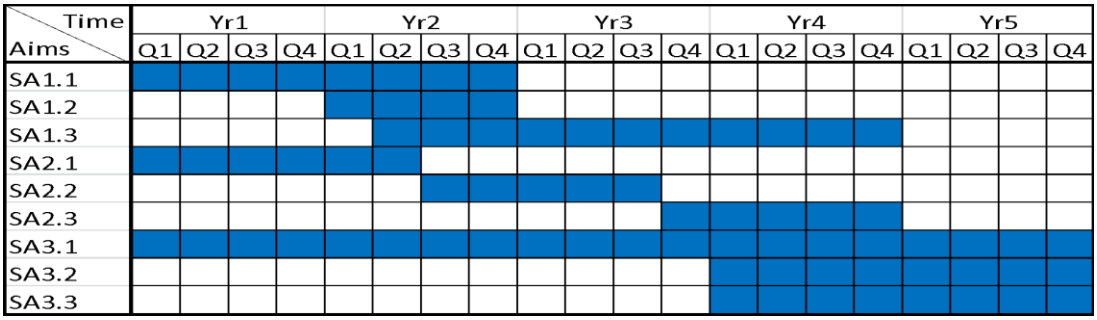

7.4 Conclusion and future directions

In concluding this project, we expect to enable several clinical trials on medium and small diameter vascular grafts. We will gain a detailed understanding of inflammatory responses to pro-healing and pro-fibrotic vascular grafts. We will develop generalizable strategies to drive the inflammation response towards healing. In future clinical trials, especially in the AV graft trial, we will conduct the same detailed study on inflammation in routinely retrieved graft samples. We will obtain knowledge of how inflammation in humans orchestrates fibrosis and healing. All

the knowledge gained will guide us to achieve our long-term goal of improving bio-integration and eliminating fibrosis associated with implantable devices and tissue engineering.

Bibliography

Abbott, William M., Joseph Megerman, Jonathan E. Hasson, Gilbert L'Italien, and David F. Warnock. 1987. "Effect of Compliance Mismatch on Vascular Graft Patency." *Journal of Vascular Surgery* 5 (2): 376–82.

Ahmed, Maqsood, George Hamilton, and Alexander M. Seifalian. 2014. "The Performance of a Small-Calibre Graft for Vascular Reconstructions in a Senescent Sheep Model." *Biomaterials* 35 (33): 9033–40.

Albrektsson, Tomas, Christer Dahlin, Torsten Jemt, Lars Sennerby, Alberto Turri, and Ann Wennerberg. 2014. "Is Marginal Bone Loss around Oral Implants the Result of a Provoked Foreign Body Reaction?" *Clinical Implant Dentistry and Related Research* 16 (2): 155–65.

Anderson, James M., Analiz Rodriguez, and David T. Chang. 2008. "Foreign Body Reaction to Biomaterials." In *Seminars in Immunology*, 20:86–100. Elsevier.

Anghelina, Mirela, Padma Krishnan, Leni Moldovan, and Nicanor I. Moldovan. 2004. "Monocytes and Macrophages Form Branched Cell Columns in Matrigel: Implications for a Role in Neovascularization." *Stem Cells and Development* 13 (6): 665–76. https://doi.org/10.1089/scd.2004.13.665.

Ashby, M. F. 2006. "The Properties of Foams and Lattices." *Philosophical Transactions of the Royal Society A: Mathematical, Physical and Engineering Sciences* 364 (1838): 15–30.

Ballyk, Peter D., Colin Walsh, Jagadish Butany, and Matadial Ojha. 1997. "Compliance Mismatch May Promote Graft–Artery Intimal Hyperplasia by Altering Suture-Line Stresses." *Journal of Biomechanics* 31 (3): 229–37.

Bascom, John U. 1961. “Gelatin Sealing to Prevent Blood Loss from Knitted Arterial Grafts.” *Surgery* 50 (3): 504–12.

Benjamin, Emelia J., Salim S. Virani, Clifton W. Callaway, Alanna M. Chamberlain, Alexander R. Chang, Susan Cheng, Stephanie E. Chiuve, Mary Cushman, Francesca N. Delling, and Rajat Deo. 2018. “Heart Disease and Stroke Statistics-2018 Update: A Report from the American Heart Association.” *Circulation* 137 (12): e67.

Böer, Ulrike, Claas Spengler, Danny Jonigk, Melanie Klingenberg, Claudia Schrimpf, Stefanie Lützner, Michael Harder, Hans-Heinrich Kreipe, Axel Haverich, and Mathias Wilhelmi. 2013. “Coating Decellularized Equine Carotid Arteries with CCN1 Improves Cellular Repopulation, Local Biocompatibility, and Immune Response in Sheep.” *Tissue Engineering Part A* 19 (15–16): 1829–42.

Bonito, V., AIPM Smits, OJGM Goor, B. D. Ippel, A. Driessen-Mol, TJAG Münker, A. W. Bosman, T. Mes, P. Y. W. Dankers, and C. V. C. Bouten. 2018. “Modulation of Macrophage Phenotype and Protein Secretion via Heparin-IL-4 Functionalized Supramolecular Elastomers.” *Acta Biomaterialia* 71: 247–60.

Boretos, John W., Don E. Detmer, and James H. Donachy. 1971. “Segmented Polyurethane: A Polyether Polymer, II. Two Years Experience.” *Journal of Biomedical Materials Research* 5 (4): 373–87.

Bostman, O., E. Hirvensalo, J. Makinen, and P. Rokkanen. 1990. “Foreign-Body Reactions to Fracture Fixation Implants of Biodegradable Synthetic Polymers.” *The Journal of Bone and Joint Surgery* 72 (4): 592–96.

Brown, Bryan N., Jolene E. Valentin, Ann M. Stewart-Akers, George P. McCabe, and Stephen F. Badylak. 2009. “Macrophage Phenotype and Remodeling Outcomes in Response to

Biologic Scaffolds with and without a Cellular Component." *Biomaterials* 30 (8): 1482–91.

Burkart, Andreas, Andreas B. Imhoff, and Eva Roscher. 2000. "Foreign-Body Reaction to the Bioabsorbable Suretac Device." *Arthroscopy: The Journal of Arthroscopic & Related Surgery* 16 (1): 91–95.

Byrom, Michael J., Paul G. Bannon, Geoffrey H. White, and Martin KC Ng. 2010. "Animal Models for the Assessment of Novel Vascular Conduits." *Journal of Vascular Surgery* 52 (1): 176–95.

Calleros, Erasmo Lopez, Felix I. Simonovsky, Shai Garty, and Buddy D. RATNER. 2020. "Crosslinked, Biodegradable Polyurethanes for Precision-porous Biomaterials: Synthesis and Properties." *Journal of Applied Polymer Science*, 48943.

Christenson, E. M., J. M. Anderson, and A. Hiltner. 2007. "Biodegradation Mechanisms of Polyurethane Elastomers." *Corrosion Engineering, Science and Technology* 42 (4): 312–23.

Chuang, Tzu-Wen, and Kristyn S. Masters. 2009. "Regulation of Polyurethane Hemocompatibility and Endothelialization by Tethered Hyaluronic Acid Oligosaccharides." *Biomaterials* 30 (29): 5341–51.

Cinat, Marianne E., Judith Hopkins, and Samuel E. Wilson. 1999. "A Prospective Evaluation of PTFE Graft Patency and Surveillance Techniques in Hemodialysis Access." *Annals of Vascular Surgery* 13 (2): 191–98.

Clowes, A. W., T. R. Kirkman, and M. A. Reidy. 1986. "Mechanisms of Arterial Graft Healing. Rapid Transmural Capillary Ingrowth Provides a Source of Intimal Endothelium and

Smooth Muscle in Porous PTFE Prostheses." *The American Journal of Pathology* 123 (2): 220–30.

Dekker, Sylvia, Daphne Van Geemen, Antoon J. Van den Bogaerdt, Anita Driessen-Mol, Elena Aikawa, and Anthal IPM Smits. 2018. "Sheep-Specific Immunohistochemical Panel for the Evaluation of Regenerative and Inflammatory Processes in Tissue-Engineered Heart Valves." *Frontiers in Cardiovascular Medicine* 5.

Dick, Sarah A., Jillian A. Macklin, Sara Nejat, Abdul Momen, Xavier Clemente-Casares, Marwan G. Althagafi, Jinmiao Chen, Crystal Kantores, Siyavash Hosseinzadeh, and Laura Aronoff. 2019. "Self-Renewing Resident Cardiac Macrophages Limit Adverse Remodeling Following Myocardial Infarction." *Nature Immunology* 20 (1): 29.

DiVincenti Jr, Louis, Robin Westcott, and Candice Lee. 2014. "Sheep (Ovis Aries) as a Model for Cardiovascular Surgery and Management before, during, and after Cardiopulmonary Bypass." *Journal of the American Association for Laboratory Animal Science* 53 (5): 439–48.

Doi, Kiyoshi, and Takehisa Matsuda. 1997. "Enhanced Vascularization in a Microporous Polyurethane Graft Impregnated with Basic Fibroblast Growth Factor and Heparin." *Journal of Biomedical Materials Research: An Official Journal of The Society for Biomaterials and The Japanese Society for Biomaterials* 34 (3): 361–70.

Drury, John K., Tim R. Ashton, John D. Cunningham, Roshan Maini, and John G. Pollock. 1987. "Experimental and Clinical Experience with a Gelatin Impregnated Dacron Prosthesis." *Annals of Vascular Surgery* 1 (5): 542–47.

Fleckenstein, Peter, and Heinz-Helmut Werner. 1990. Process for the preparation of a vessel prosthesis impregnated with crosslinked gelatin. 4,902,290, issued 1990.

Fukunishi, Takuma, Cameron A. Best, Tadahisa Sugiura, Toshihiro Shoji, Tai Yi, Brooks Udelsman, Devan Ohst, et al. 2016. "Tissue-Engineered Small Diameter Arterial Vascular Grafts from Cell-Free Nanofiber PCL/Chitosan Scaffolds in a Sheep Model 11, No. 7 (2016)." *PLoS One* 11 (7).

Gao, Hongding, Jes Sandermann, J. Prag, L. Lund, and Jes Sanddal Lindholt. 2010. "Prevention of Primary Vascular Graft Infection with Silver-Coated Polyester Graft in a Porcine Model." *European Journal of Vascular and Endovascular Surgery* 39 (4): 472–77.

Garg, K., S. A. Sell, P. Madurantakam, and G. L. Bowlin. 2009. "Angiogenic Potential of Human Macrophages on Electrospun Bioresorbable Vascular Grafts." *Biomedical Materials* 4 (3): 031001. https://doi.org/10.1088/1748-6041/4/3/031001.

Garg, Koyal, Nicholas A. Pullen, Carole A. Oskeritzian, John J. Ryan, and Gary L. Bowlin. 2013a. "Macrophage Functional Polarization (M1/M2) in Response to Varying Fiber and Pore Dimensions of Electrospun Scaffolds." *Biomaterials* 34 (18): 4439–51.

Goëau-Brissonnière, Olivier, Catherine Leport, François Bacourt, Claude Lebrault, Raymonde Comte, and Jean-Claude Pechère. 1991. "Prevention of Vascular Graft Infection by Rifampin Bonding to a Gelatin-Sealed Dacron Graft." *Annals of Vascular Surgery* 5 (5): 408–12.

Goëau-Brissonnière, Olivier, Frédéric Mercier, Marie Hélène Nicolas, François Bacourt, Marc Coggia, Claude Lebrault, and Jean Claude Pechère. 1994. "Treatment of Vascular Graft Infection by in Situ Replacement with a Rifampin-Bonded Gelatin-Sealed Dacron Graft." *Journal of Vascular Surgery* 19 (4): 739–44.

Gogolewski, S., G. Galletti, and G. Ussia. 1987. "Polyurethane Vascular Prostheses in Pigs." *Colloid and Polymer Science* 265 (9): 774–78.

Guelcher, Scott A. 2008. “Biodegradable Polyurethanes: Synthesis and Applications in Regenerative Medicine.” *Tissue Engineering Part B: Reviews* 14 (1): 3–17.

Hashi, Craig K., Yiqian Zhu, Guo-Yuan Yang, William L. Young, Benjamin S. Hsiao, Karin Wang, Benjamin Chu, and Song Li. 2007. “Antithrombogenic Property of Bone Marrow Mesenchymal Stem Cells in Nanofibrous Vascular Grafts.” *Proceedings of the National Academy of Sciences* 104 (29): 11915–20.

Hausner, Richard J, Frederick J Schoen, and K. KENDALL Pierson. 1978. “Foreign-Body Reaction to Silicone Gel in Axillary Lymph Nodes after an Augmentation Mammaplasty.” *Plastic and Reconstructive Surgery* 62 (3): 381–84.

Hibino, Narutoshi, Tai Yi, Daniel R. Duncan, Animesh Rathore, Ethan Dean, Yuji Naito, Alan Dardik, Themis Kyriakides, Joseph Madri, and Jordan S. Pober. 2011. “A Critical Role for Macrophages in Neovessel Formation and the Development of Stenosis in Tissue-Engineered Vascular Grafts.” *The FASEB Journal* 25 (12): 4253–63.

Hoerstrup, Simon P., Ian Cummings, Mario Lachat, Frederick J Schoen, Rolf Jenni, Sebastian Leschka, Stefan Neuenschwander, et al. 2006. “Functional Growth in Tissue-Engineered Living, Vascular Grafts: Follow-up at 100 Weeks in a Large Animal Model.” *Circulation* 114 (supplement I): I-159-I–166.

Hsu, S.-H. Shan-hui, and Wei-Chih Chen. 2000. “Improved Cell Adhesion by Plasma-Induced Grafting of L-Lactide onto Polyurethane Surface.” *Biomaterials* 21 (4): 359–67.

Javerliat, Isabelle, Olivier Goëau-Brissonnière, Valérie Sivadon-Tardy, Marc Coggia, and Jean-Louis Gaillard. 2007. “Prevention of Staphylococcus Aureus Graft Infection by a New Gelatin-Sealed Vascular Graft Prebonded with Antibiotics.” *Journal of Vascular Surgery* 46 (5): 1026–31.

Jenkins, Stephen J., Dominik Ruckerl, Peter C. Cook, Lucy H. Jones, Fred D. Finkelman, Nico van Rooijen, Andrew S. MacDonald, and Judith E. Allen. 2011. "Local Macrophage Proliferation, Rather than Recruitment from the Blood, Is a Signature of TH2 Inflammation." *Science* 332 (6035): 1284–88.

Jeong, Sung In, So Yeon Kim, Seong Kwan Cho, Moo Sang Chong, Kyung Soo Kim, Hyuck Kim, Sang Bong Lee, and Young Moo Lee. 2007. "Tissue-Engineered Vascular Grafts Composed of Marine Collagen and PLGA Fibers Using Pulsatile Perfusion Bioreactors." *Biomaterials* 28 (6): 1115–22.

Jeschke, Marc G., Valentin Hermanutz, Steven E. Wolf, and Gerhard B. Köveker. 1999. "Polyurethane Vascular Prostheses Decreases Neointimal Formation Compared with Expanded Polytetrafluoroethylene." *Journal of Vascular Surgery* 29 (1): 168–76.

Jesús Fernández-Aceñero, Ma, Elena Zamora, and Jesús Borbujo. 2003. "Granulomatous Foreign Body Reaction against Hyaluronic Acid: Report of a Case after Lip Augmentation." *Dermatologic Surgery* 29 (12): 1225–26.

Jonas, Richard A., Gerhard Ziemer, Frederick J. Schoen, Lewis Britton, and Aldo R. Castaneda. 1988. "A New Sealant for Knitted Dacron Prostheses: Minimally Cross-Linked Gelatin." *Journal of Vascular Surgery* 7 (3): 414–19.

Jun, Ho-Wook, Lakeshia J. Taite, and Jennifer L. West. 2005. "Nitric Oxide-Producing Polyurethanes." *Biomacromolecules* 6 (2): 838–44.

Kadoba, Keishi, Frederick J. Schoen, and Richard A. Jonas. 1992. "Experimental Comparison of Albumin-Sealed and Gelatin-Sealed Knitted Dacron Conduits: Porosity Control, Handling, Sealant Resorption, and Healing." *The Journal of Thoracic and Cardiovascular Surgery* 103 (6): 1059–67.

Kang, Jungmee, Gabor Erdodi, Christopher M. Brendel, Daniel Ely, and Joseph P. Kennedy. 2010. “Polyisobutylene-based Polyurethanes. V. Oxidative-hydrolytic Stability and Biocompatibility.” *Journal of Polymer Science Part A: Polymer Chemistry* 48 (10): 2194–2203.

Kelly, Burnett, Murad Melhem, Jianhua Zhang, Gerald Kasting, Jinsong Li, Mahesh Krishnamoorthy, Sue Heffelfinger, Steven Rudich, Pankaj Desai, and Prabir Roy-Chaudhury. 2006. “Perivascular Paclitaxel Wraps Block Arteriovenous Graft Stenosis in a Pig Model.” *Nephrology Dialysis Transplantation* 21 (9): 2425–31.

Kidson, IG. 1983. “The Effect of Wall Mechanical Properties on Patency of Arterial Grafts.” *Annals of the Royal College of Surgeons of England* 65 (1): 24.

Kirkton, Robert D., Maribel Santiago-Maysonet, Jeffrey H. Lawson, William E. Tente, Shannon LM Dahl, Laura E. Niklason, and Heather L. Prichard. 2019. “Bioengineered Human Acellular Vessels Recellularize and Evolve into Living Blood Vessels after Human Implantation.” *Science Translational Medicine* 11 (485): eaau6934.

Klinge, U., B. Klosterhalfen, M. Müller, and V. Schumpelick. 1999. “Foreign Body Reaction to Meshes Used for the Repair of Abdominal Wall Hernias.” *European Journal of Surgery* 165 (7): 665–73.

Kohler, Ted R., and Thomas R. Kirkman. 1999. “Dialysis Access Failure: A Sheep Model of Rapid Stenosis.” *Journal of Vascular Surgery* 30 (4): 744–51.

Koshiko, Susumu, Tadahiro Sasajima, Senichi Muraki, Nobuyoshi Azuma, Kohsuke Yamazaki, Kaoru Chiba, Mineji Tachibana, and Masashi Inaba. 2002. “Limitations in the Use of Rifampicin-Gelatin Grafts against Virulent Organisms.” *Journal of Vascular Surgery* 35 (4): 779–85.

Kuijpers, Alma J., Gerard HM Engbers, Jeroen Krijgsveld, Sebastian AJ Zaat, Jacob Dankert, and Jan Feijen. 2000. “Cross-Linking and Characterisation of Gelatin Matrices for Biomedical Applications.” *Journal of Biomaterials Science, Polymer Edition* 11 (3): 225–43.

Lachapelle, Kevin, Alan M. Graham, and James F. Symes. 1994. “Antibacterial Activity, Antibiotic Retention, and Infection Resistance of a Rifampin-Impregnated Gelatin-Sealed Dacron Graft.” *Journal of Vascular Surgery* 19 (4): 675–82.

Lawson, Jeffery H., Marc H. Glickman, Marek Ilzecki, Tomasz Jakimowicz, Andrzej Jaroszynski, Eric K. Peden, Alison Pilgrim, et al. 2016. “Bioengineered Human Acellular Vessels for Dialysis Access in Patients with End-Stage Renal Disease: Two Phase 2 Single-Arm Trials.” *The Lancet* 387 (No. 10032): 2026–34. https://doi.org/10.1016/S0140-6736(16)00557-2.

L’heureux, Nicolas, Stéphanie Pâquet, Raymond Labbé, Lucie Germain, and François A. Auger. 1998. “A Completely Biological Tissue-Engineered Human Blood Vessel.” *The FASEB Journal* 12 (1): 47–56.

Luttikhuizen, Daniël T., Martin C. Harmsen, and Marja JA Van Luyn. 2006. “Cellular and Molecular Dynamics in the Foreign Body Reaction.” *Tissue Engineering* 12 (7): 1955–70.

Maguire Jr, James K., Michael F. Coscia, and Michael H. Lynch. 1987. “Foreign Body Reaction to Polymeric Debris Following Total Hip Arthroplasty.” *Clinical Orthopaedics and Related Research* 216: 213–23.

Manju, Saraswathy, Chirathodi Vayalappil Muraleedharan, Adathala Rajeev, Attipettah Jayakrishnan, and Roy Joseph. 2011. “Evaluation of Alginate Dialdehyde Cross-linked

Gelatin Hydrogel as a Biodegradable Sealant for Polyester Vascular Graft." *Journal of Biomedical Materials Research Part B: Applied Biomaterials* 98 (1): 139–49.

Martin, Darren J., Laura A. Poole Warren, Pathiraja A. Gunatillake, Simon J. McCarthy, Gordon F. Meijs, and Klaus Schindhelm. 2000. "Polydimethylsiloxane/Polyether-Mixed Macrodiol-Based Polyurethane Elastomers: Biostability." *Biomaterials* 21 (10): 1021–29.

Mathur, Anshu B., Terry O. Collier, W. John Kao, Michael Wiggins, Mark A. Schubert, Anne Hiltner, and James M Anderson. 1997. "In Vivo Biocompatibility and Biostability of Modified Polyurethanes." *Journal of Biomedical Materials Research* 36 (2): 246–57.

McAllister, Todd N., Marcin Maruszewski, Sergio A. Garrido, Wojciech Wystrychowski, Nathalie Dusserre, Alicia Marini, Krzysztof Zagalski, Alejandro Fiorillo, Hernan Avila, and Ximena Manglano. 2009. "Effectiveness of Haemodialysis Access with an Autologous Tissue-Engineered Vascular Graft: A Multicentre Cohort Study." *The Lancet* 373 (9673): 1440–46.

Mehta, Rupal I., Arnob K. Mukherjee, Tyler D. Patterson, and Michael C. Fishbein. 2011. "Pathology of Explanted Polytetrafluoroethylene Vascular Grafts." *Cardiovascular Pathology* 20 (4): 213–21.

Niklason, L. E., J. Gao, W. M. Abbott, K. K. Hirschi, S. Houser, R. Marini, and R. Langer. 1999. "Functional Arteries Grown in Vitro." *Science* 284 (5413): 489–93.

Ratner, B.D., K. W. Gladhill, and T. A. Horbett. 1988. "Analysis of in Vitro Enzymatic and Oxidative Degradation of Polyurethanes." *Journal of Biomedical Materials Research* 22 (6): 509–27.

Roh, Jason D., Rajendra Sawh-Martinez, Matthew P. Brennan, Steven M. Jay, Lesley Devine, Deepak A. Rao, Tai Yi, Tamar L. Mirensky, Ani Nalbandian, and Brooks Udelsman.

2010. “Tissue-Engineered Vascular Grafts Transform into Mature Blood Vessels via an Inflammation-Mediated Process of Vascular Remodeling.” *Proceedings of the National Academy of Sciences* 107 (10): 4669–74.

Rossitch, Eugene, Dennis E. Bullard, and W. Jerry Oakes. 1987. “Delayed Foreign-Body Reaction to Silk Sutures in Pediatric Neurosurgical Patients.” *Child’s Nervous System* 3 (6): 375–78.

Roy-Chaudhury, Prabir, Burnett S. Kelly, Mary Ann Miller, Anita Reaves, Janice Armstrong, Nuwan Nanayakkara, and Sue C. Heffelfinger. 2001. “Venous Neointimal Hyperplasia in Polytetrafluoroethylene Dialysis Grafts.” *Kidney International* 59 (6): 2325–34.

Salzmann, Dennis Lee. 1997. “Macrophage Response to Polymeric Vascular Grafts.” http://arizona.openrepository.com/arizona/handle/10150/288765.

Samterre, J. P., K. Woodhouse, G. Laroche, and R. S. Labow. 2005. “Understanding the Biodegradation of Polyurethanes: From Classical Implants to Tissue Engineering Materials.” *Biomaterials* 26 (35): 7457–70.

Sarkar, S., H. J. Salacinski, G. Hamilton, and A. M. Seifalian. 2006. “The Mechanical Properties of Infrainguinal Vascular Bypass Grafts: Their Role in Influencing Patency.” *European Journal of Vascular and Endovascular Surgery* 31 (6): 627–36.

Sauvage, Lester R., and Henry N. Harkins. 1953. “Experimental Vascular Grafts: An Evaluation Relating to Types, Means of Preservation, and Methods of Suture in the Growing Pig.” *Surgery* 33 (4): 587–635.

Seifalian, Alexander M., Henryk J. Salacinski, Alok Tiwari, Alan Edwards, Staffan Bowald, and George Hamilton. 2003. “In Vivo Biostability of a Poly (Carbonate-Urea) Urethane Graft.” *Biomaterials* 24 (14): 2549–57.

Shofti, R., A. Zaretzki, E. Cohen, A. Engel, and Y. Bar-El. 2004. “The Sheep as a Model for Coronary Artery Bypass Surgery.” *Laboratory Animals* 38 (2): 149–57.

Sievers, Hermine, and Dietrich von Domarus. 1984. “Foreign-Body Reaction against Intraocular Lenses.” *American Journal of Ophthalmology* 97 (6): 743–51.

Simmons, Anne, Jari Hyvarinen, and Laura A. Poole-Warren. 2006. “The Effect of Sterilisation on a Poly (Dimethylsiloxane)/Poly (Hexamethylene Oxide) Mixed Macrodiol-Based Polyurethane Elastomer.” *Biomaterials* 27 (25): 4484–97.

Soffer, Leah, Xianyan Wang, Xiaohui Zhang, Jonathan Kluge, Luis Dorfmann, David L. Kaplan, and Gary Leisk. 2008. “Silk-Based Electrospun Tubular Scaffolds for Tissue-Engineered Vascular Grafts.” *Journal of Biomaterials Science, Polymer Edition* 19 (5): 653–64.

Soldani, Giorgio, Paola Losi, Massimo Bernabei, Silvia Burchielli, Dante Chiappino, Silvia Kull, Enrica Briganti, and Dario Spiller. 2010. “Long Term Performance of Small-Diameter Vascular Grafts Made of a Poly (Ether) Urethane–Polydimethylsiloxane Semi-Interpenetrating Polymeric Network.” *Biomaterials* 31 (9): 2592–2605.

Soletti, Lorenzo, Yi Hong, Jianjun Guan, John J. Stankus, Mohammed S. El-Kurdi, William R. Wagner, and David A. Vorp. 2010. “A Bilayered Elastomeric Scaffold for Tissue Engineering of Small Diameter Vascular Grafts.” *Acta Biomaterialia* 6 (1): 110–22.

Spiller, Kara L., Rachel R. Anfang, Krista J. Spiller, Johnathan Ng, Kenneth R. Nakazawa, Jeffrey W. Daulton, and Gordana Vunjak-Novakovic. 2014. “The Role of Macrophage Phenotype in Vascularization of Tissue Engineering Scaffolds.” *Biomaterials* 35 (15): 4477–88. https://doi.org/10.1016/j.biomaterials.2014.02.012.

Spiller, Kara L., Sina Nassiri, Claire E. Witherel, Rachel R. Anfang, Johnathan Ng, Kenneth R. Nakazawa, Tony Yu, and Gordana Vunjak-Novakovic. 2015. “Sequential Delivery of

Immunomodulatory Cytokines to Facilitate the M1-to-M2 Transition of Macrophages and Enhance Vascularization of Bone Scaffolds." *Biomaterials* 37: 194–207.

Stokes, Ken, Rick McVenes, and James M. Anderson. 1995. "Polyurethane Elastomer Biostability." *Journal of Biomaterials Applications* 9 (4): 321–54.

Sussman, Eric M., Michelle C. Halpin, Jeanot Muster, Randall T. Moon, and Buddy D. Ratner. 2014. "Porous Implants Modulate Healing and Induce Shifts in Local Macrophage Polarization in the Foreign Body Reaction." *Annals of Biomedical Engineering* 42 (7): 1508–16.

Suzuki, Yoshihisa, Yoshihiko Nishimura, Masao Tanihara, Kyoko Suzuki, Tatsuo Nakamura, Yasuhiko Shimizu, Yoshio Yamawaki, and Yoshimi Kakimaru. 1998. "Evaluation of a Novel Alginate Gel Dressing: Cytotoxicity to Fibroblasts in Vitro and Foreign-body Reaction in Pig Skin in Vivo." *Journal of Biomedical Materials Research* 39 (2): 317–22.

Syedain, Zeeshan H., Melanie L. Graham, Ty B. Dunn, Timothy O'Brien, Sandra L. Johnson, Robert J. Schumacher, and Robert T. Tranquillo. 2017. "A Completely Biological 'off-the-Shelf' Arteriovenous Graft That Recellularizes in Baboons." *Science Translational Medicine* 9 (414): eaan4209.

Syedain, Zeeshan H., Lee A. Meier, Mathew T. Lahti, Sandra L. Johnson, and Robert T. Tranquillo. 2014. "Implantation of Completely Biological Engineered Grafts Following Decellularization into the Sheep Femoral Artery." *Tissue Engineering Part A* 20 (11–12): 1726–34.

Tai, N. R., H. J. Salacinski, A. Edwards, G. Hamilton, and A. M. Seifalian. 2000a. "Compliance Properties of Conduits Used in Vascular Reconstruction." *British Journal of Surgery* 87 (11): 1516–24.

Takahara, Atsushi, Arthur J. Coury, Rogert W. Hergenrother, and Stuart L. Cooper. 1991. "Effect of Soft Segment Chemistry on the Biostability of Segmented Polyurethanes. I. In Vitro Oxidation." *Journal of Biomedical Materials Research* 25 (3): 341–56.

Taylor Jr, Lloyd M., Guenther Mueller-Velten, Allen Koslow, Glenn Hunter, Thomas Naslund, Ronald Kline, and Beriplast P. Investigators. 2003. "Prospective Randomized Multicenter Trial of Fibrin Sealant versus Thrombin-Soaked Gelatin Sponge for Suture-or Needle-Hole Bleeding from Polytetrafluoroethylene Femoral Artery Grafts." *Journal of Vascular Surgery* 38 (4): 766–71.

Teebken, O. E., A. Bader, G. Steinhoff, and A. Haverich. 2000. "Tissue Engineering of Vascular Grafts: Human Cell Seeding of Decellularised Porcine Matrix." *European Journal of Vascular and Endovascular Surgery* 19 (4): 381–86.

Tyler, B. J., and B. D. Ratner. 1995. "Oxidative Degradation of Biomer™ Fractions Prepared by Using Preparative-Scale Gel Permeation Chromatography." *Journal of Biomaterials Science, Polymer Edition* 6 (4): 359–73.

Tymoszuk, Piotr, Hanneke Evens, Vanessa Marzola, Katarzyna Wachowicz, Marie-Helene Wasmer, Sebak Datta, Elisabeth Müller-Holzner, Heidi Fiegl, Günther Böck, and Nico van Rooijen. 2014. "In Situ Proliferation Contributes to Accumulation of Tumor-associated Macrophages in Spontaneous Mammary Tumors." *European Journal of Immunology* 44 (8): 2247–62.

Ueberrueck, Torsten, Joerg Tautenhahn, Lutz Meyer, Olaf Kaufmann, Hans Lippert, Ingo Gastinger, and Thorsten Wahlers. 2005. "Comparison of the Ovine and Porcine Animal Models for Biocompatibility Testing of Vascular Prostheses." *Journal of Surgical Research* 124 (2): 305–11.

Uttayarat, Pimpon, Anat Perets, Mengyan Li, Pimchanok Pimton, Stanley J. Stachelek, Ivan Alferiev, Russell J. Composto, Robert J. Levy, and Peter I. Lelkes. 2010. "Micropatterning of Three-Dimensional Electrospun Polyurethane Vascular Grafts." *Acta Biomaterialia* 6 (11): 4229–37.

Walden, Raphael, J. L. Gilbert, Joseph Megerman, and William M. Abbott. 1980. "Matched Elastic Properties and Successful Arterial Grafting." *Archives of Surgery* 115 (10): 1166–69.

Wang, Yang, Mahesh Krishnamoorthy, Rupak Banerjee, Jianhua Zhang, Steven Rudich, Christy Holland, Lois Arend, and Prabir Roy-Chaudhury. 2008. "Venous Stenosis in a Pig Arteriovenous Fistula Model—Anatomy, Mechanisms and Cellular Phenotypes." *Nephrology Dialysis Transplantation* 23 (2): 525–33.

Wang, Zhihong, Yun Cui, Jianing Wang, Xiaohu Yang, Yifan Wu, Kai Wang, Xuan Gao, Dong Li, Yuejie Li, Xi-Long Zheng, et al. 2014. "The Effect of Thick Fibers and Large Pores of Electrospun Poly(ε-Caprolactone) Vascular Grafts on Macrophage Polarization and Arterial Regeneration." *Biomaterials* 35 (22): 5700–5710. https://doi.org/10.1016/j.biomaterials.2014.03.078.

Wiggins, Michael J., Matt MacEwan, James M. Anderson, and Anne Hiltner. 2004. "Effect of Soft-segment Chemistry on Polyurethane Biostability during in Vitro Fatigue Loading." *Journal of Biomedical Materials Research Part A* 68 (4): 668–83.

Wissink, M. J. B., R. Beernink, A. A. Poot, G. H. M. Engbers, T. Beugeling, W. G. Van Aken, and J. Feijen. 2000. "Improved Endothelialization of Vascular Grafts by Local Release of Growth Factor from Heparinized Collagen Matrices." *Journal of Controlled Release* 64 (1): 103–14.

Xu, Weilin, Fei Zhou, Chenxi Ouyang, Weigang Cui, Mu Yao, and Xungai Wang. 2008. "Small Diameter Polyurethane Vascular Graft Reinforced by Elastic Weft-Knitted Tubular Fabric of Polyester/Spandex." *Fibers and Polymers* 9 (1): 71–75.

Xu, Weilin, Fei Zhou, Chenxi Ouyang, Wenxiang Ye, Mu Yao, and Bugao Xu. 2010. "Mechanical Properties of Small-diameter Polyurethane Vascular Grafts Reinforced by Weft-knitted Tubular Fabric." *Journal of Biomedical Materials Research Part A: An Official Journal of The Society for Biomaterials, The Japanese Society for Biomaterials, and The Australian Society for Biomaterials and the Korean Society for Biomaterials* 92 (1): 1–8.

Yavuz, Kivilcim, Serdar Geyik, Dusan Pavcnik, Barry T. Uchida, Christopher L. Corless, David E. Hartley, Ahmet Goktay, et al. 2006. "Comparison of the Endothelialization of Small Intestinal Submucosa, Dacron, and Expanded Polytetrafluoroethylene Suspended in the Thoracoabdominal Aorta in Sheep." *Journal of Vascular and Interventional Radiology* 17 (5): 873–82.

Zhang, L. 2013. "Zwitterionic Hydrogels Implanted in Mice Resist the Foreign-Body Reaction." *Nature Biotechnol.* 31: 553–56. https://doi.org/10.1038/nbt.2580.

Zhang, Ze, Zhaoxu Wang, Shuqin Liu, and Makoto Kodama. 2004. "Pore Size, Tissue Ingrowth, and Endothelialization of Small-Diameter Microporous Polyurethane Vascular Prostheses." *Biomaterials* 25 (1): 177–87.

Zhao, Q., N. Topham, J. M. Anerson, Anne Hiltner, G. Lodoen, and C. R. Payet. 1991. "Foreign-body Giant Cells and Polyurethane Biostability: In Vivo Correlation of Cell Adhesion and Surface Cracking." *Journal of Biomedical Materials Research* 25 (2): 177–83.

Zhu, Yabin, Changyou Gao, Tao He, and Jiacong Shen. 2004a. “Endothelium Regeneration on Luminal Surface of Polyurethane Vascular Scaffold Modified with Diamine and Covalently Grafted with Gelatin.” *Biomaterials* 25 (3): 423–30.

Ziegler-Graham, Kathryn, Ellen J. MacKenzie, Patti L. Ephraim, Thomas G. Travison, and Ron Brookmeyer. 2008. “Estimating the Prevalence of Limb Loss in the United States: 2005 to 2050.” *Archives of Physical Medicine and Rehabilitation* 89 (3): 422–29. https://doi.org/10.1016/j.apmr.2007.11.005.

Vita

EDUCATION:

ISTITUTION AND LOCATION	DEGREE	YEAR	FIELD OF STUDY
University of Washington, Seattle, WA, USA	**PhD**	**2020**	**Chemical Engineering**
Oregon State University, Corvallis, OR, USA	**MS**	**2014**	**Chemical Engineering**
Beijing University of Chemical Technology, Beijing, China	**BEng**	**2011**	**Polymer Science & Engineering**

RESEARCH EXPERIENCE:

2015-2020 **Graduate Research Assistant, University of Washington, Seattle, WA (Prof. Buddy Ratner's lab)**

- Developing immunomodulatory porous regenerative elastic scar-free scaffolds for *in-situ* vascular engineering
- Synthesized novel bio-stable polyurethane material to match the mechanical properties of blood vessels
- Study healing and immune responses to biomaterials in mice and sheep models

2013-2014 **Graduate Research Assistant, Oregon State University, Covallis, OR (Laboratory of Prof. Gregory Rorrer)**

- Maintained cell culture with aseptic technique
- Developed biosilica-based biosensor by surface functionalization of biosilica with antibody
- Evaluated biosensor performance using multiple analysis techniques such as PL spectroscopy, Raman spectroscopy and epifluorescence microscope.

2009-2011 **Undergraduate Research Assistant, State Key Laboratory of Chemical Resources, Beijing University of Chemical Technology, Beijing, China (Prof Wu Yixian's Lab)**

- Synthesized elastomers under anhydrous, nitrogen protection and extreme temperatures
- Optimized reaction conditions for synthesizing petroleum resin
- Characterized reaction products using Gel Permeation Chromatography and FTIR

PUBLICATIONS:

[1] Zhen, L., Ford, N., Gale, D. K., Roesijadi, G., & Rorrer, G. L. (2016). Photoluminescence detection of 2, 4, 6-trinitrotoluene (TNT) binding on diatom frustule

biosilica functionalized with an anti-TNT monoclonal antibody fragment. *Biosensors and Bioelectronics*, *79*, 742-748.

[2] J. Yang, L. Zhen, F. Ren, J. Campbell, G. L. Rorrer, and A. X. Wang, "Ultra-sensitive immunoassay biosensors using hybrid plasmonic-biosilica nanostructured materials," *J. Biophotonics*, vol. 9999, 2014.

PATENTS:

[1] Ratner, B.D., Zhen, L., Simonovsky, F. and Himmelfarb, J., University of Washington, 2018. *Pro-healing elastic angiogenic microporous vascular graft*. U.S. Patent Application 15/879,301.

PRESENTATIONS:

[1] L. Zhen, F. Simonovsky, S. Creason, E. Quiroga, D. C. Bonafonte, P. Roy-Chaudhury, B. Ratner, "A Precision-Porous Polyurethane Material for In-situ Tissue-Engineered Vascular Grafts", SFB, 2019.

[2] L. Zhen, M. Mecwan, S. Zhang, F. Simonovsky, and B. Ratner, " Albumin and Fibrinogen Adsorption on New Fluorinated Polyurethanes as an Indication of Blood-compatibility," Pacsurf, 2018

[3] L. Zhen, B. Ratner, " Precision-engineered Porous Polyurethane Resists Foreign Body Capsule Formation and Promotes Vascularization by Modulating Macrophage Response," SFB, 2018

[4] L. Zhen, S. Creason, and B. Ratner, " An Elastic, Precision-Engineered Porous Polyurethane Material Mitigates Foreign Body Capsule Formation and Promotes Tissue Integration *In Vivo,*" SFB, 2017

[5] L. Zhen and B. Ratner, " Precision-engineered Porous Material with Tunable Mechanical Property for Vascular Graft Application, " BMES, 2016

[6] L. Zhen and B. Ratner, "Improving Vascular Graft Performance with Pro-angiogenic Microporous Material," presented at the STS, Seattle, 21-Jan-2016.

[7] L. Zhen, "Detecting Water Pollutant TNT with Single-celled Algae," presented at the Biomaterial Seminar, Seattle, 09-Apr-2015.

[8] J. Yang, F. Ren, L. Zhen, J. Campbell, G. L. Rorrer, and A. X. Wang, "Surface-Enhanced Raman Scattering Immuno-Assay Using Diatom Frustules," in *CLEO: Science and Innovations*, 2014, p. STh4H. 1.

Thesis:

[1] L. Zhen, "Immunomodulatory Porous Regenerative Scar-free Scaffold for In-situ Vascular Engineering (IMPRESSIVE)," PhD Thesis, University of Washington, Seattle, 2020.

[2] L. Zhen, "2, 4, 6-trinitrotoluene detection using photoluminescence response of diatom biosilica functionalized with single-chain variable fragment," MS Thesis, Oregon State University, Corvallis, 2014.

[3] L. Zhen, "Synthesis and Characterization of C10 Petroleum Resin," Beijing University of Chemical Technology, Beijing, 2011.

Honors:

- Student Travel and Recognition (STAR) Award from the Society for Biomaterials (2018)
- Graduate Assistant in Areas of National Need (GAANN) fellowship (9/2015 – 6/2016)
- Prototype Funding for Health Innovation Challenge (12/2015)
- A. Pat Miller Endowed Fellowship (Autumn 2014)

UNDERGRADUATE MENTEES:

Jason Dang; Nicholas Zhen Hung Soo; Isaac Lam; Melissa Gile; Rebecca (Becky) Darrow; Tanmay Sapre; Louis Chen; Chaoyang (Tango) Tang; Lahari Gorantla; Manjari Anant; Luojun (Tommy) Qian.

EXTRACURRICULAR ROLES:

Summer 2008 **Volunteer for Huiyuan Media Village in Games of XXIX Olympiada**